



**CAPTURING COMPLEX MICROENVIRONMENTS FOR  
DIRECTED STEM CELL DIFFERENTIATION**

**A BIOMIMETIC APPROACH TO MULTIFACETED, COMPLEX  
BIOMATERIAL DESIGN FOR SPECIFIC TISSUE REGENERATION**

Michael Louis Floren

E-mail: Michael.floren@colorado.edu

Approved by:

Prof. -----, Advisor  
Department of -----  
*University of -----, Country.*

Prof. -----,  
Department of -----  
*University of -----, Country.*

Ph.D. Commission:

Prof. -----,  
Department of -----  
*University of -----, Country.*

Prof. -----,  
Department of -----  
*University of -----, Country.*

Prof. -----,  
Department of -----  
*University of -----, Country.*

University of Trento,  
Department of -----

September 2015

**University of Trento - Department of**  
.....

**Doctoral Thesis**

**Name - 2013**

**Published in Trento (Italy) – by University of Trento**

**ISBN: .....**

*Dedicated to:*  
*Elizabeth Susan Floren*  
*1951 –2002*



# Abstract

Loss of vascular function associated with cardiovascular disease, such as atherosclerosis, represents the leading medical epidemic in the United States and typically requires surgical intervention through synthetic or autologous vascular grafts. To overcome the limitations associated with adult cell sources, which are often restricted by supply or compromised by disease, mesenchymal stem cells (MSCs) have emerged as potential candidates for vascular tissue engineering. While evidence suggests the roles of several factors influencing MSC differentiation into vascular phenotypes, including matrix rigidity, geometry and chemistry, the phenomena associated with these events are still largely unknown. Further, the development of mature vascular phenotypes, such as vascular smooth muscle cells (vSMCs), with functional behavior remains elusive to the research community.

This thesis proposed to engineer and direct specific and mature vascular differentiation from MSCs by way of highly tailored matrices mimicking the vascular niche environment. Taking inspiration from natural organization, we contend that a biomimetic design approach to tissue scaffolds that display features of the natural cellular microenvironment whilst mimicking the bulk tissue properties may elicit highly specific differentiation of MSCs to vascular phenotypes. To validate our hypothesis, we employed a systemic approach incorporating physical and chemical microenvironmental cues, i.e. stiffness, biological ligands and chemical factors, with the aim to augment vascular phenotype expression, functionality, and final incorporation into a tailored biomaterial scaffolds.

First, we present a novel technique for the preparation of silk hydrogels directly from high pressure CO<sub>2</sub> environments without the need for crosslinking agents or additional additives such as surfactants or co-solvents. Through this novel method, we demonstrate the utility of CO<sub>2</sub> as a volatile electrolyte, capable of sufficiently influencing the sol-gel transition of silk proteins, resulting in the formation of stable hydrogels with properties suitable for biomedical applications.

Second, we hypothesized that suitable soluble factor regimen and matrix rigidity can instruct MSC differentiation towards more mature, functional vSMCs. To

address this, we investigated cellular differentiation on tunable SF hydrogels prepared using a solvent-free CO<sub>2</sub> processing method. The focus of this portion of the thesis is on exploiting the combined use of substrate stiffness and growth factor (TGF- $\beta$ 1) on SF matrices, with the aim of correlating the effects on the vascular commitment of human mesenchymal stem cells (hMSCs). Our data reveal that hMSC differentiation into mature SMCs can be achieved within modest culture periods (72 h) by combining appropriate SF hydrogel stiffness (33 kPa) with growth factor (TGF- $\beta$ 1). These findings advance our understanding of how complex multicomponent biomaterials, whereby mimicking the intricacy of natural tissue environments, can play a significant role in developing optimal stem cell differentiation protocols.

Third, we postulated that the presentation of ECM proteins on 3D matrices with tunable stiffness will augment the differentiation of MSCs to vascular lineages. To address this, we established a high-throughput ECM platform based on soft, fibrous PEG hydrogels meanwhile highly-tunable in stiffness and 3-dimensional geometry. Using this technique, we identified several microenvironments supporting MSC adhesion, spreading and differentiation toward early vascular lineages. This portion of the thesis supports the hypothesis that a complex milieu exists coupling protein functional behavior with substrate rigidity and that this phenomenon may potentially be exploited through proper application of high-throughput screening methodologies.

In the final work of this thesis, we explored the integration of ECM-derived small engineered peptides with 3D soft matrices to refine the differentiation of MSCs to vascular phenotypes, and further successfully recapitulate the complex vascular niche necessary for specific and efficient MSC differentiation into vascular lineages. In line with this, we report the development of a microarray platform based on electrospun nanofibrous hydrogels of photoclickable thiol-ene poly(ethylene glycol) (PEG) hydrogels. Here, we demonstrate the ability to control primary cell adhesion to soft, fibrous hydrogels functionalized with RGD peptide. However, future work will be focused on designing combinatorial peptide studies, whereby, the integration of several biological ligands of interest with tunable physical properties can instruct stem cell differentiation in a highly specific manner.

This thesis has provided fundamental insights into the effects of physiological stimuli on vascular differentiation of MSC in terms of the specificity and maturity of the final differentiated cells. Better understanding of such mechanisms will prove paramount in the sequential stages of MSC differentiation to mature vascular cells. Additionally, the findings of this thesis will help to better define the process of regenerating functional healthy vascular tissue from MSCs. Altogether, a combinatorial approach investigating the effects of matrix elasticity, biological ligands and growth factors on MSC differentiation in a 3D nanofiber culture will be critical towards understanding and recapitulating MSC differentiation in the *in vivo* vascular environment.



2.2.4. Aim 4 .....	30
--------------------	----

**Chapter III**

**Carbon Dioxide Induced Silk Protein Gelation for Biomedical**

<b>Applications .....</b>	<b>32</b>
<b>3.1. Introduction.....</b>	<b>33</b>
<b>3.2. Materials &amp; Methods.....</b>	<b>36</b>
<b>3.2.1. Preparation of Silk Fibroin Solution .....</b>	<b>36</b>
<b>3.2.2. Fabrication of Silk Hydrogels .....</b>	<b>37</b>
<b>3.2.2.1. Atmospheric Conditions .....</b>	<b>37</b>
<b>3.2.2.2. High Pressure Conditions .....</b>	<b>37</b>
<b>3.2.2.3. Determination of Gelation Kinetics .....</b>	<b>39</b>
<b>3.2.3. Gel Physical Properties .....</b>	<b>39</b>
<b>3.2.3.1. Structural Analysis by Fourier Transform</b>	
<b>Infrared Spectroscopy .....</b>	<b>39</b>
<b>3.2.3.2. Environmental Scanning Electron Microscopy</b>	
<b>.....</b>	<b>39</b>
<b>3.2.3.3. Scanning Electron Microscopy .....</b>	<b>40</b>
<b>3.2.3.4. Swelling Ratio .....</b>	<b>40</b>
<b>3.2.3.5. Mechanical Properties in Compression .....</b>	<b>40</b>
<b>3.2.4. Statistical Analysis .....</b>	<b>41</b>
<b>3.3. Results &amp; Discussion .....</b>	<b>41</b>
<b>3.3.1. Gross Examination of Prepared Silk Hydrogels ....</b>	<b>41</b>
<b>3.3.2. Gelation Kinetics .....</b>	<b>42</b>
<b>3.3.2.1. In situ observation .....</b>	<b>42</b>
<b>3.3.2.2. Gelation Screening .....</b>	<b>42</b>
<b>3.3.3. Monitoring of Silk Structural Changes by FTIR .....</b>	<b>44</b>
<b>3.3.4. Hydrogel Physical Characteristics .....</b>	<b>46</b>
<b>3.3.4.1. Microstructure .....</b>	<b>46</b>
<b>3.3.4.2. Hydrogel Swelling Behavior .....</b>	<b>49</b>
<b>3.3.5. Properties in Compression .....</b>	<b>51</b>
<b>3.3.6. Phenomenological Description .....</b>	<b>54</b>
<b>3.3.6.1. Acidification Kinetics using Carbon Dioxide</b>	
<b>.....</b>	<b>54</b>
<b>3.3.6.2. Influence of High Pressure Environment ....</b>	<b>63</b>

<b>3.4. Conclusion .....</b>	<b>64</b>
------------------------------	-----------

## **Chapter IV**

<b>Human MSCs Cultured on Silk Hydrogels with Variable Stiffness and Growth Factor Differentiate into Mature SMC Phenotype .....</b>	<b>66</b>
--------------------------------------------------------------------------------------------------------------------------------------	-----------

<b>4.1. Introduction.....</b>	<b>67</b>
<b>4.2. Materials &amp; Methods.....</b>	<b>69</b>
<b>4.2.1. SF Hydrogel Preparation .....</b>	<b>69</b>
<b>4.2.2. Hydrogel Structural Characterization .....</b>	<b>70</b>
<b>4.2.2.1. Thermal analysis by differential scanning calorimetry .....</b>	<b>70</b>
<b>4.2.2.2. Fourier-Transform Infrared Spectroscopy (FTIR) analysis .....</b>	<b>70</b>
<b>4.2.2.3. Morphology Assessment .....</b>	<b>71</b>
<b>4.2.2.4. Mechanical Properties in Compression .....</b>	<b>71</b>
<b>4.2.3. Cell Culture methods .....</b>	<b>71</b>
<b>4.2.4. Cell Characterization methods .....</b>	<b>72</b>
<b>4.2.4.1. Quantitative real-time polymerase chain reaction (qPCR) .....</b>	<b>72</b>
<b>4.2.4.2. Immunofluorescent Staining .....</b>	<b>73</b>
<b>4.2.4.3. Confocal Imaging .....</b>	<b>73</b>
<b>4.2.5. Statistical analysis .....</b>	<b>74</b>
<b>4.3. Results .....</b>	<b>74</b>
<b>4.3.1. Hydrogel Fabrication and Characterization .....</b>	<b>74</b>
<b>4.3.2. Hydrogel Pore Characteristics .....</b>	<b>77</b>
<b>4.3.3. Hydrogel Compressive Properties .....</b>	<b>78</b>
<b>4.3.4. Effect of SF Hydrogel Rigidity on hMSC attachment and spreading in Low-Serum or TGF<math>\beta</math>-1 Fortified Media .....</b>	<b>79</b>
<b>4.3.5. Effect of SF Hydrogel Rigidity and TGF-<math>\beta</math>1 on Vascular SMC Commitment of hMSCs .....</b>	<b>81</b>
<b>4.4. Discussion .....</b>	<b>84</b>
<b>4.5. Conclusion .....</b>	<b>89</b>

## Chapter V

### Three-Dimensional, Soft Neotissue Arrays as High Throughput Platforms for the Interrogation of Engineered Tissue Environments

.....	90
<b>5.1. Introduction</b> .....	<b>91</b>
<b>5.2. Materials &amp; Methods</b> .....	<b>92</b>
<b>5.2.1. Materials</b> .....	<b>92</b>
<b>5.2.2. Fabrication of PEGDM Soft Matrices</b> .....	<b>93</b>
<b>5.2.3. Characterization of PEGDM Soft Matrices</b> .....	<b>94</b>
<b>5.2.3.1. FTIR Analysis</b> .....	<b>94</b>
<b>5.2.3.2. Scanning Electron Microscopy Imaging</b> .....	<b>94</b>
<b>5.2.3.3. Fluorescent Imaging</b> .....	<b>94</b>
<b>5.2.3.4. Rheology</b> .....	<b>95</b>
<b>5.2.4. ECM Protein Array Preparation</b> .....	<b>95</b>
<b>5.2.5. Cell Seeding and Cell Culture</b> .....	<b>96</b>
<b>5.2.6. Immunofluorescent Staining</b> .....	<b>97</b>
<b>5.2.7. Confocal Imaging</b> .....	<b>97</b>
<b>5.2.8. Image &amp; Statistical Analysis</b> .....	<b>98</b>
<b>5.3. Results</b> .....	<b>98</b>
<b>5.3.1. Characterization of 3-dimensional Fibrous Soft         Hydrogel Matrix</b> .....	<b>98</b>
<b>5.3.2. Design and Optimization of 3-dimensional Protein         Microarray</b> .....	<b>100</b>
<b>5.3.3. Stem Cell Adhesion and Spreading within 3-         dimensional Neotissue Arrays</b> .....	<b>103</b>
<b>5.3.4. Effect of Protein Environment and Matrix Elasticity on         MSC Adhesion and Spreading</b> .....	<b>104</b>
<b>5.3.5. Effects of Matrix Elasticity and Adhesive Protein         Environment on MSC Fate Commitment in 3-         dimensional Engineered Neotissues</b> .....	<b>107</b>
<b>5.4. Discussion</b> .....	<b>110</b>
<b>5.5. Conclusion</b> .....	<b>116</b>

## Chapter VI

<b>Nanofibrous Photoclickable Hydrogel Microarrays for High-Throughput Screening of Cellular Microenvironments .....</b>	<b>117</b>
<b>6.1. Introduction.....</b>	<b>118</b>
<b>6.2. Materials &amp; Methods.....</b>	<b>119</b>
<b>6.2.1. Macromer synthesis .....</b>	<b>119</b>
<b>6.2.2. Electrospinning .....</b>	<b>119</b>
<b>6.2.3. Scanning Electron Microscopy .....</b>	<b>120</b>
<b>6.2.4. Peptide Synthesis .....</b>	<b>120</b>
<b>6.2.5. Fluorescent Peptide Synthesis .....</b>	<b>121</b>
<b>6.2.6. Engineered Peptide Array Preparation .....</b>	<b>121</b>
<b>6.2.7. Cell Seeding &amp; Cell Culture .....</b>	<b>122</b>
<b>6.2.8. Immunofluorescent Staining .....</b>	<b>122</b>
<b>6.2.9. Confocal Imaging .....</b>	<b>122</b>
<b>6.2.10. Statistical analysis .....</b>	<b>123</b>
<b>6.3. Results .....</b>	<b>123</b>
<b>6.3.1. Characterization of 3-dimensional fibrous PEG thiol-ene hydrogel matrix .....</b>	<b>123</b>
<b>6.3.2. Engineered Peptide Synthesis and Array Fabrication .....</b>	<b>124</b>
<b>6.3.3. Primary Cell Adhesion and Spreading within Peptide Functionalized PEG thiol-ene Matrices .....</b>	<b>125</b>
<b>6.3.4. Primary Cell Adhesion and Spreading within PEG thiol-ene Peptide Functionalized Arrays .....</b>	<b>127</b>
<b>6.4. Discussion .....</b>	<b>128</b>
<b>6.5. Conclusion .....</b>	<b>129</b>
<b>Chapter VII</b>	
<b>Conclusion and Future Perspectives .....</b>	<b>130</b>
<b>7.1. Conclusions .....</b>	<b>130</b>
<b>7.2. Future Directions .....</b>	<b>133</b>

<b>List of abbreviation and acronyms .....</b>	<b>136</b>
<b>References .....</b>	<b>137</b>
<b>Scientific Production .....</b>	<b>165</b>
<b>Participation to <i>Congresses, Schools and Workshops</i>.....</b>	<b>166</b>
<b>Acknowledgements.....</b>	<b>168</b>

# Chapter I

## Introduction & Background

### **1. Motivation**

#### **1.1. Cardiovascular Disease: Motivation for New Therapies**

There is a pressing need to develop advanced strategies for the treatment of cardiovascular diseases (CVD). Cardiovascular disease (CVD) is the leading cause of death in the United States associated with 1 out of every 4 deaths as reported in 2009 (Kochanek, 2009). Current therapies rely on surgical intervention using autologous vascular bypass grafts such as the saphenous vein; however, these therapies are restricted in practice as they require surgical harvest and may be limited by a prior disease state or previous use (Weintraub, 1994). Approximately 1.5 million cases are alternatively treated with synthetic vascular grafts; however, these grafts commonly fail due to stenosis, an abnormal narrowing of the vessel, or thrombosis, formation of a blood clot in the vessel. These conditions arise because current synthetic vascular grafts fail to successfully integrate with the local vasculature at the implant site. Various recent studies have attempted to improve the biorecognition and integration of synthetic grafts by loading the substrates with primary vascular cells. Nonetheless, such methods still represent limited successful outcomes due to the need for invasive surgery and the limited expansion and functionality of these primary cells *in vitro*.

#### **1.2. Tissue Engineering Therapies**

Tissue engineering and regenerative medicine seek to provide therapeutic solutions to repair or replace damaged tissue (Langer, 1993). Traditionally, tissue engineering has relied on cultivating a cell source, usually a biopsy of the host tissue, onto a structural matrix (scaffold) and subsequently implanted at the site of defect. The ability to design scaffolds that imitate the natural cellular micro-environment of the replacement tissue is vital for the success of such implants and usually involves the fine-tuning of engineered matrices on various scales. Vascular

tissues are highly organized, ranging from nanoscale matrix proteins, providing a medium for biological cues between adjacent cells, to macroscopic structures that influence the architecture and mechanical function of such vessels. This stunning organization found in nature at all size scales allows tissues to perform functions beyond the single cell. Vascular tissues rely on the viable and functional extra cellular matrix (ECM) to impart the necessary requisites of mammalian vasculature (Cleary, 2012). Taking inspiration from this natural organization, several reports have focused on preparing vascular tissue scaffolds that display features of the natural cellular environment whilst mimicking the bulk architecture; together mirroring the essential building blocks for functional vasculature.

### **1.3. Stem Cells in Tissue Regeneration**

#### **1.3.1. Vascular Regeneration**

Stem cell therapy promises to revolutionize the treatment of vascular diseases with the potential to regenerate vascular tissues *in vitro* or *in vivo* (Krawiec, 2012). Mesenchymal stem cells (MSCs) are multipotent cells capable of differentiating into several tissues including vascular phenotypes, can be easily obtained and are rapidly expandable *in vitro*, thereby providing several advantages for their utility in vascular tissue regeneration (Kan, 2005). There is growing evidence that MSCs reside in a perivascular niche which is thought to interact largely with vascular signals *in vivo* and may play a significant role in local tissue regeneration and homeostasis of the vasculature (da Silva Meirelles, 2008). Further, a recent study developed a protocol to produce functional vascular SMCs from induced pluripotent stem cells (iPSCs) via an MSC intermediate (Bajpai, 2012). The iPSC-derived MSC were found to be both highly proliferative and capable of differentiating into highly contractile SMCs. The preceding citations lend credibility to the hypothesis that MSCs represent a potent cell source for the regeneration of highly specific and functional vascular tissues.

However, despite significant progress in regenerating vascular tissues using MSCs and other stem cells, there are still considerable challenges associated with the production of vascular phenotypes with high cell specificity, maturity and

functional behavior. The vascular niche constitutes a complex microenvironment which conveys a variety of signals, eliciting specific biological responses and maintaining tissue function and homeostasis. Further resolution of the mechanisms and environmental signaling which regulate MSC differentiation towards vascular phenotypes has profound implications towards cell-based vascular tissue engineering and regeneration.

#### 1.4. Microenvironmental Cues Direct Stem Cell Fate Decisions

There is abundant evidence to suggest that local signals from the tissue specific ECM microenvironments, through cell-ligand, cell-molecule or cell-matrix activation, significantly affect MSC differentiation and mature phenotype expression (Reilly, 2010; Suzuki, 2010; Engler, 2006) (Fig. 1). Substrate physical properties such as elasticity (Engler, 2006; Discher, 2005) and geometry (Cukierman, 2001; Huebsch, 2010) have been implicated to strongly influence MSC differentiation. Our

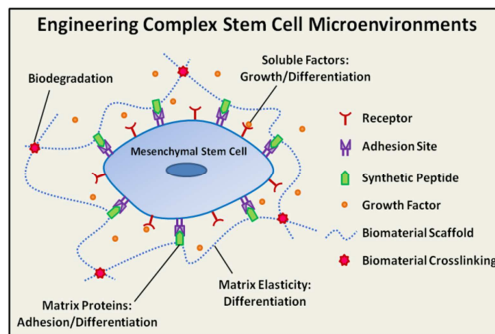


**Figure 1 - 1.** The ECM microenvironment confers a variety of physical and chemical cues which direct MSC growth, adhesion and differentiation.

group has previously demonstrated that 3D nanofibrous PEG gel substrates with elasticity that mimics the natural vascular stiffness ( $E = 8$  to  $15$  kPa) can direct MSC differentiation

toward vascular phenotypes within 24 hours (Wingate, 2012). Besides substrate physical properties, MSC differentiation and phenotype commitment are also greatly influenced by matrix chemical markers such as growth factors or matrix chemistry.

Together, these signals impart an instructional environment whereby MSC behavior and differentiation are directed in a highly specific manner. However, successful recreation of this complex milieu which directs MSCs to vascular phenotypes in vitro as well as the underlying mechanisms governing these events is still widely unknown. A biomimetic approach, incorporating several environmental signals, such as cell-matrix and cell-biomolecule interactions, will help to establish more robust and specific MSC differentiation protocols.

#### **1.4.1. Biological Ligands Instruct Stem Cell Differentiation**

Cell-matrix and cell-biomolecule interactions play a critical role in diversity of biological events including cell adhesion, growth, differentiation, and apoptosis (Discher, 2009; Kuraitis, 2012). Growing evidence shows that MSCs acquire tissue-specific characteristics when co-cultured with mature cells types or exposed to preformed biological matrices in vitro and that this instructive differentiation is elicited by the specific signals of the microenvironment (Philp, 2005). However, matrix and soluble factor (SF) signals are often observed independently to differentiate cells on 2D substrates, an environment vastly different from the way cells are presented naturally in vivo, i.e. a 3D tissue context which elicits multiple signal inputs to regulate cell fate. It is likely that crosstalk of these environmental factors on intracellular signaling molecules may be required to direct MSC differentiation toward desired cell type and function. Several reports have focused on the influence of different matrix signals such as ECM proteins, ECM-derived peptides and SFs on regulating MSC differentiation to vascular lineages (Table 1). A recent report demonstrated the potential of small peptides incorporated into 2D rigid substrates to guide MSC differentiation towards osteogenic or adipogenic lineages respectively (Frith, 2012). However, while this study provides insight into small peptide directed MSC differentiation; systematic studies of tailored peptides to instruct MSC differentiation to vascular phenotypes on soft 3D substrates are absent.

#### **1.4.2. Soluble Factors as Critical Signals for MSC Differentiation**

Recent evidence suggests that precise, complex SF regimens can result in highly specific and mature VSMCs from iPSCs (Lachaud, 2013; El-Mounayri, 2013). However, these protocols are often time consuming, utilizing multiple factors and requiring weeks to reach maturity. Studying the activity of early cell signaling events in the presence of SFs may help to refine current factor protocols. Several pathways mediating SF effects on VSMC differentiation from iPSCs have also been revealed recently. Though largely unexplored, the potential crosstalk sites between signaling induced by matrix adhesion and chemical signaling for vascular morphogenesis include ERK, AKT, RhoA or JNK (Discher, 2009; Martino, 2009; Park, 2011). Reports suggest inhibition of ERK activation in MSCs induces spontaneous VSMC differentiation, whereas RhoA mediating TGF- $\beta$  signaling transduction or integrin mechanotransduction signaling leads to Smad activation for VSMC differentiation (Han, 2011). Despite considerable progress towards mechano-chemical signaling phenomena during cellular processes, questions remain as to how these mechanisms direct early instruction of MSC differentiation. Further, systematic studies evaluating the effect of growth factor regimens on early MSC differentiation processes is yet to be explored.

**Table 1. Effect of Various Matrix Signals on hMSC Growth & Differentiation**

<b>Matrix Signal</b>	<b>Outcome</b>	
<u>ECM Protein</u>		
Collagen I	↑ SMC markers <sup>19</sup>	(Gong, 2008)
Collagen IV	↑growth, ↑ SMC markers <sup>19</sup>	(Gong, 2008)
Elastin	↑ Osteogenic markers	(Gong, 2008)
Laminin	↑ SMC markers <sup>9</sup>	(Suzuki, 2013)
Fibronectin	↑ SMC markers <sup>19</sup>	(Gong, 2009)
<u>Engineered Peptide</u>		
RGD	↑Viability <sup>20</sup> , ↑adhesion <sup>21</sup>	(Nuttelman, 2005; Hersel, 2003)
IKVAV	↑Osteogenic markers <sup>18</sup>	(Frith, 2012)
GKDGEA	↑Osteogenic markers <sup>18</sup>	(Frith, 2012)
YGISR	↑Adipogenic markers <sup>18</sup>	(Frith, 2012)
VAPGVG	↑ Osteogenic markers <sup>18</sup>	(Frith, 2012)
<u>Soluble Factor</u>		
TGF- $\beta$ 1	↓ Proliferation <sup>22</sup> ↑ SMC differentiation <sup>22</sup>	(Narita, 2008)
PDGF	↑ Proliferation <sup>19,23</sup> ↓ SMC differentiation <sup>23</sup>	(Gong, 2008; Vazao, 2011)
bFGF	↑ Proliferation <sup>24</sup> ↓ SMC differentiation <sup>19,24</sup>	(Gong, 2008; Han, 2010)
Ascorbic Acid (AA)	↑ Proliferation <sup>22</sup> ↑ SMC differentiation <sup>22</sup>	(Narita, 2008)

## **1.5. Biomimetic Scaffolds for Stem Cells**

### **1.5.1. Scaffold Requirements**

The design of 3D tissue scaffolds is essential to the success of an engineered tissue in order to permit cell adhesion, proliferation, differentiation, permeability for nutrients as well as structural support for tissue growth (Langer, 1993). To achieve this, a scaffold should include several criteria such as suitable porosity, pore size, permeability for nutrients, material biocompatibility and degradation, whilst mirroring the mechanical behavior of the intended tissue (Chua, 2001; Stevens, 2010). Ideally, a scaffold with high porosity improves cell infiltration as well nutrient diffusion. However, scaffold physical properties, such as porosity and cell geometry, influence the mechanical behavior of such constructs (Gibson, 1982). In this regard, a careful balance between mechanical function and elicited biological response must be considered when designing a tissue scaffold. Particularly with biodegradable polymers, as the material degrades mechanical properties diminish; thereby presenting the necessity to prepare scaffolds that maintain the required support for tissue growth before degradation. This concept is particularly significant for load bearing tissues, such as bone or vasculature, which provides appropriate mechanical properties due in part to its unique architecture and internal anisotropy (Fratzl, 2007).

### **1.5.2. Material Selection**

Material properties, such as chemistry, surface properties, and biocompatibility, are significant factors that must be considered when preparing a tissue scaffold. In particular, when a material is implanted within the body a cascade of chemical signaling is initiated as the body recognizes the material as “foreign”. Most notably these events are recognized by local inflammation and the formation of a fibrous capsule encasing the foreign material. In tissue engineering, the encouragement of

tissue infiltration and tolerance of the foreign material are necessary to encourage new tissue formation. By adjusting the properties of the material utilized, the body's response to foreign materials can be controlled such that cells can proliferate and infiltrate.

#### **1.5.2.1. Synthetic Polymers**

Synthetic polymers offer several advantages as materials for developing tissue engineering scaffolds including the ability to tailor mechanical properties and degradation kinetics to meet various applications. Specifically, synthetic polymers are attractive because they can be fabricated into various shapes with desired morphologies and features which can be permissive for cell maintenance and in-growth (Gunatillake, 2003). For example, synthetic polymers can be produced reproducibly with specific molecular weights, block structures, degradable moieties, and crosslinking mechanisms. These properties in turn, govern material formation dynamics, crosslinking density, and material mechanical and degradation properties. PEO and poly(ethylene glycol) (PEG) are hydrophilic polymers that can be photocrosslinked by modifying each end of the polymer with either acrylates or methacrylates (Cruise, 1998; West, 1999; Mann, 2001). Hydrogels can then be prepared when the modified PEO or PEG is mixed with the appropriate photoinitiator and crosslinked via UV exposure (West, 1999; Bryant, 2001). Synthetic hydrogels are often attractive materials for their inert properties since they lack cell adhesion receptors and proteins often do not readily adsorb to them. Specifically, PEG has been used to prevent post-operative adhesions (West, 1996) and to prevent intimal thickening of arteries after damage (West, 1996). However, while synthetic materials are attractive for their cost, reproducible fabrication and facile manufacturing, their lack of cell-recognition sites as well as potential for toxic degradation products causing undesirable inflammation are often disadvantageous (Seo, 2013).

#### **1.5.2.1. Natural Polymers**

In nature, fibrous proteins represent the foundation for mechanically robust structures (i.e. collagen fibrils), provide recognition sites for cell binding and

hierarchical organization, as well as providing anchoring sites for other extracellular matrix components. Among naturally derived fibrous proteins, silk fibroin, the primary structural protein of natural Bombyx Mori silk fibers, is a natural polymer that has been studied extensively for tissue engineering applications in part to its excellent mechanical properties, biocompatibility, and controllable degradation rate. Silk proteins have found significant utility in biomedicine due to their high biocompatibility, tunable biodegradability and material format versatility. Perhaps its earliest biomaterial rendition, natural silk fibers have been employed as sutures for wound ligation for centuries (Moy, 1991). Wound dressings have also been prepared using pure silk electrospun nets (Schneider, 2009) or with silk blends of PEG (Kweon, 2008) or carboxymethyl keratin (Lee, 1999), demonstrating improved inflammation response and wound healing kinetics. Silk fibroin coatings are also attractive for implant materials. Improved adhesion of human fibroblasts has been reported on silk fibroin coated polyurethane (Petriani, 2001) and polycarbonate (Chiarini, 2003) surfaces. Other adaptations of silk fibroin implant technologies include anterior cruciate ligament (ACL) reconstruction (Altman, 2002) knee meniscus repair (Mandal, 2011) and nerve guidance conduits (Yang, 2007).

### **1.5.3. Fabrication Techniques**

A number of techniques to prepare tissue scaffolds have been described by previous authors such as porogen leaching, thermally induced phase separation, gas foaming, electrospinning and 3D printing among (Chua, 2001; Stevens, 2010). Each method has advantages and disadvantages over others in regard to fabrication time, reproducibility and employed solvents. Moreover, the ability to tune scaffolds at specific length scales is also dependent on the method utilized. At the cellular level, cells interact with a plethora of structures, from matrix proteins to adjacent cells. The organization and size of such structures can guide cells to form functional groups which are the building blocks of macroscopic tissue. Electrospinning polymer nets can produce nanofibers which resemble the shape and size of matrix proteins (Wingate, 2012, Bonani 2012). It is speculated that the likeness of the nanofibers with natural ECM proteins enhances cell activity. One limitation, however, of

nanofibers meshes is the absence of macroscopic structures which support porosity and interconnectivity, severely limiting cell infiltration and nutrient diffusion.

Recent studies have highlighted the importance of 3-dimensional, fibrous matrices to optimize stem cell niche environments (Carlson, 2012; Lim, 2009). One potential solution is the use of hydrogels which present both a fibrous microstructure reminiscent of the natural ECM combined with excellent nutrient diffusion. Hydrogels are networks of polymer chains that are stabilized either by chemical or physical crosslinking and dispersed throughout an immobilized water phase. The stability of the polymer network allows for the penetration and uptake of water (swelling) without dissolving, thus lending itself to a variety of attractive and practical applications. Hydrogels have become excellent material candidates for a wide selection of biomedical applications because of their high water content (allowing for efficient transport of biological molecules), improved biocompatibility and innate similarity to the physiochemical nature of natural tissues (Drury, 2003; Peppas, 2006).

## **1.6. Tailoring Microenvironments to Control Stem Cell Fate**

### **1.6.1. Current State of the Art**

There has been a considerable drive in recent years to develop engineered microenvironments which capture the complex SC niche found *in vivo*. The previous sections discussed how both physical and biological cues can individually direct stem cell fate processes. However, it is difficult to achieve tailored differentiation of stem cells with regard to both the efficiency of stem cell differentiation into desired lineages as well as mature tissue functionality merely from the introduction of limited signals (i.e. simple growth factor regimens or non-specific physical cues). The culmination of such signals is likely to drive the future for complex SC differentiation protocols and specificity. Several reports have attempted to elucidate the synergistic roles of combined bio-physical cues, such as substrate elasticity and biological factor, in stem cell fate processes (Table 2). One of the earlier studies performed by Park et al. elucidated the importance of the synergy involved between substrate elasticity and growth factor TGF $\beta$ -1 to instruct specific MSC differentiation (Park,

2011). Here it was found that substrate elasticity could invoke different SC fate commitments in the presence of growth factor which alone was not sufficient. Expanding on this theory, Wingate et al. combined VEGF administration with a soft, three-dimensional substrate optimally designed for endothelial cells (ECs). The authors reported that the substrate combined with growth factor were significantly more effective at directing stem cell fate towards EC lineage than growth factor alone (Wingate, 2014). The two preceding citations provide compelling evidence that a synergistic role of individual environmental factors can assist in the MSC differentiation process. Challenges in the future will be in the discovery of multiple signal effectiveness for specific SC lineage commitment as well as platforms designed for end-user tunability.

**Table 2. Review of Biomaterials for Stem Cell Differentiation by Variable**

Year	Material	Geometry	Elasticity	Biological Ligand	Soluble Factor	Ref
2006		2D planer	soft	-	-	Engler, 2006
2008	PGA mesh	3D scaffold	stiff	ECM proteins	Various	Gong, 2008
2010	PEGDM Gel	3D gel	soft	RGD	-	Huebsch, 2010
2011	Collagen I/PA gel	2D planer	soft	-	TGF- $\beta$ 1	Park, 2011
2012	PS-PEO copolymer	2D planer	stiff	engineered peptides	-	Frith, 2012
2012	PEGDM Nanofiber Gel	3D nanofibers	soft	-	-	Wingate, 2012
2013	Pegylated-Fibrin Gel	2D/3D gel	soft	-	TGF- $\beta$ 1	Stowers, 2013
2014	PEGDM Nanofiber Gel	3D nanofibers	soft	-	VEGF	Wingate, 2014

### 1.6.2. Systemic Approaches to Multivariate Studies

High through-put approaches have emerged in recent years to circumvent the limitations of traditional low through-put techniques (i.e. conventional cultureware), with the promise to develop complex platforms for combined biomolecule/substrate discovery. An early example of such technology, Flaim et al. developed an ECM microarray to investigate the role of specific proteins on SC differentiation (Flaim, 2005). By spotting proteins onto acrylamide coated slides, the authors presented 32 different protein conditions in the form of discrete protein dots on the order of 200 $\mu$ m. The technology was reproducible and capable of producing multiple microarrays with significantly less protein requirement than traditional methods. The authors investigated the influence of the different protein conditions in the presence of both primary hepatocytes and mouse embryonic SCs. Interrogation of the respective cell

lines indicated several protein combinations which either maintained hepatocyte function or persuaded SC differentiation. While this report lends strong credibility to high through-put techniques, the incorporation of multiple signals within designed microarrays has proven to be a challenge within the field. An approach developed by Gobaa et al. has proven an important step as it provides the opportunity to analyze a greater number of variables and more rapidly than previous attempts (Gobaa, 2011). In particular, the authors designed individual hydrogel microwells, with both modular stiffness as well as variable protein composition. This report represents a paradigm shift in study of SC differentiation events from the traditional methods of single specimen culture ware to the sample robust high through-put capabilities. The development of complex high through-put platforms to investigate SC differentiation with combinatorial signaling will likely prove instrumental towards the design of future biomaterial platforms.

### **1.6.3. Translational Methods to Integrate Complex Stem Cell Environments**

Integration of complex cellular signaling environments into biomaterial scaffolds presents a considerable challenge to the tissue engineering community (Kim, 2012). Protein materials represent an interesting platform as they often mimic the organization found in natural tissues as well as impart improved biological responses (Kim, 2012). We have found that silk proteins offer tremendous advantage as substrate platforms for scaffolds and vascular grafts due to its excellent mechanical properties, biocompatibility, controllable degradation rate, and mild inflammatory response in vivo (Murphy, 2009; Motta, 2012). Previously, we have developed a novel technique to produce silk hydrogels with tunable elasticity using the green solvent carbon dioxide (CO<sub>2</sub>) (Floren, 2012). Due to its tunable elasticity approaching vascular tissues ( $E = 10\text{-}30$  kPa), combined with clean fabrication, we propose to use this matrix as a next-generation platform that integrates vascular niches for MSCs to be used in vascular tissue engineering. The production of tunable vascular graft materials, comprised of compatible biomaterials, and further

specialized with engineered vascular niche environments will be of considerable value to the research community.

## **1.7. Significance & Motivation for this Research**

While there have been several important contributions in the literature that elucidate stem cell differentiation events associated with microenvironment discovery and design, there is still much uncertainty surrounding specific and controlled stem cell fate decisions. There is a growing consensus among the scientific community that recapitulation of the complex stem cell niche environment can lead to more robust and controlled stem cell differentiation processes and maintenance. Our interest in vascular regeneration prompted us to adopt a holistic approach to capture the complex vascular niche environment. We aim to engineer complex vascular niche environments by 1) resolving the mechanisms associated with MSC-matrix interactions, 2) establish simple, precise SF regimen protocols into these complex environments and 3) translate these optimized vascular niches to well established biomaterial platforms. Successful completion of this project will provide fundamental understanding of the effects of physiological stimuli on vascular differentiation of MSC in terms of the specificity and maturity of the final differentiated cells. Better understanding of such mechanisms will prove paramount in the sequential stages of MSC differentiation to vascular cells. Additionally, the results will help to better define the process of regenerating functional healthy vascular tissue from MSCs. In summary, a combinatorial approach investigating the effects of matrix elasticity, biological ligands and growth factors on MSC differentiation in a 3D nanofiber culture will be critical towards understanding and recapitulating MSC differentiation in the in vivo vascular environment.

## **Chapter II**

### **Specific Objectives**

#### **2.1. *Introduction***

The main objective of this thesis is to engineer and instruct specific and mature vascular differentiation from MSCs by way of highly tailored matrices mimicking the natural vascular niche environment. Taking inspiration from natural organization, we propose that a biomimetic approach to vascular tissue scaffolds that display features of the natural cellular microenvironment whilst mimicking the bulk tissue properties may elicit highly specific differentiation of MSCs to vascular phenotypes. Previous work in our laboratory suggests a holistic approach for directing MSC differentiation to vascular phenotypes, encompassing the combined effects of matrix rigidity, growth factor presentation and synthetic peptides, to enhance the vascular differentiation of MSCs (Wingate, 2012; Wingate, 2014). To this aim, we hypothesize that the convergence of several mechanochemical cues may recapitulate the complex vascular niche compulsory to instruct MSC differentiation into mature vascular tissues and enabling functional vascular regeneration *in vitro*. To validate our hypothesis, we will take a novel approach by resolving the mechanisms ascribed to MSC differentiation towards VSMCs in a systematic approach, i.e. stiffness, biological ligands and chemical factors, to augment vascular

phenotype expression and functionality, via relevant biomaterial scaffolds. We expand on these aims as follows:

## **2.2. Aims of this Thesis**

### **2.2.1. Aim 1**

The first objective of this thesis was to develop tunable hydrogel systems based on the natural polymer silk fibroin. Silk fibroin (SF), a natural protein extracted from *Bombyx mori* silkworms, is an attractive material for tissue engineering due to its excellent mechanical properties, biocompatibility, tunable degradation rate, and mild inflammatory response in vivo [Wang, 2008]. A diversity of regenerative tissues has been reported using SF-based constructs including bone [Meinel, 2005; Fini, 2005], cartilage (Wang, 2010), vascular (Soffer, 2008; Bondar, 2008; Bonani, 2011), skin (Unger, 2004), nervous (Yang, 2007), hepatic (Gotoh, 2004) and ocular (Lawrence, 2009) amongst others (Kundu, 2013). In light of these reports, the future and relevance of silk biomaterials for therapies catered to the biomedical community are believed to be great (Motta, 2012).

Hydrogels have become excellent material candidates for a wide selection of biomedical applications because of their high water content (allowing for efficient transport of biological molecules), improved biocompatibility and innate similarity to the physiochemical nature of natural tissues (Drury, 2003; Peppas, 2006). Recently, porous natural-based hydrogels have been chemically crosslinked under high pressure CO<sub>2</sub> without the necessity for surfactants or co-solvents (Partap, 2006; Annabi, 2009; Annabi, 2010). Hydrogels produced using high pressure CO<sub>2</sub> generally exhibit greater porosity and improved crosslinking, resulting in improved gel stiffness as well as an enhanced capacity to support cell and tissue infiltration (Annabi, 2010). The potential of CO<sub>2</sub> to induce silk protein gelation without the need for extensive chemical processes, circumventing complex materials fabrication protocols and avoiding complications to biological systems, would presumably be of considerable value to the biomaterials community.

Here, for the first time, we present a novel technique for the preparation of silk hydrogels directly from high pressure CO<sub>2</sub> environments without the need for crosslinking agents or additional additives such as surfactants or co-solvents.

Through this novel method, we demonstrate the utility of CO<sub>2</sub> as a volatile electrolyte, capable of sufficiently influencing the sol-gel transition of silk proteins, resulting in the formation of stable hydrogels with properties suitable for biomedical applications. The influence of CO<sub>2</sub> pressure, silk protein concentration and processing time were investigated in regard to the gelation kinetics, physical and mechanical properties of the prepared gels (Chapter III).

### **2.2.2. Aim 2**

The second objective of this thesis was to study the influence of growth factor (TGF- $\beta$ 1) combined with silk fibroin hydrogels of varying stiffness, as prepared in Aim 1, on the differentiation of MSCs into a mature SMC phenotype.

Cell interactions with the local microenvironment are recognized in several important biological events including cell adhesion, growth, differentiation, and apoptosis [5, 6]. In particular, substrate biophysical properties such as rigidity (Engler, 2006; Discher, 2005), geometry (Cukierman, 2001; Huebsch, 2010) biological ligand (Suzuki, 2010; Gong, 2008), soluble factor (Narita, 2008), or combination thereof (Wingate, 2014) have been revealed to influence MSC differentiation events. However, integration of complex cellular signaling environments into biomaterial scaffolds presents a considerable challenge to the tissue engineering community (Kim, 2012). We previously developed a technique to produce porous, SF hydrogels with tunable stiffness and morphology using the green solvent, carbon dioxide (CO<sub>2</sub>), see Aim 1. Hydrogel elastic moduli approaching soft tissues ( $E = 6\text{-}30$  kPa), combined with ease of fabrication and biocompatibility, motivated us to use these SF materials as a platform to instruct stem cell differentiation towards the vascular smooth muscle cell (SMC) lineage in a precise manner.

We hypothesized that suitable soluble factor regimen and matrix rigidity can instruct MSC differentiation towards more mature, functional vSMCs. In the present study, we address cellular differentiation on tunable SF hydrogels prepared from a solvent-free CO<sub>2</sub> processing method. The transforming growth factor  $\beta$  (TGF- $\beta$ ) family is a potent regulator of several cell functions such as proliferation, spreading (Derynck, 1997) and is strongly associated with vascular smooth muscle cell (vSMC)

differentiation of stem cells (Narita, 2008). Therefore, the focus of this objective is on exploiting the combined use of substrate stiffness and growth factor (TGF- $\beta$ 1) on SF matrices, with the aim of correlating the effects on the vascular commitment of human mesenchymal stem cells (hMSCs).

### **2.2.3. Aim 3**

Despite accumulated knowledge regarding individual and combined roles of various mechanochemical ECM signals in stem cell activities, the intricacy exhibited by cellular microenvironments poses a considerable challenge in resolving the mechanisms ascribed to stem cell behavior and fate determination processes. This complexity mandates a systemic approach whereby integrative studies must be expanded to capture a more comprehensive understanding of the determinants which direct stem cell differentiation toward desired cell type and function.

High through-put approaches have emerged in recent years to circumvent the limitations of traditional low through-put techniques (i.e. conventional cultureware), with the promise to develop complex platforms for combined biomolecule/substrate discovery. However, despite the versatility afforded by current microarray technologies, the incorporation of multiple signals within engineered microarrays remain limited. Meanwhile the integration of current combinatorial microarray technologies in three-dimensions, coupled with other biophysical properties, such as tunable stiffness and geometry, have yet to reach fruition.

For this objective, we postulated that the presentation of ECM proteins on 3D matrices with tunable stiffness will augment the differentiation of MSCs to vascular lineages. To address this, we established a high-throughput ECM platform based on soft, fibrous matrices meanwhile highly-tunable in elasticity and 3-dimensional geometry. The technology we demonstrate here is amenable to manipulation of several matrix properties, such as elasticity and geometry, in concert with customizable ECM protein micro-dot combination. Altogether, we demonstrate the practical adaptation of high-throughput technology to facilitate the screening of various tunable mechano-ligand microenvironments in three dimensions with the aim to optimize stem cell fate decisions.

#### **2.2.4. Aim 4**

Stem cell (SC) therapy promises to revolutionize the treatment of various diseases with the potential to regenerate functional tissues *in vitro* or *in vivo*. Several recent studies have demonstrated that cellular microenvironments such as ligand-activated cell-matrix interactions and/or matrix physical properties such as elasticity and geometry have significant role in directing the differentiation processes in stem cells (Lutolf, 2009; Wingate, 2012). Microarrays have emerged as an important tool for studying stem cell processes in a high-throughput manner (Gupta, 2010; Gobba, 2011). Nevertheless, most of the existing ECM arrays being either 2-D or shallow 3-D are not able to capture the effects of biophysical and chemical cues on stem-cell fate completely.

Here we hypothesize that the integration of ECM-derived small engineered peptides into 3D soft matrices may refine the differentiation of MSCs to vascular phenotypes, and further successfully recapitulate the complex vascular niche necessary for specific and efficient MSC differentiation into vascular lineages. In line with this, we report the development of a microarray platform based on electrospun nanofibrous hydrogels of photoclickable thiol-ene poly(ethylene glycol) (PEG) hydrogels. Thiol-ene polymerizations proceed by an orthogonal, step-growth mechanism where one thiol reacts with one ene leading to a highly homogenous distribution in crosslinks, thus imparting tunable substrate stiffness with high fidelity (Hoyle, 2010). Furthermore, it allows for the subsequent covalent post-modification of PEG thiol-ene hydrogel substrates with small engineered peptides with high reactivity and specificity. Taken together, the manipulation of the matrix properties, such as stiffness and geometry, in concert with engineered peptides will facilitate the interrogation of multiple and distinct SC microenvironments. To this end, we demonstrate the potential application of this high-throughput technology for screening of a variety of engineered 3D microenvironments for stem cell fate optimization.

## Chapter III

# Carbon Dioxide Induced Silk Protein Gelation for Biomedical Applications

*Part of this chapter has been published in:*

Michael L. Floren, Sara Spilimbergo, Antonella Motta, Claudio Migliaresi. "Carbon Dioxide Induced Silk Protein Gelation for Biomedical Applications". *Biomacromolecules*, 13 (2012) 2060-2072.

**Abstract:** We present a novel method to fabricate silk fibroin hydrogels using high pressure carbon dioxide (CO<sub>2</sub>) as a volatile acid without the need for chemical crosslinking agents or surfactants. The simple and efficient recovery of CO<sub>2</sub> post processing results in a remarkably clean production method offering tremendous benefit towards materials processing for biomedical applications. Further, with this novel technique we reveal that silk protein gelation can be considerably expedited under high pressure CO<sub>2</sub> with the formation of extensive  $\beta$ -sheet structures and stable hydrogels at processing times less than 2 hours. We report a significant influence of the high pressure CO<sub>2</sub> processing environment on silk hydrogel physical properties such as porosity, sample homogeneity, swelling behavior and compressive properties. Microstructural analysis revealed improved porosity and homogenous composition amongst high pressure CO<sub>2</sub> specimens in comparison to

the less porous and heterogeneous structures of the citric acid control gels. The swelling ratios of silk hydrogels prepared under high pressure CO<sub>2</sub> were significantly reduced compared to the citric acid control gels, which we attribute to enhanced physical crosslinking. Mechanical properties were found to increase significantly for the silk hydrogels prepared under high pressure CO<sub>2</sub>, with a 2 and 3 fold increase in the compressive modulus of the 2 and 4 wt% silk hydrogels over the control gels, respectively. We adopted a semi-empirical theoretical model to elucidate the mechanism of silk protein gelation demonstrated here. Mechanistically, the rate of silk protein gelation is believed to be a function of the kinetics of solution acidification from absorbed CO<sub>2</sub> and potentially accelerated by high pressure effects. The attractive features of the method described here include the acceleration of stable silk hydrogel formation, free of residual mineral acids or chemical crosslinkers, reducing processing complexity, and avoiding adverse biological responses, whilst providing direct manipulation of hydrogel physical properties for tailoring toward specific biomedical applications.

### **3.1. Introduction**

Hydrogels are networks of polymer chains that are stabilized either by chemical or physical crosslinking and dispersed throughout an immobilized water phase. The stability of the polymer network allows for the penetration and uptake of water (swelling) without dissolving, thus lending itself to a variety of attractive and practical applications. Hydrogels have become excellent material candidates for a wide selection of biomedical applications because of their high water content (allowing for efficient transport of biological molecules), improved biocompatibility and innate similarity to the physiochemical nature of natural tissues (Drury, 2003; Peppas, 2006).

Much of the performance of hydrogels depends on the selection of the appropriate material to address the necessary design prerequisites. Synthetic polymers are widely chosen for hydrogel fabrication as their properties can be precisely controlled whilst being readily reproducible (Drury, 2003); by comparison, hydrogels prepared from naturally derived sources generally lack versatility in tunable chemistries and reproducibility when compared to their synthetic

counterparts. However, despite these limitations, natural polymers generally present improved biocompatibility and cellular interactivity, thereby enhancing their utility in the fabrication of biomaterials (Lee, 2001).

Among naturally derived proteins, silk fibroin, the primary structural protein of *Bombyx mori* (mulberry silkworm) silk fibers, is a natural polymer that has been studied extensively for biomedical applications due to its excellent mechanical properties, biocompatibility, and controllable degradation rate (Altman, 2003). The high content of hydrophobic domains in silk proteins allows for the self-assembly and formation of strong intra- and intermolecular  $\beta$ -sheet structures, providing the basis for the exceptional strength observed in natural silk fibers (Bini, 2004). The combination of the impressive mechanical performance in its natural form as well as excellent biocompatibility and controllable degradation highlights silk fibroin as an ideal biomaterial candidate meeting several therapeutic requirements. Silk proteins have been fashioned into several material formats such as films (Servoli, 2005; Motta, 2002; Motta, 2011), sponges (Nazarov, 2004; Kim, 2005; Li, 2001), fibrous networks (nano and micrometric) (Unger, 2004; Bondar, 2008; Silva, 2008; Kim, 2003; Jin, 2002), microspheres (Wang, 2007), and hydrogels (Ayub, 1993; Kim, 2004; Wang, 2008; Motta, 2004; Silva, 2008; Fini, 2005; Zhang, 2011). Remarkable progress has been reported toward the application of silk hydrogels for tissue engineering and drug delivery therapies. Fini et al. demonstrated the healing of confined critical-sized cancellous defects in the femoral condyles of New Zealand rabbits using injectable silk hydrogels (Fini, 2005). Silk hydrogels have also found value as drug delivery vehicles. Zhang et al. combined sonicated silk hydrogels with vascular endothelial growth factor (VEGF) and bone morphogenetic protein 2 (BMP-2) to successfully palliate defects in the rabbit maxillary sinus floor (Zhang, 2011). In light of these advances, the future and relevance of silk hydrogels for therapies catered to the biomedical community are believed to be great (Motta, 2012).

The mechanism of silk fibroin gelation occurs primarily through the encouragement of macromolecular interactions from the hydrophobic side chains, initiating hydrogen bonding and resulting in physical crosslinking of the silk proteins (Ayub, 1993). Aqueous solutions of silk fibroin with ample protein concentration (>25 wt%) can form hydrogels directly through protein self-assembly, resulting in physical

crosslinking and a stabilized hydrogel network. Conversely, at modest protein concentrations (<5 wt%) gelation is particularly time expensive, requiring days to reach complete gel formation. The sol-gel transition of aqueous silk fibroin solutions can be improved through the manipulation of the physicochemical environment such as protein concentration, temperature, ionic strength, low pH, or, alternatively, by physical methods such as sonication, shear vortexing and electrogelation (Ayub, 1993; Kim, 2004; Wang, 2008; Motta, 2004; Silva, 2008; Fini, 2005; Zhang, 2011; Motta, 2012; Matsumoto, 2006; Hanawa, 1995; Yucel, 2009; Servoli, 2008). For instance, reports have demonstrated a significant reduction in gelation time, from days to a matter of hours, at reduced solution pH near to the isoelectric point of silk fibroin (pH = 3.8-4.0) (Ayub, 1993; Matsumoto, 2006; Hanawa, 1995). However, the addition of solution electrolytes at non-physiological concentrations, such as mineral acids or metal ions, may have unfavorable effects on cellular activity and function when placed in a living subject; therefore, ideally the fabrication of such materials should proceed without the necessity for chemical processes.

High pressure carbon dioxide (CO<sub>2</sub>) has emerged in recent years as an environmentally benign alternative to conventional organic solvents commonly employed for fashioning various biomaterials, such as facilitating porosity in tissue scaffolds as well as processing materials with thermally sensitive therapeutic agents (proteins) (Kazarian, 2000; Howdle, 2001; Floren, 2011). Recently, porous natural-based hydrogels have been chemically crosslinked under high pressure CO<sub>2</sub> without the necessity for surfactants or co-solvents (Partap, 2006; Annabi, 2009; Annabi, 2010). Hydrogels produced using high pressure CO<sub>2</sub> generally exhibit greater porosity and improved crosslinking, resulting in improved gel stiffness as well as an enhanced capacity to support cell and tissue infiltration (Annabi, 2010). Nonetheless, although these improvements are significant, it is important to note that residual crosslinking agents not recovered after processing or released during material degradation may result in adverse effects to biological systems (Jayakrishnan, 1996).

An alternative approach involves directly employing CO<sub>2</sub> as a volatile electrolyte to invoke changes in the physicochemical environment, influencing the sol-gel transition of proteins and the formation of stable gel networks. Carbon

dioxide has been used extensively as a volatile electrolyte for the controlled isoelectric precipitation of food proteins such as soy and casein (Hofland, 2000; Hofland, 1999). Volatile acids are advantageous to conventional mineral acid processing, such as sulfuric and hydrochloric acids which are frequently employed by conventional precipitation processes, as their high volatility in atmospheric conditions allows for their efficient recovery (Thiering, 2001). Additionally, unlike conventional mineral acids, solution pH can be maintained simply by tuning the electrolyte solubility within solution, which here is a function of pressure and temperature. Appreciable pH drops of aqueous solutions have been reported at modest fractions of dissolved CO<sub>2</sub> (Bortoluzzi, 2011). Li et al. reported the pH of CO<sub>2</sub>-H<sub>2</sub>O systems approaching 4 at modest pressures (5 bar) (Li, 2007). The slow, homogenous acidification of aqueous solutions by CO<sub>2</sub> has generally been reported to improve the precipitation and recovery of proteins or molecules which exhibit sensitivity to extreme drops in pH (Thiering, 2001). Thus, the ability to experience considerable drops in solution pH at relatively low fractions of absorbed CO<sub>2</sub> permits its utility as a viable alternative to conventional mineral acids. The potential of CO<sub>2</sub> to induce silk protein gelation without the need for extensive chemical processes, circumventing complex materials fabrication protocols and avoiding complications to biological systems, would presumably be of considerable value to the biomaterials community.

Here, for the first time, we present a novel technique for the preparation of silk hydrogels directly from high pressure CO<sub>2</sub> environments without the need for crosslinking agents or additional additives such as surfactants or co-solvents. Through this novel method, we demonstrate the utility of CO<sub>2</sub> as a volatile electrolyte, capable of sufficiently influencing the sol-gel transition of silk proteins, resulting in the formation of stable hydrogels with properties suitable for biomedical applications. The influence of CO<sub>2</sub> pressure, silk protein concentration and processing time were investigated in regard to the gelation kinetics, physical and mechanical properties of the prepared gels. Gelation time could be significantly improved depending on the processing conditions employed. Moreover, the physical and mechanical properties of silk hydrogels prepared under high pressure CO<sub>2</sub> exhibited superior qualities in comparison to the control gels prepared by

conventional acid titration. Mechanistically, reduction in solution pH by CO<sub>2</sub> absorption, governed by diffusion limitations, and potentially the high pressure environment, both influence the gelation of silk proteins as presented here. The use of high pressure CO<sub>2</sub> as a volatile electrolyte to precisely control and accelerate silk protein gelation, providing the direct tailoring of hydrogel physical properties, whilst being readily recoverable post processing, potentially offers tremendous benefit as a clean and efficient method toward silk hydrogel fabrication.

## **3.2. Materials & Methods**

### **3.2.1. Preparation of Silk Fibroin Solution**

Neat silk fibroin was obtained from cocoons of *Bombyx mori* silkworms and subsequently degummed to remove the exterior sericin proteins. Degumming was achieved by washing the extracted silk fibroin in boiling solutions of Na<sub>2</sub>CO<sub>3</sub> at 1.1 g/L and 0.4 g/L both for 1.5 hours. Fibroin solution was prepared by dissolving the obtained fibers in 9.3M LiBr (Fluka Chemicals, Buchs, Switzerland) aqueous solution (10% w/v) at 65 °C for 4 hours and filtered to eliminate impurities. Filtered fibroin solution was then placed in Slide-A-Lyzer cassette (Pierce, 3500 Da MWCO) and dialyzed against distilled water for 3 days at room temperature to remove the residual salts. Following dialysis, solution protein concentration was determined using a NanoDrop ND-1000 spectrophotometer (Delaware). Solution volume was adjusted with distilled water to reach the desired concentration, namely 2 and 4 wt%.

### **3.2.2 Fabrication of Silk Hydrogels**

#### **3.2.2.1 Atmospheric Conditions**

Silk hydrogels prepared at atmosphere using a conventional acid titration method were employed as a control gel in this study. Silk fibroin solution (2 and 4 wt%) was titrated below the isoelectric point (pH 3.8-4.0)<sup>19</sup> using a citric acid solution (0.1M) and kept at 37 °C until gelation occurred (approximately 8 hours). After gelation, silk hydrogels were placed in PBS solution and stored at 4 °C to be utilized for further analysis.

### 3.2.2.2 High Pressure Conditions

A schematic of the high pressure CO<sub>2</sub> processing protocol is detailed in Figure 1. The high pressure apparatus consisted of two configurations: a large volume steel reactor (450 ml) custom fabricated in house for the preparation of large specimens, and a smaller volume (200 ml) high pressure quartz view cell reactor (Separex, France) which allowed for direct in situ observation during processing. Vessel temperature was controlled via an internal water-jacketed heat exchanger fed from an external water bath (MPM Instruments, Italy). The high pressure CO<sub>2</sub> atmosphere was achieved via a HPLC pump (Gilson, mod 307 drive module with a maximum flow rate of 25 ml/min) set to the desired operating pressure. The high pressure vessel consisted of both a temperature and pressure transducer which allowed for accurate monitoring of both variables over the experimental times. Silk fibroin solution (5 ml) at different concentrations (2 & 4 wt%) were syringed into a 25 ml Teflon beaker (h: 35 mm, Ø 30mm) and placed into the high pressure vessel. Once the system had been sealed and thermal equilibrium established (40 °C), CO<sub>2</sub> was introduced into the vessel under various pressures, namely 5, 30, 60, 100 and 150 bar. Once pressure and temperature had reached stability, specimens were isolated and maintained at the set conditions for specific processing times (0-8 hours). Following processing, the system was depressurized slowly (approximately 30 minutes) to avoid sample rupture due to the high pressure release and maintain hydrogel integrity. Collected hydrogel specimens were immediately placed in distilled water and stored at 4 °C for future characterization.

Two sample preparations, hydrated and dry specimens, for the silk hydrogels were utilized for the measurements in this study. Hydrated samples were taken directly from the high pressure CO<sub>2</sub> apparatus and characterized without further modification for the ESEM, swelling ratio and mechanical compression measurements. To prepare dry hydrogel specimens, wet silk hydrogels were first quenching in liquid nitrogen for 5 minutes and subsequently lyophilized for 48 hours to remove water. Dry hydrogel specimens were used to perform the structural and SEM analysis.

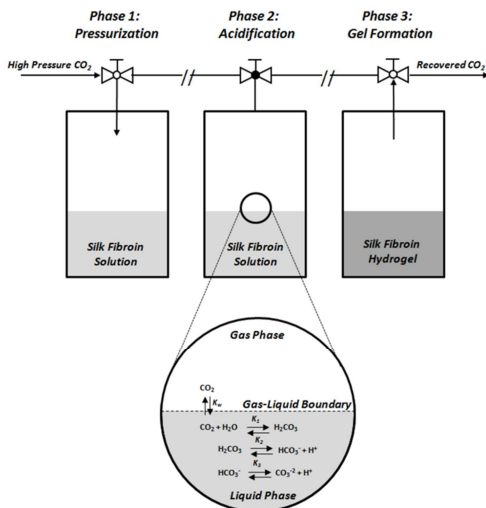


**Figure III - II.** Schematic diagram of silk gelation using high pressure CO<sub>2</sub>. Phase 1: Pressurization, Phase 2: Acidification through carbonic acid formation, Phase 3: Protein aggregation and gelation.

### 3.2.2.3 Determination of Gelation Kinetics

To establish the gelation time of silk fibroin solution under different conditions of high pressure carbon dioxide, 5 ml volumes of silk fibroin 2 and 4 wt% were pipetted into a 25 ml Teflon beaker and exposed to high pressure carbon dioxide (5-150 bar) at constant temperature 40 °C. Gelation time was determined upon examination of specimens removed from the high pressure environment at set pressures and processing times. Gelation was confirmed by the formation of a homogenous, opaque gel lacking sufficient viscosity to flow from an inverted beaker.

### 3.2.3 Gel Physical Properties

#### 3.2.3.1 Structural Analysis by Fourier Transform Infrared Spectroscopy

Silk hydrogel structural characteristics were investigated using Fourier Transform Infrared Spectroscopy (FTIR) Spectrum One (Perkin Elmer, Waltham, MA, USA) with a zinc selenide crystal. To monitor the kinetics of silk structural

transition during gelation, 5 ml volumes of 2 wt% silk solutions, 0.6cm thickness, were submitted to high pressure CO<sub>2</sub> (60 bar) for 0-2 hours and collected every 15 minutes for structural characterization. A second set of samples was used to access the structural features of the silk hydrogels after 8 hours processing time. To preserve the secondary structure of the obtained silk hydrogels, specimens were immediately quenched in liquid nitrogen after treatment by high pressure CO<sub>2</sub> and subsequently lyophilized for 48 hours to obtain dry samples for characterization. We performed preliminary experiments comparing the spectra of lyophilized and hydrated gels obtained directly after processing in high pressure CO<sub>2</sub> and found similar data produced by both conditions. Structural data was acquired by loading lyophilized silk hydrogel specimens onto the IR apparatus and sample spectrums were collected as a mean of 32 acquisitions (between 4000 cm<sup>-1</sup> and 400 cm<sup>-1</sup>) with a spectral resolution of 4 cm<sup>-1</sup>.

### **3.2.3.2 Environmental Scanning Electron Microscopy**

To evaluate silk hydrogel surface morphology in the native state, wet specimens were examined using an environmental scanning electron microscope (ESEM, Philips XL 30 ESEM, Philips, Eindhoven, Netherlands) at a working distance 10-15 μm and voltage of 15 kV. Gel specimens were observed without any further treatment at a vacuum range (5-7 Torr) at constant temperature (5 °C).

### **3.2.3.3. Scanning Electron Microscopy**

Dry imaging of hydrogel specimens was obtained using a scanning electron microscope (SEM) (Quanta 200 Scanning Electron Microscope – FE – operating mode: low vacuum, gaseous secondary electron GSE detector). Wet silk hydrogels were first quenched in liquid nitrogen for 5 minutes and subsequently lyophilized for 48 hours to prepare dry cross sections for imaging. Prior to imaging, lyophilized cross sections were sputter coated (Biorad SC500, Hemel Hempstead, UK) with a thin layer of gold to avoid charging of the sample.

### **3.2.3.4. Swelling Ratio**

The swelling behavior of hydrogel specimens was performed by submerging hydrated samples in PBS at 37 °C for 24 hours. Once removed, the wet weight of

the swollen silk hydrogels was recorded ( $W_{wet}$ ). Subsequently, the samples were quenched in liquid nitrogen for 5 minutes followed by lyophilization for 48 hours to obtain the dry mass ( $W_{dry}$ ). The swelling ratio was then calculated from the following relation:

$$\text{Swelling Ratio (g PBS/g protein)} = \frac{(W_{wet} - W_{dry})}{W_{dry}}$$

### **3.2.3.5. Mechanical Properties in Compression**

The mechanical performance of hydrated specimens was performed in the unconfined state by a uniaxial compression mechanical tester (Bose ELF3400) with a 50 N load cell. For testing specimens, cylindrical plugs (10 mm diameter, 6-7 mm height) were punched out of a large volume silk hydrogel (5 ml) and subsequently submerged in PBS at room temperature. Samples were let to stand no more than 1 hour prior to the mechanical testing. The mechanical properties of the gel samples were tested in the wet state, in PBS, at room temperature. Strain (mm) and load (N) were recorded using Wintest software at a cross speed of 20  $\mu\text{m/s}$  up to 60% strain level. To ensure proper sample placement and flatness, samples were cyclically preconditioned at 1% strain for 10 cycles. From the collected data, a stress-strain plot was rendered and the compressive modulus extrapolated from the tangent slope at 10% strain of the stress-strain curve.

### **3.2.4. Statistical analysis**

All tests were performed in triplicate. Statistical significance of collected data was determined at each condition using an independent Student's t-test. Data are presented as mean  $\pm$  standard deviation (SD) and was considered statistically significant at 95% confidence ( $p < 0.05$ ).

## **3.3. Results and Discussion:**

### **3.3.1. Gross Examination of Prepared Silk Hydrogels**

The macrostructure of silk hydrogels prepared using high pressure  $\text{CO}_2$  and from the citric acid control are presented in Figure 2. The hydrogels prepared under high pressure  $\text{CO}_2$  Figure 2(b) displayed superior homogeneity in comparison to the

soft, heterogeneous consistency of hydrogels prepared at atmospheric conditions using citric acid (Figure 2(a)). Mechanical integrity as well as elastic properties was also apparent from the 4 wt% silk hydrogels prepared under high pressure (Figure 2 (c,d)). Gel consistency and rigidity between the two protein concentrations was noticeably different, with higher concentrations (4 wt%) exhibiting more resilient mechanical stiffness compared to lower concentrations (2 wt%) which were often too soft for simple handling. The mechanical performance of silk hydrogels prepared under high pressure CO<sub>2</sub> will be further evaluated in the mechanical properties section of this paper.

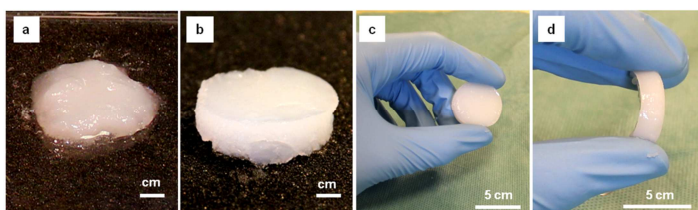


**Figure III - 2.** Silk hydrogels at 2 wt% protein concentration prepared by conventional citric acid titration (a) and under high pressure CO<sub>2</sub> (b). Demonstration of the handling properties of a 4 wt% silk hydrogel prepared under high pressure CO<sub>2</sub> (c,d).

### 3.3.2. Gelation Kinetics

#### 3.3.2.1. In situ observation

Silk fibroin aqueous solutions at 2 and 4 wt% protein concentrations were processed under high pressure carbon dioxide at several pressures (5-150 bar) and processing times (2-8 hours). In situ gelation observations permitted from the high pressure quartz view cell reactor are presented in Figure 3. The introduction of high pressure CO<sub>2</sub> resulted in a transition of the transparent silk solution to a slightly turbid consistency at short processing times (1 min.), followed by a progressive increase in turbidity with time (60 min.) and finally reaching complete gelation with the formation of an opaque gel (90 min.). The presence of a turbid solution prior to gelation is consistent with other reports for silk protein gelation and is likely due to the formation of small (<10 μm) protein precipitates rich in β-sheet crystals (Matsumoto, 2006). Interestingly, turbidity was detectable upon the immediate contact with high pressure CO<sub>2</sub> as evidenced in Figure 3. As the diffusion of CO<sub>2</sub>

into the solution under stagnant conditions can be considered slow even at elevated pressures (Thiering, 2001), the evidence of a turbid solution immediately upon submission to high pressure CO<sub>2</sub> indicates the potential role of the hydrostatic pressure environment, the effects of which will be discussed further in the phenomenological section of this paper.

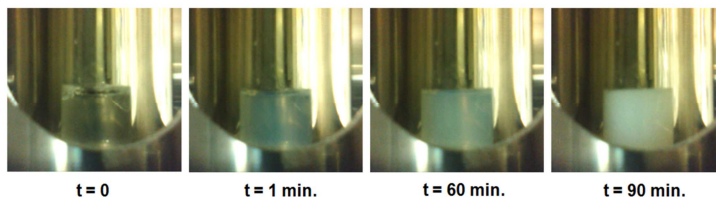


**Figure IV - 3.** In situ observation of silk protein gelation induced under high pressure CO<sub>2</sub>. Conditions: 2 wt% silk fibroin solution, Pressure (CO<sub>2</sub>) = 60 bar.

### 3.3.2.2. Gelation Screening

Figure 4 reports the gelation time for silk solutions submitted to several CO<sub>2</sub> pressures. To ascertain the role of solution concentration on gelation kinetics, two solution concentrations were prepared, 2 and 4 wt%, and evaluated under the various processing conditions. When pressure was increased, gelation time was markedly reduced from approximately 6-8 hours for samples prepared at atmosphere (citric acid control) to less than 2 hours at pressures above 60 bar regardless of the starting concentration. For each pressure step, gelation time reduced significantly up to 60 bar ( $p < 0.05$ ), after which the application of higher pressures was found to have no significant impact on gelation time. Interestingly, silk gelation could not be achieved at low CO<sub>2</sub> pressures (5 bar, data not shown), which is likely a consequence of the poor CO<sub>2</sub> solubility in water at reduced pressures (Li, 2007). Short processing times (< 1.5 hours) resulted in incomplete gelation regardless of the operating pressure. These findings suggest that a potential minimum reaction time under high pressure CO<sub>2</sub> is required to achieve full gelation. Protein concentration is generally reported to influence the rate of silk protein gelation (Ayub, 1993; Kim, 2004) which is evident here from the spread of gelation times found at both concentrations from the citric acid control gels. However, contrary to previous findings we report negligible differences in gelation time between the 2 and 4 wt%

concentrations when processed under high pressure CO<sub>2</sub>. Such an observation indicates that other processing parameters, rather than protein concentration, impose a considerable influence on silk protein assembly. The mechanistic effects of high pressure CO<sub>2</sub> processing on silk protein assembly will be elucidated further in the phenomenological section of this paper.

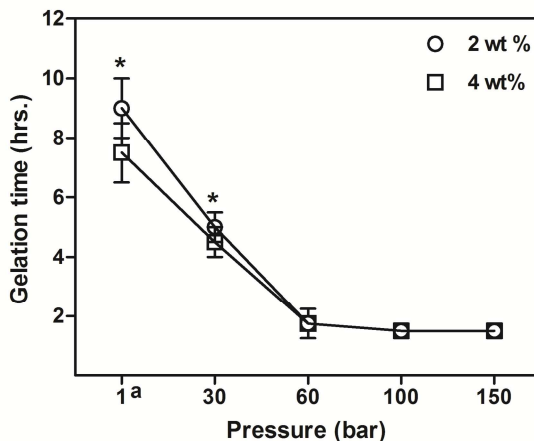


**Figure III – 4.** Gelation kinetics of silk fibroin solutions (2 and 4 wt%) submitted to various pressures CO<sub>2</sub>. Constant sample volume of 5 ml and thickness of 0.6 cm were utilized. Values presented as mean ± standard deviation. Significance determined by performing a student t-test on all samples compared to 60 bar processing condition (\*p < 0.05). Abbreviations: (a) citric acid control samples prepared at atmosphere.

### 3.3.3. Monitoring of Silk Structural Changes by FTIR

To investigate the structural transition of the silk proteins during the gelation process, sample silk solutions were collected periodically after processing under high pressure CO<sub>2</sub> and studied by FTIR. Preliminary results comparing spectra of hydrogels obtained from different protein concentrations produced similar data, thus the results presented here will be reserved to the 2 wt% silk samples. Figure 5 depicts the spectra obtained for 2 wt% silk solutions processed under high pressure CO<sub>2</sub> (60 bar) from 0-8 hours and compared against the citric acid control. Here the infrared region (1700-1500 cm<sup>-1</sup>) was investigated encompassing assignments for amide I (1700-1600 cm<sup>-1</sup>) and amide II (1600-1500 cm<sup>-1</sup>) peptide backbones both commonly utilized in the study of silk fibroin secondary structures (Ayub, 1993;

Hanawa, 1995; Hu, 2006). Several structural resonances have been identified for the amide I and amide II spectral domain including  $\beta$ -sheet structures (Hu, 2006; Hu, 2011) (1620-1630  $\text{cm}^{-1}$ , 1697-1700  $\text{cm}^{-1}$ , amide I; 1515  $\text{cm}^{-1}$ , amide II), random coils (Hu, 2006, Um, 2001) (1640-1649  $\text{cm}^{-1}$ , amide I; 1540  $\text{cm}^{-1}$ , amide II),  $\alpha$ -helix (Hu, 2006) (1652  $\text{cm}^{-1}$ , amide I), turns (Hu, 2006) (1663-1696  $\text{cm}^{-1}$ , amide I) and side chain residues (1605-1615  $\text{cm}^{-1}$ , amide I) (Hu, 2006). The presence of  $\beta$ -sheet structures is believed to play a critical role in the formation of silk hydrogels (Matsumoto, 2006). Initially, the unprocessed silk solution exhibited peaks centered at 1552  $\text{cm}^{-1}$  (Amide II) and 1640  $\text{cm}^{-1}$  (Amide I) which constitute random coil structures, and 1654  $\text{cm}^{-1}$  (Amide I) which indicates  $\alpha$ -helix structures. After submission to high pressure  $\text{CO}_2$ , the formation of peaks centered at 1610-1630  $\text{cm}^{-1}$  and 1700  $\text{cm}^{-1}$  (Amide I) appeared signifying the presence of  $\beta$ -sheet structures. Simultaneously, the 1510-1520  $\text{cm}^{-1}$  (Amide II) peak increased indicating the dense packing of  $\beta$ -sheet structures (Hu, 2011). Concomitant to the formation of  $\beta$ -sheet structures, a decrease in the  $\alpha$ -helix (1654  $\text{cm}^{-1}$ ) and random coil (1552  $\text{cm}^{-1}$ , 1640  $\text{cm}^{-1}$ ) peak contributions was realized. Based on the progressive augmentation of the  $\beta$ -sheet structure peaks, increasing processing time under high pressure  $\text{CO}_2$  encouraged the formation of  $\beta$ -sheet structures with the preparation of stable silk hydrogels attained after 90 minutes processing. Notably, the strong  $\beta$ -sheet absorbance peak centered at 1623  $\text{cm}^{-1}$  attains the greatest intensity increase between 60 and 90 minutes processing time, with processing times longer than 2 hours resulting in only trivial changes to the absorbance intensity. These transitions are in agreement with the gelation data presented in the previous section, whereby stable silk hydrogels were only achievable after a minimum of 90 minutes processing under high pressure  $\text{CO}_2$  (60 bar). The structural transitions observed here are consistent with previous studies on silk hydrogels produced in acidic environments (Ayub, 1993; Hanawa, 1995), which suggests that the transition to the stable  $\beta$ -sheet conformation under high pressure  $\text{CO}_2$  may proceed in an analogous fashion. Curiously, varying the processing pressure did not result in significant changes to the hydrogel secondary structure upon inspection after 8 hours processing time (data not shown), indicating that the effect of different pressures had no considerable outcome on the obtained protein secondary structure. This is consistent with previous studies

on the high pressure CO<sub>2</sub> (<200 bar) treatment of aqueous α-elastin solutions, whereby negligible changes to the protein secondary structure were reported both during and post high pressure processing (Dehghani, 2008). Thus, the application of pressure, at least at the magnitude applied in this study, does not seem to invoke significant modifications to the silk structural conformations. It is obvious that a more comprehensive study is necessary to establish these findings, in particular the probing of silk structural changes whilst submitted to high pressure environments. A high pressure study employing in situ spectroscopy techniques as recently described (Dehghani, 2008) may better elucidate the events during the gelation of silk proteins under high pressure CO<sub>2</sub>.

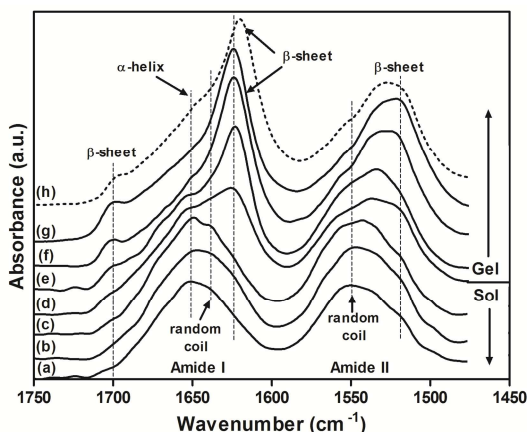


**Figure III – 5.** Dynamic β-sheet formation during silk gelation evaluated by FTIR for 2 wt% silk solutions submitted to high pressure CO<sub>2</sub> (60 bar): (a) 0 min., (b) 30 min., (c) 60 min., (d) 75 min., (e) 90 min., (f) 2 hrs., (g) 8hrs., (h) citric acid control. Constant sample volume of 5 ml and thickness of 0.6 cm were utilized.

### 3.3.4. Hydrogel Physical Characteristics

#### 3.3.4.1. Microstructure

Hydrogel microstructures were evaluated both in the wet and dry state to ascertain the effects of the processing conditions on microstructure formation. Environmental scanning electron microscopy (ESEM) was employed to image wet samples directly following processing with no further modification (Figure 6). ESEM

analysis demonstrated that silk hydrogels prepared under high pressure CO<sub>2</sub> were distinctly more homogenous when compared to the citric acid controls. By comparison, hydrogels prepared at atmospheric conditions with citric acid were considerably more heterogeneous, seemingly comprised predominantly of aggregate-like structures.

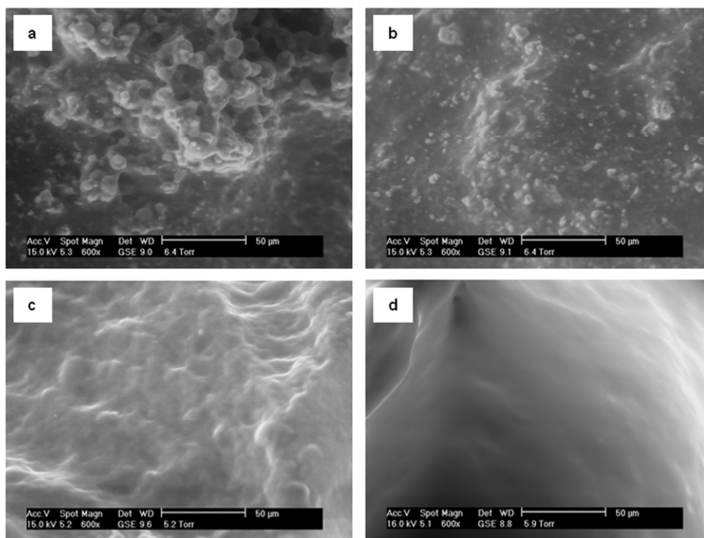


**Figure III – 6.** Environmental Scanning Electron Microscopy (ESEM) images of wet silk hydrogels prepared by citric acid titration (a) 2 wt% and (b) 4 wt% and under high pressure CO<sub>2</sub> (c) 2 wt% and (d) 4 wt%.

Dry imaging was also performed using conventional scanning electron microscopy (SEM) techniques to better investigate the microstructures of the prepared hydrogels at various pressures (Figure 7). Comparison of the micrographs of silk hydrogels prepared by high pressure CO<sub>2</sub> or by citric acid at atmosphere indicated the formation of homogenous pores and reduced pore size for the specimens prepared with high pressure CO<sub>2</sub>. Utilizing image analysis software (ImageJ) the equivalent pore diameter of the pores was obtained. Specimens prepared at higher protein concentration exhibited an increase in the average pore size from  $2.22 \pm 0.5 \mu\text{m}$  to  $5.62 \pm 1.4 \mu\text{m}$  for 2 and 4 wt% respectively. By comparison, average pore sizes for silk hydrogels prepared at atmospheric

conditions with citric acid could not be measured as the specimens lacked a sufficient population of pores for tabulation. The disordered network observed for the hydrogels prepared with citric acid indicates a lack of homogenous gelation when compared to the more homogenous microstructure displayed by the samples prepared under high pressure CO<sub>2</sub>.

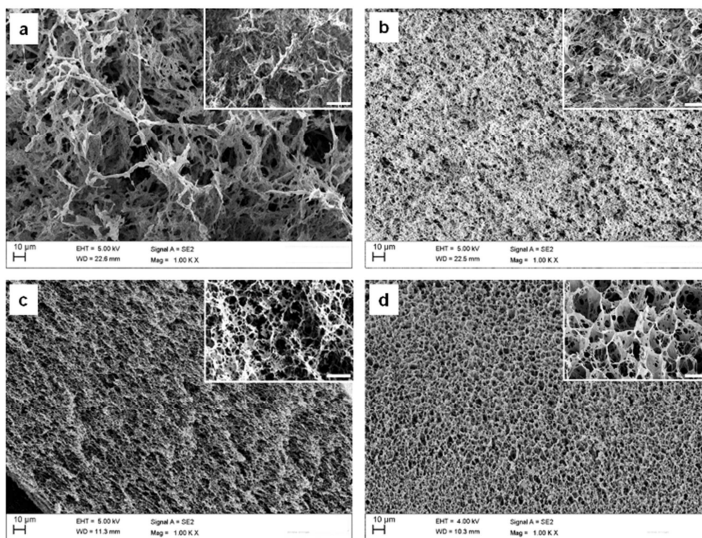


**Figure III – 7.** Scanning Electron Microscopy (SEM) images of lyophilized silk hydrogels prepared by citric acid titration (a) 2 wt% and (b) 4 wt% and under high pressure CO<sub>2</sub> (c) 2 wt% and (d) 4 wt%. Insets represent 4000X magnification with 5 µm scale bars respectively.

Pore microstructures with high interconnectivity and reduced pore sizes have been reported for several natural polymer hydrogels fabricated under high pressure CO<sub>2</sub> such as chitosan (Ji, 2011), dextran (Palocci, 2007), alginate (Partap, 2006) and  $\alpha$ -elastin (Annabi, 2009). The mechanism of pore formation under high pressure CO<sub>2</sub> compared to atmospheric conditions is believed to proceed by a phase inversion process in which CO<sub>2</sub>, acting as an anti-solvent, partitions the solution into a polymer-rich and polymer-lean phase (Annabi, 2009). The subsequent removal of CO<sub>2</sub> from the aqueous phase (polymer-lean phase) during the depressurization process results in the formation of a porous construct (polymer-rich phase) (Annabi, 2010). Carbon dioxide has a weak affinity for water, therefore the rate of diffusion

between the nonsolvent (CO<sub>2</sub>) and solvent (water) is poor, inhibiting pore nucleation and resulting in the tendency for reduced pore size.

Recently authors have reported on the capacity to modify hydrogel microstructures prepared under high pressure CO<sub>2</sub> by manipulating the depressurization rate (Annabi, 2010). Annabi et al. employed both slow and fast venting rates (1 bar/min and 60 bar/min respectively) in the preparation of recombinant tropoelastin/ $\alpha$ -elastin hydrogels under high pressure CO<sub>2</sub> and reported a significant decrease in pore size attained under the fast venting rate when compared to the slower rate (Annabi, 2010). We performed preliminary experiments by adjusting the venting rate of the silk hydrogels prepared here ranging from 1 bar/min. to 10 bar/min. and found no significant modifications to the obtained hydrogel microstructure. It should be noted that in the present work we chose to avoid venting rates faster than 10 bar/min. as this often resulted significant shearing effects from the rapid escape of CO<sub>2</sub> sufficient to rupture the silk hydrogels. Nevertheless, despite our preliminary findings, we anticipate that further manipulations to the degassing stage during silk gelation may result in the fabrication hydrogels with a diversity of properties. The optimization of the CO<sub>2</sub> venting rate and its relation to silk hydrogel microstructure and properties will be the topic of a future paper.

#### **3.3.4.2. Hydrogel Swelling Behavior**

The swelling properties of silk hydrogels prepared at various protein concentrations, processing media and processing times are presented in Figure 8. The processing media had a profound effect on the swelling nature of the prepared gels. Silk hydrogels prepared under 60 bar high pressure CO<sub>2</sub> at 2 and 4 wt% absorbed  $32.4 \pm 1.4$  g and  $20.0 \pm 1.9$  g PBS/g protein respectively after 8 hours processing time. By comparison, hydrogels prepared under atmospheric conditions with citric acid absorbed  $42.6 \pm 0.5$  g and  $25.36 \pm 1.8$  g PBS/ g protein at 2 and 4 wt% respectively. Adjustment of the processing pressure did not result in a significant change on hydrogel swelling capacity (data not shown). The reduced swelling observed for the high pressure CO<sub>2</sub> specimens may be correlated to a higher degree of crosslinking (Anseth, 1996). Interestingly, no significant variation in hydrogel swelling was found

for specimens processed at different processing times under high pressure CO<sub>2</sub>, despite the 2 wt% specimens prepared at 2 hours. Presumably, this is a result of the gel locking in its structure upon initial gelation, which is observed at times considerably less than 8 hours under high pressure CO<sub>2</sub>. Hydrogels prepared at greater protein concentrations exhibited a two-fold decrease in absorbed PBS than at lower protein concentration, regardless of the processing environment. Generally, hydrogels with greater protein concentration have more polymer chains available to participate in crosslinking; thus, the resultant gel network is stiffer, thereby effectively reducing the capacity to absorb fluid.

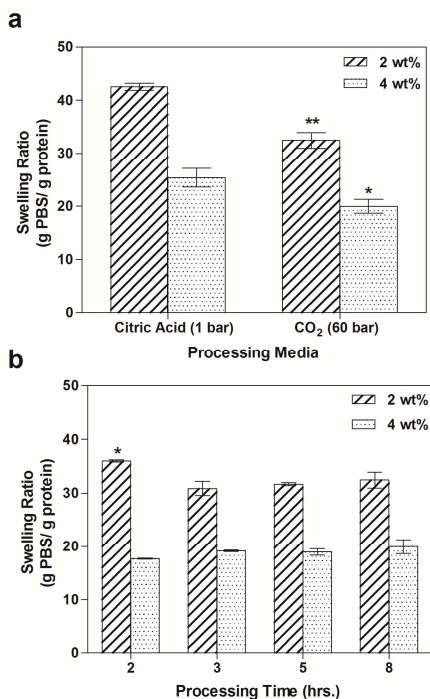


**Figure III – 8.** Swelling ratio of silk hydrogels produced by citric acid titration and under high pressure CO<sub>2</sub> environments (a) and at various processing times using high pressure CO<sub>2</sub> (60 bar)(b). Student's t-test performed on the groups with a significance \*p < 0.05 and \*\*p < 0.005 reported.

Swelling properties reported here are generally higher than those reported for other natural polymer hydrogels prepared under high pressure CO<sub>2</sub> (see Table 1). The swelling ratio of 2 wt% silk hydrogels prepared here ( $32.4 \pm 1.4$  g PBS/ g protein) was significantly higher than those reported for 1.5 wt% chitosan hydrogels crosslinked with genipin or glutaraldehyde under high pressure CO<sub>2</sub> (17.2 and 25.7 g PBS/g protein for genipin and glutaraldehyde crosslinkers respectively) (Ji, 2011). The decreased swelling properties of chemically crosslinked natural polymers compared to the silk hydrogel prepared here is potentially a result of different crosslinking mechanisms. It is important to note that an obvious deviation in the absorbed fluid could be a result of the individual and unique chemistries of the different natural polymers. Nonetheless, the comparable swelling properties of silk hydrogels prepared here to other natural-based hydrogel systems demonstrates the capacity to retain several of the attractive features of high pressure CO<sub>2</sub> processing without the necessity for crosslinking agents.

### **3.3.5. Properties in Compression**

To ascertain the mechanical performance of silk hydrogels prepared under high pressure CO<sub>2</sub>, mechanical compression experiments were performed and the resultant elastic moduli computed and presented in Figure 9. The compressive modulus increased for hydrogels prepared under high pressure CO<sub>2</sub> when compared to the specimens produced at atmosphere using citric acid Figure 9(a). The compressive moduli of silk hydrogels produced at 60 bar high pressure CO<sub>2</sub> for 8 hours processing time were  $18.91 \pm 2.34$  and  $63.98 \pm 2.97$  kPa for 2 and 4 wt% respectively. By comparison, the moduli computed for the 2 and 4 wt% silk hydrogels prepared at atmospheric conditions were  $9.40 \pm 1.89$  and  $15.96 \pm 0.89$  kPa respectively. The compressive moduli were higher for silk hydrogels with greater protein concentration both prepared under high pressure CO<sub>2</sub> and atmospheric conditions. This is to be expected as the greater protein concentration will result in higher degree of crosslinking and improved mechanical properties (Anseth, 1996). Interestingly, the compressive properties of silk hydrogels prepared under different processing pressures were not found to have a significant impact on hydrogel mechanical properties (data not shown), suggesting that the improved

mechanical properties reported here may be a result of other mechanisms. Silk hydrogel compressive properties were also monitored over different processing times as shown in Figure 9(b). As processing time increased from 2 to 8 hours, the compressive moduli increased from  $14.12 \pm 2.88$  kPa to  $18.91 \pm 2.34$  kPa and  $39.70 \pm 3.24$  kPa to  $63.98 \pm 2.97$  kPa for 2 and 4 wt% silk hydrogels respectively. Thus, as a consequence of longer processing times, the silk hydrogels produced under high pressure CO<sub>2</sub> became stiffer.

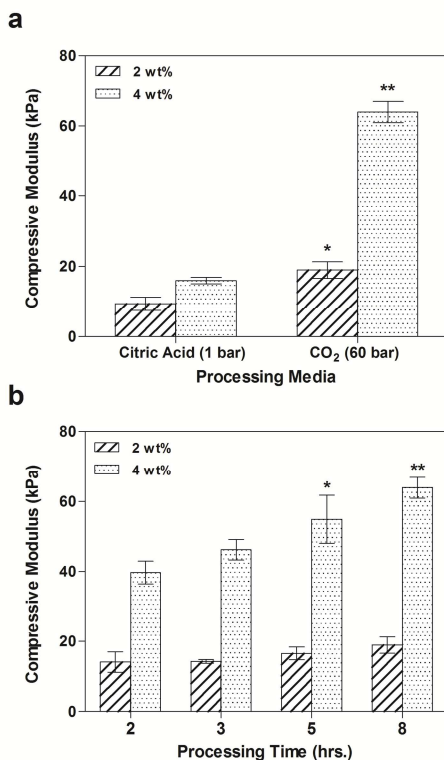


**Figure III – 9.** Compressive moduli of silk hydrogels prepared by citric acid titration and under high pressure CO<sub>2</sub> environments (a) and at several processing times under high pressure CO<sub>2</sub> (60 bar) (b). Student's t-test performed on all specimens compared to the citric acid controls (a) and (b) at 2 hours processing time. Significance was reported for \*p < 0.05 and \*\*p < 0.005 respectively.

Generally, hydrogel mechanical performance is intimately linked to the swelling properties of the said material, namely that the swelling ratio negatively correlates to gel stiffness (Anseth, 1996). Remarkably, in comparison with the swelling data presented in the previous section, as processing time increases mechanical performance of the hydrogel increases at no significant expense to the swelling properties. A potential explanation for this result is the ability for residual protein chains, not already associated with the gel network, to coat and crosslink with the preformed gel network after prolonged processing times. Verheul et al. postulated that only a fraction of available proteins are initially involved in forming the primary structural network of heat-induced whey protein isolate gels (Verheul, 1998). After which, prolonged processing times resulted in the coating of these residual proteins onto available gel surfaces. The condensation and decoration the porous gel with residual free proteins reinforces the gel network at modest expense to the overall gel spatial structure. We propose that a similar phenomenon to that reported by Verheul et al. is likely to have occurred here as well for silk hydrogels processed under high pressure CO<sub>2</sub>. At extended processing times under high pressure CO<sub>2</sub>, residual free silk proteins will associate and condense onto the free surfaces within the gel network, improving mechanical properties while maintaining the fluid content. Presumably, this effect would be more pronounced for hydrogels prepared under high pressure CO<sub>2</sub>, as the local solution pH is believed to be homogenous at all points of space (Thiering, 2001). Utilizing a mineral acid would not achieve this as the presence of local proton-rich domains would in fact trigger protein nucleation points, and once gelation has completed the diffusion of free protons amongst the formed aggregates would be significantly hindered (Hofland, 2003). The lack of available free protons to participate in the gelation of the residual proteins would thus inhibit gelation at later stages of processing.

Silk proteins have been studied extensively for biomaterial applications in part due to the exceptional mechanical properties found in natural silk fibers. The physical properties of several natural polymer hydrogels prepared under high pressure CO<sub>2</sub> are presented in Table 1.

**Table III - 1.** Comparative physical properties of several naturally derived hydrogels fabricated under high pressure CO<sub>2</sub>

Natural Polymer	Crosslinking agent/Surfactant	Swelling Ratio (g PBS/ g protein)	E (kPa)	Ref
Silk Fibroin	-	19.5-34.8	14.1-64.0	This study
Chitosan	GP	17.2	73.9	(Ji, 2011)
	GA	25.7	41.6	(Ji, 2011)
Alginate	CaCO <sub>3</sub> / PFPE-	-	33.8	(Partap, 2006)
	NH <sub>4</sub>			
Tropoelastin/ $\alpha$ -elastin	GA	4.6-7.0	4.9-11.8	(Annabi, 2010)
	HDMI/DMSO	6.81	8.62	(Annabi, 2009)

Abbreviations: E: Compressive Modulus (kPa), GP: Genipin, GA: Glutaraldehyde, PFPE-NH<sub>4</sub>: Ammonium perfluoropolyether, HDMI: Hexamethylene diisocyanate, DMSO: Dimethyl sulfoxide.

When compared to other natural polymer hydrogels produced under higher pressure CO<sub>2</sub>, such as crosslinked tropoelastin/ $\alpha$ -elastin, chitosan, or alginate gels, silk fibroin hydrogels exhibited either comparable or improved mechanical performance. Concomitantly, silk hydrogels produced under high pressure CO<sub>2</sub> also displayed high levels of fluid retention coupled with improved mechanical properties. Compared to other hydrogels processed under high pressure CO<sub>2</sub>, the silk hydrogels prepared here performed formidably without the need for chemical crosslinking agents. Thus, the method described here to produce silk hydrogels may offer a clean and time efficient alternative to several other naturally derived hydrogel systems produced under high pressure CO<sub>2</sub>, which otherwise require chemical processes.

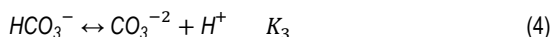
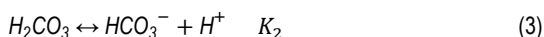
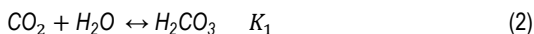
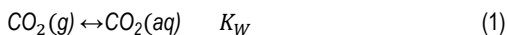
### 3.3.6. Phenomenological Description

In this study, the potential of utilizing high pressure carbon dioxide as a volatile acid for the isoelectric gelation of silk fibroin was investigated. The considerably more rapid gelation of silk proteins under high pressure CO<sub>2</sub> warranted further inquiry into

the specific stimulus of the processing environment such as solution acidification through carbonic acid formation and submission to high hydrostatic pressure.

### 3.3.6.1. Acidification Kinetics using Carbon Dioxide

The acidification of an aqueous solution with CO<sub>2</sub> proceeds through two equilibrium steps: an interfacial mass transfer step of gaseous CO<sub>2</sub> into the liquid (eq. 1) and a subsequent aqueous phase reaction to form carbonic acid (eq 2) (Thiering, 2001).



This acidic process is an outcome of carbon dioxide reacting with water to form carbonic acid and other constituent ions in solution (eq. 3 and 4) (see Figure 1 for illustration). Henry's Law dictates that the driving force for dissolution and reaction of carbon dioxide in water is enhanced at higher pressures; therefore, pressure will have a direct impact on the rate of acidification.

The kinetics of CO<sub>2</sub> dissolution, reaction to form carbonic acid and subsequent diffusion of free protons (H<sup>+</sup>) is generally perceived to be rapid (Salt, 1982); therefore, the acidification of an aqueous solution by CO<sub>2</sub> is rate-limited by the interfacial transport across the vapor/liquid-phase boundary (eq. 1). It is generally supported that through the steady addition of CO<sub>2</sub>, combined with the rapid rate of proton diffusion throughout the bulk fluid, that the solution experiences a controlled, homogenous reduction in pH with all proteins exhibiting identical net electrostatic charge at all points of time (Salt, 1982). This homogenous acidification cannot be achieved with conventional mineral acids without inducing localized regions of high ion concentration, resulting in pH overshoots which can potentially induce damage to the protein structure (Thiering, 2001).

Herein we adopt a semi-empirical mathematical approach to elucidate the events which lead to aqueous solution acidification in contact with CO<sub>2</sub>. The approach employed here is to rely on the calculation of absorbed CO<sub>2</sub> within the bulk solution over time, coupled with the dissociation reaction kinetics of the formation of

carbonic acid to yield a prediction of free protons in solution. Once knowledge of the free protons in the bulk solution is obtained the pH may be estimated. We introduce this model with the following assumptions:

1. pH reduction is presumed to occur homogenously at all points of time within the bulk protein solution.
2. Mass transport of CO<sub>2</sub> into the bulk solution may be modeled by conventional Fickian diffusion constraints.
3. Pressure effects on the equilibrium constants may be considered negligible.
4. Solubility and activity of CO<sub>2</sub> in silk fibroin solution can be approximated by CO<sub>2</sub>-H<sub>2</sub>O binary data obtained from the literature.

The prediction of the CO<sub>2</sub> mass fraction in solution over a specific diffusion length and time begins with the diffusion equation. The mass transport of CO<sub>2</sub> into a non-agitated liquid phase may be defined by a mass balance in the unsteady-state condition expressed by Fick's second law of diffusion (Walas, 1991):

$$\frac{\partial C}{\partial t} = D \frac{\partial^2 C}{\partial x^2} \quad (5)$$

where D is the gas phase diffusivity of CO<sub>2</sub> and C represents the concentration of CO<sub>2</sub> in the liquid phase at a given distance (x) and time (t). In our system, there is only one accessible face for diffusion thus the boundary conditions may be constrained to a semi-infinite region:

$$\begin{aligned} C(x, 0) &= 0, \text{ initially} \\ C(0, t) &= C_s, \text{ at the surface} \\ C(\infty, t) &= 0, \text{ at infinity} \end{aligned}$$

where C<sub>s</sub> represents the soluble concentration limit of CO<sub>2</sub> in water at the surface, which is both a function of pressure and temperature. The solution to equation 5 may be obtained using a combination of variables approach and can be written as such:

$$\frac{C(x,t)}{C_s} = 1 - \operatorname{erf}\left(\frac{x}{\sqrt{4Dt}}\right) \quad (6)$$

where erf represents the error function of  $x\sqrt{4Dt}$ . Duan et al. provided tabulated solubility data of CO<sub>2</sub>-H<sub>2</sub>O binary systems at several temperatures and pressures (Duan, 2006). To obtain CO<sub>2</sub> solubility data for this model, we chose an interpolation routine based on the CO<sub>2</sub> solubility data reported by Duan et al. (see Table 2). Using the interpolated solubility limits of CO<sub>2</sub> in water at specific pressures, we can obtain a discrete solution to equation 6 at various diffusion lengths. Figure 10 plots solutions for dimensionless CO<sub>2</sub> concentration at several diffusion lengths over time at constant pressure. Clearly evident is the prohibitively long time scale required for CO<sub>2</sub> diffusion to reach even modest distances under stagnant conditions. With the CO<sub>2</sub> concentration profile defined, calculation of the bulk absorbed CO<sub>2</sub> fraction in solution can be obtained, and an expression for the pH as a function of time can be formulated.

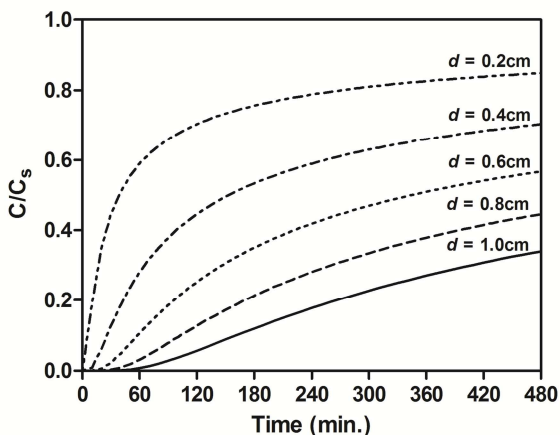


Figure V – 10. Dimensionless CO<sub>2</sub> concentration ( $C/C_s$ ) over time at various diffusion lengths (0.2-1.0 cm).

Several modeling approaches have been proposed to predict the pH of complex aqueous solutions in contact with carbon dioxide (Bortoluzzi, 2011; Li, 2007; Meyssami, 1992). Generally, the pH of a complex solution of discrete ions ( $i$ ) can be defined by an electroneutrality condition:

$$\sum_i v_i m_i = 0 \quad (7)$$

where  $v$  is the valence and  $m$  the molality associated with the individual ions. In the case of an aqueous solution in contact with high pressure  $\text{CO}_2$ , eq 7 can be written as:

$$C_{H^+} - C_{OH^-} - C_{HCO_3^-} - 2C_{CO_3^{2-}} = 0 \quad (8)$$

where  $C$  is the molal concentration of component  $i$  in  $\text{mol kg}^{-1}$ . Regarding complex aqueous solutions, the need to account for the buffer capacity of the additional constituents (proteins) becomes essential. Hofland et al. proposed a method to account for the buffer capacity of proteins in solution by calculating the total proton uptake from the proteins in solution obtained from an experimental titration curve (Hofland, 1999). By subtracting the number of protons in free solution from the number of protons added during titration the authors were able to calculate the total number of protons buffered by the protein. To avoid elaborate modeling, we chose to adopt a method similar to that proposed by Hofland et al. (Hofland, 2003) for the prediction of the pH of silk protein solutions in contact with  $\text{CO}_2$ . Accounting for the buffer capacity of silk proteins, the electroneutrality condition may be modified:

$$C_{H^+} - C_{OH^-} - C_{HCO_3^-} + \text{Silk}_{\text{uptake}(H^+)} = 0 \quad (9)$$

where  $\text{Silk}_{\text{uptake}(H^+)}$  ( $\text{mol H}^+/\text{g silk protein}$ ) is the amount of protons absorbed per a mass of silk protein which can be obtained by a titration curve (Coleman, 1947) and is expressed as such:

$$\text{Silk}_{\text{uptake}(H^+)} = 0.0025pH^{-2.416} \quad (10)$$

The concentration of protons in solution ( $C_{H^+}$ ) may be correlated to solution pH by the following expression:

$$C_{H^+} = 10^{-pH}/\gamma \quad (11)$$

where  $\gamma$  is the activity coefficient of the monovalent ions in solution. Adopting the description by Hofland et al. (Hofland, 2003) equation 9 may be represented as follows:

$$\frac{10^{-pH}}{\gamma} - \frac{K_a}{10^{-pH}\gamma} C_{CO_2} + \text{Silk}_{\text{uptake}(H^+)} = 0 \quad (12)$$

where  $K_a$  is the overall dissociation constant of  $CO_2$  and  $C_{CO_2}$  is the solubility of carbon dioxide in solution at time  $t$ . The relevant variables employed from literature to solve equations 6 and 12 are presented in Table 2.

**Table III - 2.** Summary of variables Employed for pH Model Prediction of Complex Solutions

<b>Parameter</b>	<b>Value</b>	<b>Ref</b>
$D$ (Diffusivity $CO_2(g)$ ) ( $m^2/s$ )	$1.91 \times 10^{-9}$	(Weast, 2010)
$K_a$ (Overall dissociation constant of $CO_2$ )	$5.02 \times 10^{-7}$	(Edwards, 1978)
$\gamma$ (Activity Coefficient $H^+$ ) (kg/mol)	0.830	(Meysami, 1992)
$CO_2$ Solubility in Water (mol/ kg $H_2O$ )*		(Duan, 2006)
5 bar	0.12	-
30 bar	0.57	-
60 bar	0.98	-
100 bar	1.24	-
150 bar	1.32	-

\*Data obtained by interpolation

The solution to equation 12 provides a theoretical pH time profile for a complex aqueous solution with a known fraction of absorbed  $CO_2$ , which here is a function of time, diffusion length and the equilibrium  $CO_2$  solubility (pressure). To demonstrate the buffering capacity of the silk proteins, we prepared a data plot of the theoretical pH time profile at different protein concentrations in comparison to pure water (Figure 11(a)). As can be seen from the model, solution pH reduces exponentially in the

early time frame (<60 minutes) for the experiments followed by asymptotic behavior at longer time points (>120 minutes). The kinetic behavior exhibited here for solution acidification using CO<sub>2</sub> is in agreement with other model predictions and empirical data available from the literature (Bortoluzzi, 2011; Li, 2007; Meysami, 1992). As demonstrated by the theoretical pH calculation, protein content significantly affects the magnitude of the pH reduction achievable. At silk protein concentrations 2 and 4 wt%, the equilibrium pH increased to 3.72 and 3.92 under 60 bar CO<sub>2</sub> respectively. By comparison, the equilibrium pH prediction of pure water under 60 bar CO<sub>2</sub> was 3.21. It can therefore be projected that even at modest protein concentrations significant perturbations in solution pH may be anticipated. From a processing perspective, if such a phenomenon holds true, then it is entirely plausible that a critical upper limit for protein concentration may exist for processing of silk fibroin under high pressure CO<sub>2</sub>. This is an inherent consequence of the weak acidic properties of CO<sub>2</sub> in water.

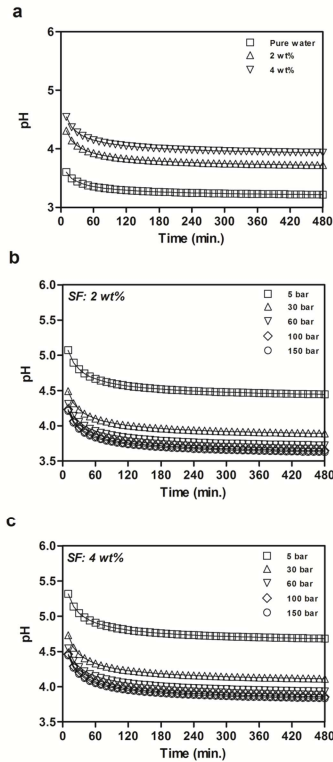


**Figure III – 11.** Theoretical pH time profiles estimated from eq. 12. a) equilibrium pH as a function of protein concentration at 60 bar CO<sub>2</sub>. Estimated pH time profiles for silk solutions 2 and 4 wt% (b,c) submitted to various pressures CO<sub>2</sub>.

We further investigated the influence of processing parameters (pressure) on the rate of solution acidification with potential ramifications on the reported gelation times. The predicted pH time profiles at several pressures of CO<sub>2</sub> over time for the different protein concentrations are presented in Figure 11(b,c). Under stagnant conditions, it is clear that considerable lengths of time are required to reduce the solution pH to near the isoelectric point of silk fibroin (pH: 3.8-4.0)<sup>19</sup> regardless of solution starting concentration. Solution acidification is more strongly influenced at lower pressures (5-60 bar) compared to elevated pressures where only modest adjustments to final pH are reported (Chen, 2007). Characteristic to all pressures

utilized, solution pH experienced rapid reductions early in the processing time followed by an asymptotic behavior at extended times.

To investigate the processing times associated with sufficient pH for silk gelation, we calculated the estimated processing time to achieve a theoretical solution pH of 4 for 2 and 4 wt% silk solutions (Figure 12). Evident from the theoretical pH time profiles, for the 2 wt% silk solution a pH of 4 is attained at approximately 120 and 35 minutes for 30 and 60 bar respectively and 20 minutes for both 100 and 150 bar pressure. By comparison, the 4 wt% protein solutions exhibited considerably longer times to reach a pH of 4 with 180, 90 and 80 minutes for 60, 100 and 150 bar respectively; at 30 bar it was only capable of achieving an equilibrium pH of 4.11. The kinetic data reported for the 2 wt% silk hydrogels prepared under high pressure CO<sub>2</sub> (Figure 4) generally agree with the model prediction, with the onset of suitable pH reduction followed by a period of time (lag phase) prior to final gelation. Previous reports have postulated a three phase nucleation dependent mechanism for silk protein gelation. Using time-resolved FTIR studies on ethanol stabilized silk fibroin films, Chen et al. proposed a three phase conformational mechanism of silk protein assembly: a lag phase characterized by the propagation of  $\beta$ -sheet formation and nucleation, followed by a rapid growth of  $\beta$ -sheet crystals and finally a slowing phase involving a perfection of the  $\beta$ -sheet structure (Chen, 2007). The presence of a lag period prior to rapid gelation is also observed here from the time intervals recorded for gelation and the pH model predictions for obtaining sufficient pH. Comparing the model prediction of pH reduction with the measured kinetic data we see that as pressure increases the lag phase between the onset of the acidic environment with reported gelation is reduced. From this viewpoint, it seems appropriate to propose that variations in the lag period could be influenced by other external factors such as the hydrostatic pressures submitted during processing, as discussed in the following section.

Interestingly, the theoretical pH time profiles estimated for the 4 wt% silk fibroin solutions are considerably longer than the actual kinetic data reported here (Figure 4). One reason for this discontinuity is the failure of the model to account for protein concentration effects on gelation. Generally, gelation time is positively correlated to protein concentration. Hanawa et al. observed gelation of silk solutions at various

concentrations and reported an approximately inverse relationship to concentration. Geltime scales  $1/C$  (curve fit from tabulated data) (Hanawa, 19995), i.e. gelation time is effectively halved by doubling the protein concentration. This behavior agrees reasonably well with the silk hydrogels prepared under atmospheric conditions with citric acid where 4 wt% hydrogels were produced in less than 6 hours, in comparison to the 2 wt% hydrogels which required a minimum of 8 hours. Thus, while the model presented here may predict a foreseeable working limit for solution concentrations to reach sufficiently reduced pH, it will not be strictly accurate without considering the positive correlation between protein concentration and gelation kinetics.

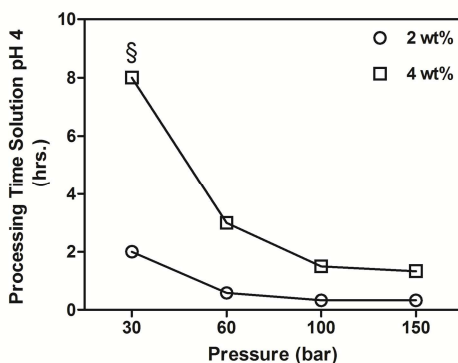


**Figure III – 12.** Estimated processing times for 2 and 4 wt% silk solutions at various processing pressures CO<sub>2</sub> to achieve a solution pH of 4. Abbreviations: (\$) pH of 4.11.

The protracted theoretical pH time profile illustrates the critical role of the mass transport of CO<sub>2</sub> into the silk solution to induce gelation. Clearly the model demonstrates that processing times less than 1 hour may result in an inadequate pH reduction to achieve silk gelation, which is in agreement with the kinetic data presented earlier. What is more, as the sample thickness plays a vital role in the predicted CO<sub>2</sub> concentration profiles (Figure 10), processing of samples with decreased thickness would conceivably reduce the gelation time. A systematic study adjusting sample thickness in the presence of high pressure CO<sub>2</sub> could confirm the precision of the model presented here.

### 3.3.6.2. Influence of High Pressure Environment

Conformational transitions of proteins and the process of assembly (aggregation) involve a multitude of molecular processes encompassing both protein-solvent and protein-protein interactions. Similar to temperature, pressure is a significant thermodynamic parameter which can have profound implications on these protein events. Pressure is believed to induce changes in the partial molar volume of proteins, protein folding mechanics and conformational transitions (Mozhaev, 1996). These modifications can be either elastic (reversible) or plastic (irreversible) depending on the magnitude of pressure and the protein under study (Gross, 1994). The dynamics of protein interactions under pressure can be summarized by Le Chatelier's principal, which dictates that the application of pressure shifts equilibrium of the physical system to the state that occupies the lesser volume (Mozhaev, 1996; Gross, 1994; Mozhaev, 1994). Accordingly, under high pressure, those systems experiencing transitions which involve a reduction in total volume will be favored as compared to those whose total volume increases. Under high pressures, minimal modifications are observed for protein compressibility and internal energy, whereas considerable structural deviations of water at the surface of proteins have been reported (Kitchen, 1992). Hydrophobic hydration of proteins results in the formation of a densely packed water shell encompassing the protein (Edsall, 1983). The unique structuring and disassembly of water molecules relative to hydrophobic hydration permits proteins to exist in an extended/unfolded state under pressure and it's all in accordance with reduced volume states (Urry, 1993).

Given the breadth of protein events influenced by high pressure, the development of a strict mechanistic model for silk protein aggregation under pressure is fraught with ambiguities. On this basis, it is likely that several physical factors associated with high pressure processing, such as changes in the hydration shell as well as the propensity for reduced volume states, could influence the rate of protein aggregation. The interaction of water with silk proteins has been previously reported to play a critical role in the in the natural assembly process of silk proteins (Bini, 2004). Accordingly, it follows that appreciable perturbations of the hydration shell of the silk proteins under pressure could result in increased hydrophobic interactions and subsequent  $\beta$ -sheet formation. Recently, the assembly

of  $\beta$ -sheet rich silk fibers has been observed through the application of high hydrostatic pressure (1-7 kbar) to aqueous silk fibroin solutions (Gebhardt, 2008). It was suggested that under pressure silk proteins unfold due to the penetration of water into the interior of the protein chain, enhancing protein solvation and resulting in a structural conformation with increased propensity for aggregation. While these findings provide insight into high pressure effects on silk protein assembly, considering the magnitude of pressures utilized in this study, approximately two orders of magnitude less, it is unclear if such protein unfolding mechanisms still prevail here. In an attempt to better elucidate the role of high pressure processing on silk protein assembly, we performed a series of preliminary experiments submitting aqueous silk solutions of reduced pH (3.5) to high pressure nitrous oxide ( $N_2O$ ) and recorded the respective gelation times.  $N_2O$  has previously been revealed to have no potential to influence the pH of aqueous media<sup>41</sup>, therefore, its application here allows for the investigation of pressure effects isolated from the acidic phenomenon previously discussed with  $CO_2$ . Our preliminary findings have revealed reduced gelation times for the silk solutions processed in the high pressure  $N_2O$  environment in a fashion similar to that reported here using high pressure  $CO_2$  (unpublished data). Thus, while no direct mechanistic model for silk protein association under high pressure can be arrived at from the current data, it would seem that our preliminary experiments provide some credibility to the suggestion that high pressure plays some role in the reduced gelation times as reported here. Despite these findings, an exact working model for the acceleration of silk protein gelation under high pressure is still inundated by a lack of tangible observations. Pressure-assisted silk protein association and gelation should be studied further in future experiments to elucidate these complex mechanisms.

### ***3.4. Conclusion:***

This work demonstrates the feasibility to produce silk fibroin hydrogels using high pressure  $CO_2$  as a volatile acid without the necessity of crosslinking agents or chemical additives, resulting in a remarkably clean process. It also illustrates several appealing features of using high pressure  $CO_2$  to fabricate silk hydrogels. Firstly, gelation time was expedited to less than 2 hours depending on the processing

conditions and regardless of protein concentration. Structural analysis of the aforementioned silk hydrogels confirmed the presence and growth of extensive  $\beta$ -sheet structures coinciding with the formation of stable hydrogels. Secondly, silk hydrogel microstructure and porosity was improved, thereby offering several benefits for a variety of biomaterial applications. Lastly, the mechanical properties of silk hydrogels prepared under high pressure were enhanced considerably compared to the control citric acid gels. Further, the properties of the silk hydrogels prepared here performed formidably against other naturally derived hydrogels fabricated using high pressure  $\text{CO}_2$ , whilst avoiding the necessity for chemical processing. Mechanistically, the absorbed  $\text{CO}_2$  reduced the solution pH in a slow fashion, governed predominantly by diffusion limitations, with pressure effects potentially contributing to the accelerated gelation. In final, the findings reported here suggest that silk hydrogels produced under high pressure  $\text{CO}_2$  may offer an appealing processing alternative to conventional silk materials fabrication, providing a simple and pure production method, and avoiding potential biological complications associated with chemical additives.

## Chapter IV

# Human MSCs Cultured on Silk Hydrogels with Variable Stiffness and Growth Factor Differentiate into Mature SMC Phenotype

*Part of this chapter has been submitted to: Acta Biomaterialia – August 2015*

Michael Floren, Walter Bonani, Anirudh Dharmarajan, Anotnella Motta, Claudio Migliaresi; Wei Tan. "Human MSCs Cultured on Silk Hydrogels with Variable Stiffness and Growth Factor Differentiate into Mature SMC Phenotype". Submitted Acta Biomaterialia – August 2015

**Abstract:** Cell-matrix and cell-biomolecule interactions play critical roles in a diversity of biological events including cell adhesion, growth, differentiation, and apoptosis. Evidence suggests that a concise crosstalk of these environmental factors may be required to direct stem cell differentiation toward matured cell type and function. However, the culmination of these complex interactions to direct stem cells into highly specific phenotypes *in vitro* is still widely unknown, particularly in the context of implantable biomaterials. In this study, we utilized tunable hydrogels based on a simple high pressure CO<sub>2</sub> method and silk fibroin (SF) the structural protein of *Bombyx mori* silk fibers. Modification of SF protein starting water solution concentration results in hydrogels of variable stiffness whilst retaining key structural parameters such as matrix pore size and  $\beta$ -sheet crystallinity. To further resolve the complex crosstalk of chemical signals with matrix properties, we chose to investigate the role of 3D hydrogel stiffness and transforming growth factor (TGF- $\beta$ 1), with the aim of correlating the effects on the vascular commitment of human mesenchymal stem cells. Our data revealed the potential to upregulate matured vascular smooth muscle cell phenotype (myosin heavy chain expression) of hMSCs by employing appropriate matrix stiffness and growth factor (within 72 h). Overall, our observations suggest that chemical and physical stimuli within the cellular microenvironment are tightly coupled systems involved in the fate decisions of

hMSCs. The production of tunable scaffold materials that are biocompatible and further specialized to mimic tissue-specific niche environments will be of considerable value to future tissue engineering platforms.

#### **4.1. Introduction**

Loss of vascular function associated with cardiovascular disease, such as atherosclerosis, represents the leading medical epidemic in the United States and typically requires surgical intervention through synthetic or autologous vascular grafts (Laslett, 2012). To overcome the limitations associated with adult cell sources, which are often restricted by source or compromised by disease, mesenchymal stem cells (MSCs) have emerged as potential candidates for vascular tissue engineering (Bajpai, 2012). However, despite their growing application, several MSC-based vascular regeneration strategies have been met with inconsistent results, and in some cases resulted in abridged vascular function. For instance, direct bolus delivery of MSCs to injured vasculature can lead to a dysfunctional endothelium, resulting in a higher incidence of vessel occlusion compromising vessel mechanics (O'Shea, 2010). Likewise, MSCs injected at the site of infarcted hearts resulted in increased levels of calcification and ossification of the surrounding cardiac tissue (Breitbach, 2007). These findings suggest a lack of fundamental understanding of the complex vascular niche environment and mechanisms accredited to MSC differentiation towards mature, functional vascular tissues.

Cell interactions with the local microenvironment are recognized in several important biological events including cell adhesion, growth, differentiation, and apoptosis (Discher, 2009; Kuraitis, 2012). In particular, substrate biophysical properties such as rigidity (Engler, 2006; Discher 2005), geometry (Cukierman, 2001; Huebsch, 2010) biological ligand (Suzuki, 2010; Gong, 2008), soluble factor (Narita, 2008), or combination thereof (Wingate, 2014) have been revealed to influence MSC differentiation events. Evidence suggests that a concise crosstalk of these environmental factors may be required to direct MSC differentiation toward desired cell type and function. These findings are supported by recent reports which reveal MSCs acquiring tissue-specific characteristics when co-cultured with mature cells

types or exposed to preformed biological matrices *in vitro*, highlighting the important regulatory role elicited by the specific signals of the microenvironment towards stem cell differentiation (Philp, 2005). However, current methods to regulate stem cell differentiation are often executed independently of other factors, i.e. stiffness or growth factor individually, or lack the amenity to integrate these parameters into a tailorable milieu. A biomimetic approach, incorporating several environmental signals, such as cell-matrix and cell-biomolecule interactions, will help to establish more robust and specific MSC differentiation protocols.

Integration of complex cellular signaling environments into biomaterial scaffolds presents a considerable challenge to the tissue engineering community (Kim, 2012). A variety of synthetically-formulated as well as natural materials have been evaluated for 3D biomaterial scaffolds (Place, 2009). Synthetic materials are attractive for their cost, reproducible fabrication and facile manufacturing yet their lack of cell-recognition sites as well as potential for toxic degradation products causing undesirable inflammation are often disadvantageous (Laflamme, 2011). On the contrary, natural materials represent an attractive scaffold platform as they have excellent biological properties, such as cellular recognition, biocompatibility and the potential to degrade through known metabolic processes (Bouten, 2011; Stegemann, 2007).

Silk fibroin (SF), a natural protein extracted from *Bombyx mori* silkworms, is an attractive material for tissue engineering due to its excellent mechanical properties, biocompatibility, tunable degradation rate, and mild inflammatory response *in vivo* (Kundu, 2013). A diversity of regenerative tissues has been reported using SF-based constructs including bone (Meinel, 2005; Fini, 2005), cartilage (Wang, 2010), vascular (Soffer, 2008; Bondar, 2008; Bonani, 2011), skin (Unger, 2004), nervous (Yang, 2007), hepatic (Gotoh, 2004) and ocular (Lawrence, 2009) amongst others (Kundu, 2013). We previously developed a technique to produce porous, SF hydrogels with tunable stiffness and morphology using the green solvent, carbon dioxide (CO<sub>2</sub>) (Floren, 2012). Hydrogel elastic moduli approaching soft tissues ( $E = 6\text{-}30$  kPa), combined with ease of fabrication and biocompatibility, motivated us to use these SF materials as a platform to instruct stem cell differentiation towards the vascular smooth muscle cell (SMC) lineage in a precise manner. In addition to

substrate rigidity, chemical signals are important for vascular development, maintenance, and regeneration and collectively constitute a complex process involving the interactions of many cellular features in vivo (Carmeliet, 2000). However, the effects of stiffness and its interaction with growth factors have yet to be sufficiently studied, the resolution of which may provide new insights into processes of cellular regeneration and tissue maintenance as they pertain to the cellular microenvironment.

In the present study, we address cellular differentiation on tunable SF hydrogels prepared from a solvent-free CO<sub>2</sub> processing method. The transforming growth factor  $\beta$  (TGF- $\beta$ ) family is a potent regulator of several cell functions such as proliferation, spreading (Derynck, 1997) and is strongly associated with vascular smooth muscle cell (vSMC) differentiation of stem cells (Narita, 2008). Therefore, the focus of this work is on exploiting the combined use of substrate stiffness and growth factor (TGF-  $\beta$ 1) on SF matrices, with the aim of correlating the effects on the vascular commitment of human mesenchymal stem cells (hMSCs). The production of tunable scaffold materials that are biocompatible and further specialized to mimic vascular niche environments will be of considerable value to future tissue engineering platforms.

## **4.2. *Materials & Methods***

### **4.2.1 SF Hydrogel Preparation**

Aqueous silk fibroin (SF) solutions were prepared from degummed cocoons of Bombyx Mori and subsequently dissolving the obtained fibers in 9.3 M LiBr (Fluka Chemicals, Buchs, Switzerland) aqueous solution (10% w/v) at 65 °C for 4 hours and filtered to eliminate impurities. The obtained SF solution was then placed in Slide-A-Lyzer cassette 3500 Da MWCO (Pierce, Thermo Scientific) and dialyzed against distilled water for 3 days at room temperature to remove residual salts. Following dialysis SF solution volume was adjusted with distilled water to reach the desired concentration. Silk hydrogels were prepared from a previously published protocol using high pressure CO<sub>2</sub> (Floren, 2012). Briefly, SF solutions at different concentrations (1.5, 2, 3 & 4 wt%) were syringed into a custom Teflon mold

consisting of 12 cylindrical specimens (h: 3 mm, Ø 10 mm) and placed within a stainless steel high pressure reaction vessel (BR-300, Berghof Products + Instruments, Eningen, Germany). The temperature of the reactor was controlled through an electrical heating jacket run by a BDL-3000 temperature controller (Berghof). Once the system had been sealed and thermal equilibrium established (40°C), CO<sub>2</sub> gas was introduced in the reactor and pressurized at a working pressure of 60 bar through a high-performance liquid chromatography (HPLC) pump (Model 426, Alltech, Deerfield, IL, USA) and isolated for specific gelation times (0-8 hours). Following the set gelation period, the system was depressurized slowly (approximately 30 minutes) to avoid sample rupture due to the high pressure release. Collected hydrogel specimens were immediately placed in PBS and stored at 4°C for future characterization.

## **4.2.2. Hydrogel Structural Characterization**

### **4.2.2.1. Thermal analysis by differential scanning calorimetry**

Following SF hydrogel formation, specimens were shock frozen in liquid nitrogen and subsequently lyophilized to prepare dry samples for thermal analysis. Silk hydrogel thermal properties were acquired using a differential scanning calorimeter (DSC) (Mettler, Model DSC30, Columbus, OH, USA) with N<sub>2</sub> gas flow, at a heating rate of 10 °C/min from 0°C to 350°C.

### **4.2.2.2. Fourier-Transform Infrared Spectroscopy (FTIR) analysis**

Silk protein structural characteristics were investigated before and after high pressure CO<sub>2</sub> treatment using FTIR Spectrum One (Perking Elmer, Waltham, MA, USA) with a zinc selenide crystal. To preserve the secondary structure of the obtained silk hydrogels, specimens were immediately quenched in liquid nitrogen after treatment by high pressure CO<sub>2</sub> and subsequently lyophilized for 48 hours to obtain dry samples for characterization. Structural data was acquired by loading lyophilized silk hydrogel specimens onto the IR apparatus and sample spectrums were collected as a mean of 32 acquisitions (between 4000 cm<sup>-1</sup> and 400 cm<sup>-1</sup>) with a spectral resolution of 4 cm<sup>-1</sup>. Fourier Self-Deconvolution (FSD) of the infrared

spectra spanning the amide I region (1595–1705  $\text{cm}^{-1}$ ) was employed to quantify the different silk secondary structures within the hydrogel specimens. Deconvolution was performed using parameters described elsewhere (Hu, 2006). Following deconvolution, Gaussian curve fitting was then performed with Origin 8.0 (OriginLab Corp., Northampton, MA).

#### **4.2.2.3. Morphology Assessment**

Imaging of dry hydrogel specimens was obtained using a scanning electron microscope (SEM) (Quanta 200 Scanning Electron Microscope – FE – operating mode: low vacuum, gaseous secondary electron GSE detector). Hydrated silk hydrogels were first quenched in liquid nitrogen and subsequently lyophilized for 48 hours to prepare dry cross sections for imaging. Prior to imaging, lyophilized cross sections were sputter coated (Biorad SC500, Hemel Hempstead, UK) with a thin layer of gold to avoid charging of the sample.

Imaging of wet hydrogel specimens was performed by submerging neat SF hydrogel matrices in 0.1 mg/ml Rhodamine123 solution (Sigma) at 4 °C for 8 hours (Rh123 is a green-fluorescent small molecule excitation 485nm, emission 535 nm) and then repeatedly washed in DI water to remove all un-bound dye. The non-specific adsorption of Rh123 within the SF matrices allows for visual observation of the wet hydrogel morphology (Elliott, 2015). Gels were then placed on glass slides for confocal imaging. Samples were imaged with Argon-ion laser at 488nm coupled with a band-pass emission filter 535/15 nm using a confocal microscope Nikon A1 model.

#### **4.2.2.4. Mechanical Properties in Compression**

Silk hydrogel mechanical properties were tested under compression. Compression tests of hydrogel specimens (8 mm diameter × 5 mm depth) were performed in the unconfined state by a mechanical tester (MTS) using a 5N load cell. The mechanical properties of the gel samples were tested in the wet state, in PBS, at room temperature. Strain (mm) and load (N) were recorded using Wintest software at a cross speed of 20  $\mu\text{m/s}$  up to 60% strain level. To ensure proper sample

placement and flatness, samples were cyclically preconditioned at 1% strain for 10 cycles. The compressive modulus was calculated from the tangent slope of the linear elastic region of the rendered stress/strain curve.

#### **4.2.3. Cell Culture methods**

Human mesenchymal stem cells (hMSCs) were purchased from Lonza (Switzerland) and maintained with Lonza's MSCGM human Mesenchymal Stem Cell Growth BulletKit. Reduced-serum medium consisted of Dulbecco's Modified Eagles Media (DMEM) (Hyclone, Logan/UT), with 1% defined FBS (Hyclone, Logan/UT) and 1% Penn/Strep (Invitrogen, Carlsbad, CA). Cells were cultured and maintained at 37°C and 5% CO<sub>2</sub> with medium being replaced every 72 h. Passages 3-6 were used for all experiments. Silk gels were briefly incubated in reduced-serum medium in 24-well plates and medium was aspirated just prior to seeding. hMSCs were seeded at 5 x 10<sup>4</sup> cells to the surface of each silk gel using a concentrated cell suspension. Cells were incubated for 1.5 h at 37°C and 5% CO<sub>2</sub> to allow for initial attachment before reduced-serum medium was added to the wells. Recombinant human Transforming Growth Factor-β1 (TGF-β1) was supplied by Novoprotein (Summit, NJ) and was maintained at 10ng/ml for experimental conditions requiring growth factor administration.

#### **4.2.4. Cell Characterization Methods**

##### **4.2.4.1. Quantitative real-time polymerase chain reaction (qPCR)**

Total RNA was extracted from samples using Trizol-chloroform method (Chomczynski, 1987) followed by further purification with RNeasy Kit Microkit (Qiagen) per the manufacturer's instructions. Quantification of RNA was performed on a Nanodrop 2000 spectrophotometer (Thermo Scientific). Single-stranded complementary DNA (ss-cDNA) was synthesized from RNA with iScript cDNA synthesis kit (Bio-Rad) using a Hybaid PCR Express thermal cycler per the manufacturer's instructions. SYBR RT2-qPCR primer assays from Qiagen were used with iTaq Universal SYBR Green Supermix (Bio-Rad) in this study. The primers used and their corresponding National Center for Biotechnology (NCBI) Reference

Sequence (RefSeq) numbers are listed in Table 1.  $\beta$ -actin was the reference gene. Quantitative real-time polymerase chain reaction (qPCR) was performed on either a Bio-rad CFX96 or iQ5 under the following reaction conditions: 95°C for 3 min and 40 cycles of 95°C for 5 s and 60°C for 30 s. Relative expression was calculated using quantification cycle (Cq) values as per the  $\Delta\Delta Cq$ -method and fold change was calculated using  $2^{-\Delta\Delta Cq}$  (Livak, 2001).

**Table 1** Gene information for qPCR

Gene	Symbol	Ref Seq no.
Actin, beta	<i>ACTB</i>	NM_001101.3
Actin, alpha 2, smooth muscle, aorta	<i>ACTA2</i>	NM_001613.2
Calponin 1, basic, smooth muscle	<i>CNN1</i>	NM_001299.4
Myosin, heavy chain 11, smooth muscle	<i>MYH11</i>	NM_022844.2

#### 4.2.4.2. Immunofluorescent Staining

Following cell culture, SF hydrogel samples were fixed with 3.7% formaldehyde at room temperature, permeated with 0.1% Triton X-100 and blocked with 3% BSA (Sigma). Immunofluorescent staining of cells for cell nuclei (DAPI)(Sigma) and cellular cytoskeleton (Alexa488-phalloidin) were utilized to observe cell adhesion and spreading respectively. Primary anti- $\alpha$ -actin (G-12), anti-MYH11 (G-4), and anti-Calponin 1(CALP) antibodies were supplied through Santa Cruz Biotechnologies. Secondary antibodies conjugated with either Alexa 488 or Alexa 647 along with Alexa 488-phalloidin cytoskeleton stain were acquired through Invitrogen, Inc. (Eugene, OR). Calponin and myosin heavy chain (MYH11) antigenic staining was performed to characterize SMC differentiation. For SMC marker immunostaining, samples were first incubated with primary anti-calponin or anti-MYH11 in 1% BSA overnight at 4° C. Following primary antibody coupling, samples were washed 3X in PBS and incubated with secondary antibody Alexa 488-IgG or Alexa 647-IgG for 2 h at room temperature. All samples were finally mounted with Fluoro-Gel (Electron Microscopy Services, Hatfield, PA) mounting medium and stored at 4° C for imaging.

#### **4.2.4.3. Confocal imaging**

Confocal images were acquired using a Nikon A1R laser scanning confocal microscope piloted by NIS-Elements 4.0 and equipped with 405 nm, 488 nm, 561 nm, and 640 nm laser lines. Unless otherwise stated, a 10x 0.5NA objective with the pinhole set to 1.2 Airy Units (AU) was used. When needed, multiple z planes were acquired in order to capture all of the cells within each SF hydrogel. A maximum intensity projection image or 3-dimensional rendering was then generated using ImageJ software.

#### **4.2.5. Statistical analysis**

All tests were performed in triplicate. Statistical significance of collected data was determined at each condition using an independent Student's t-test. Data are presented as mean  $\pm$  standard deviation (SD) and was considered statistically significant at 95% confidence ( $p < 0.05$ ). For qPCR, two-way ANOVA with Tukey's test was performed on  $\Delta Cq$  values using Graphpad's Prism software. Error is represented by standard error of the mean for three replicates.

### **4.3. Results**

In this study, the feasibility of using SF hydrogels with growth factor and tunable stiffness to promote vascular differentiation was evaluated. Silk hydrogels were prepared using high pressure CO<sub>2</sub>, whereby gelation proceeds through the progressive reduction in solution pH achieved under CO<sub>2</sub>-water binary systems (Floren, 2012). We found that silk hydrogels prepared by this method require less time to gelation and display improved physical properties compared to conventional hydrogel fabrication methods. We note that while our technique allows for stable hydrogel formation at low silk protein water solution concentrations, our study revealed that silk concentrations less than 1.5 wt% resulted in nonhomogeneous gel formation (results not shown) and therefore were not practical for further evaluation. Consequently, hydrogels from silk concentrations 1.5, 2, 3 and 4 wt% (SF1.5, SF2, SF3, and SF4 respectively) were prepared for this study and assessed for physical and mechanical properties.

### 4.3.1. Hydrogel Fabrication and Characterization

The macrostructures of hydrogels prepared under high pressure CO<sub>2</sub> at various silk protein concentrations are shown in Figure 1. Visual observation of the silk hydrogels indicate stable gelation and mechanical integrity are retained for all protein concentrations investigated. Structural changes associated with silk hydrogel formation were confirmed by FTIR-ATR and displayed in Figure 2A. Evaluation of the spectral regions within 1700–1500 cm<sup>-1</sup> relating to the peptide backbones of amide I (1700–1600 cm<sup>-1</sup>) and amide II (1600–1500 cm<sup>-1</sup>) are commonly utilized to observe the different secondary structures of SF (Hu, 2006). The unprocessed silk solution displayed peaks centered at 1552 cm<sup>-1</sup> (amide II) and 1654 cm<sup>-1</sup> (amide I) indicating random coil and  $\alpha$ -helix structures respectively. In contrast, silk hydrogels prepared by high pressure CO<sub>2</sub> resulted in peaks at 1625 cm<sup>-1</sup> (amide I) and 1518 cm<sup>-1</sup> (amide II) corresponding to silk II secondary structure and confirming the presence of extensive  $\beta$ -sheet crystals. Fourier self-deconvolution (FSD) analysis of the respective IR curves indicated a  $\beta$ -sheet content of 35 $\pm$  2% for the SF1.5 hydrogel samples with a gradual increase to 46  $\pm$  2% for the SF4 hydrogels. The increase in SF  $\beta$ -sheet content at greater protein concentrations has also been observed by others (Matsumoto, 2006) and is likely due to increased protein macromolecular interactions resulting in enhanced  $\beta$ -sheet formation. Figure 2B displays the thermal scans obtained by DSC for both unprocessed SF solution (a) and silk hydrogels prepared by high pressure CO<sub>2</sub> (b-e). A broad endothermic peak between 60-90°C representing bound water was observed for all samples. Unprocessed SF solution revealed a non-isothermal crystallization peak at 225°C representing the transition of amorphous silk domains into  $\beta$ -sheet structures (Hu, 2006). All silk hydrogel specimens lacked a glass transition region as well as crystallization peak due to the formation of extensive  $\beta$ -sheet structures during the CO<sub>2</sub> hydrogel fabrication process. Thermal degradation of the unprocessed silk solution occurred at a lower temperature (about 282 °C) compared to the gradual increase from 283°C to 289 °C for SF1.5 and SF4 hydrogels respectively. The lower degradation temperature observed for the SF1.5 samples compared to the SF4 specimens agrees with the lower  $\beta$ -sheet content revealed by FTIR. Collectively,

these observations indicate silk-CO<sub>2</sub> hydrogels exhibit extensive  $\beta$ -sheet crystal domains, permitting stable gel formation at all protein concentrations investigated.

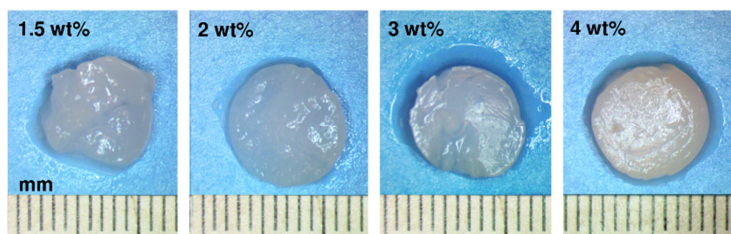


Figure IV - 1. Gross characterization of SF hydrogel matrices prepared at different protein concentrations.

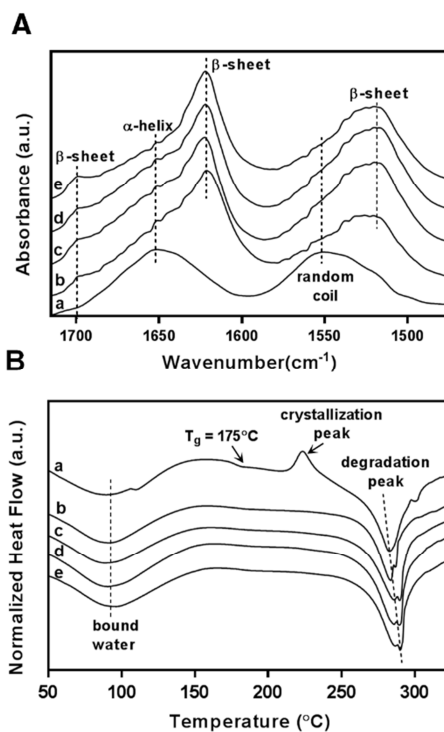
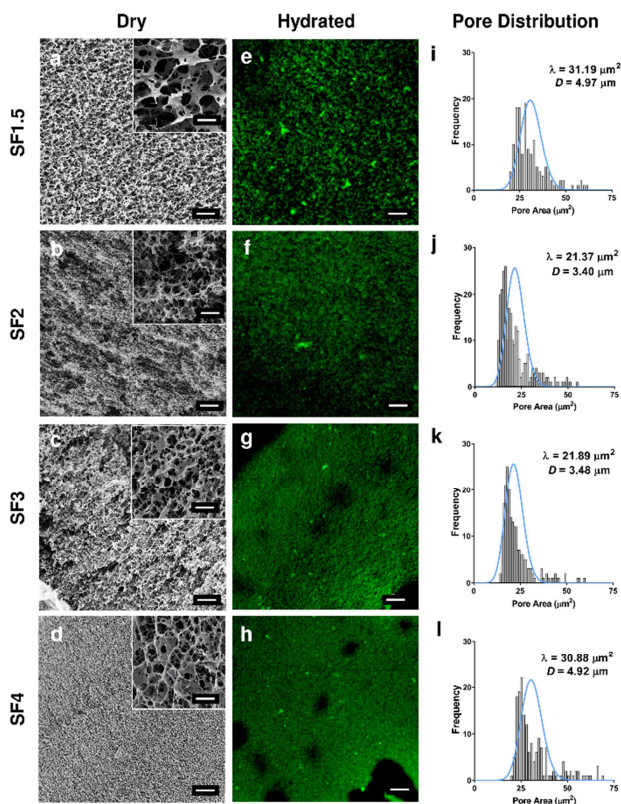


Figure IV - 2. Structural properties of SF hydrogels prepared by high pressure CO<sub>2</sub>. (A) FTIR-ATR spectra reveal the presence of extensive  $\beta$ -sheet crystalline secondary structures in prepared hydrogel specimens; unmodified silk solution (a), prepared silk hydrogels SF1.5 (b), SF2 (c), SF3 (d), and SF4 (e). (B) DSC curves demonstrate stability under thermal scans for

unmodified silk solution (a) and prepared silk hydrogels SF1.5 (b), SF2 (c), SF3 (d), and SF4 (e).

#### **4.3.2. Hydrogel Pore Characteristics**

SF hydrogel morphology characteristics were evaluated using SEM in the dry state (Figure 3a-d) and compared against wet state imaging (Figure 3e-h) using CLSM. Dry state imaging revealed a porous matrix with average pore sizes ranging from  $3.40 \pm 0.58$  -  $4.97 \pm 1.28$   $\mu\text{m}$  for all SF hydrogel concentrations. A slight decrease in pore size was observed for SF2 and SF3 hydrogel specimens at  $3.40 \pm 0.58$   $\mu\text{m}$  and  $3.48 \pm 0.42$   $\mu\text{m}$  average pore size, respectively. By comparison, the average pore sizes for SF1.5 and SF4 were greater at  $4.97 \pm 1.28$  and  $4.92 \pm 0.83$   $\mu\text{m}$ , respectively. Analysis of SF hydrogel pore distributions were not found to be significantly different. Comparison of the dry state pore size and distribution were in good agreement with the complimentary measurements achieved using wet state imaging. The average pore sizes reported here correlate well with SF hydrogels prepared in our previous work (Floren, 2012).



**Figure IV – 3.** Morphology assessment of silk hydrogel matrices. (a-d) Scanning electron microscopy images of silk hydrogels in dry state; inset magnification scale bars 5  $\mu\text{m}$ . (e-h) Hydrated silk hydrogel images obtained by confocal laser microscopy. Scale bars 20  $\mu\text{m}$ . (i-l) Silk hydrogel pore distributions, with respective Poisson distributions (blue lines), and pore size quantified by image analysis of respective micrographs (a-h).

#### 4.3.3. Hydrogel Compressive Properties

To assess SF hydrogel mechanical properties, we evaluated the mechanical response of all specimens in compression. Figure 4a represents the stress-strain curves of SF1.5, SF2, SF3 and SF4 hydrogel specimens tested in compression. All SF hydrogel samples displayed a linear response up to 10% strain level, demonstrating the elasticity of fabricated hydrogels. The compressive modulus of the hydrogel samples increased as SF concentration increased (Figure 4b). The

compressive modulus increased by 10-fold from SF1.5 ( $6.41 \pm 0.47$  kPa) to SF4 hydrogels ( $63.98 \pm 2.42$  kPa). The elastic moduli of SF hydrogels displayed here, ~6 – 64 kPa, represent a biologically relevant stiffness range for native vasculature, suggesting their potential use for vascular tissue engineering substrates (Wingate, 2012).

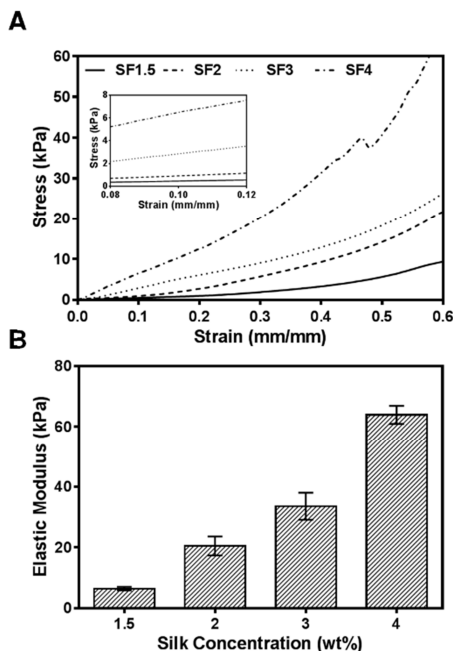


**Figure IV – 4.** Mechanical properties of SF hydrogels prepared by high pressure CO<sub>2</sub>. (A) Stress vs. strain relationships for several hydrogel matrices prepared with different silk protein content. Inset represents linear region used to determine mechanical properties. (B) Elastic moduli of these matrices.

#### 4.3.4. Effect of SF Hydrogel Rigidity on hMSC attachment and spreading in Low-Serum or TGFβ-1 Fortified Media

Serum-containing media, including more defined serum mixtures for stem cell culture, is often not well defined, incorporating several combinations of factors as well as high variability among lots (El-Mounayri, 2013). From this stance, serum-based differentiation protocols do not allow for unadulterated manipulation of the biochemical milieu necessary to define concise spatiotemporal microenvironments.

Therefore, to suppress the potential for compounding effects of soluble factors, we chose low-serum (1% defined FBS) culture conditions for all experiments.

To confirm the biocompatibility of our SF hydrogels, we cultured hMSCs for 72 h in media either with low serum or TGF- $\beta$ 1 (+) (10ng/ml) supplemented low serum, and evaluated cell attachment and spreading (Figure 5a-h). Human MSC attachment was observed for all SF hydrogel formulations. Utilizing image analysis, we measured hMSC density after culturing on SF hydrogels for 72 h with variable stiffness. Human MSC density increased from  $150 \pm 30$  cells/mm<sup>2</sup> to  $622 \pm 87$  cells/mm<sup>2</sup> for 6 kPa (SF1.5) and 64 kPa (SF4) hydrogels in low-serum culture conditions respectively (Figure 5j). Likewise, supplementing low-serum media with 10 ng/ml of TGF- $\beta$ 1 resulted in a significant ( $p < 0.05$ ) increase in the cell density for all SF hydrogel elasticities studied with an increase from  $427 \pm 28$  cells/mm<sup>2</sup> to  $798 \pm 26$  cells/mm<sup>2</sup> for 6 kPa (SF1.5) and 64 kPa (SF4) hydrogels, respectively. This data suggests that hMSC attachment positively correlates with SF hydrogel stiffness and TGF- $\beta$ 1 administration.

Significant cell spreading was observed (Figure 5a-h) and distinct cellular morphologies revealed for all SF hydrogel samples (Figure 5i) irrespective of growth factor intervention. Cell spreading area was quantified using image analysis and normalized to the respective cell density of each specimen. We found no significant differences in cell spreading area for SF hydrogels of different stiffness or growth factor protocol with the exception of the 6 kPa (SF1.5) hydrogel under low-serum conditions. The discrepancy in cell spreading area for the 6 kPa (SF1.5) low-serum condition is likely due to the reduced cell density measured for these samples, which could facilitate enhanced cellular spreading throughout the substrate. Altogether, our findings suggest that the SF hydrogels produced here provide a sustainable microenvironment for hMSC attachment and spreading in the presence of low-serum or TGF- $\beta$ 1 fortified media.

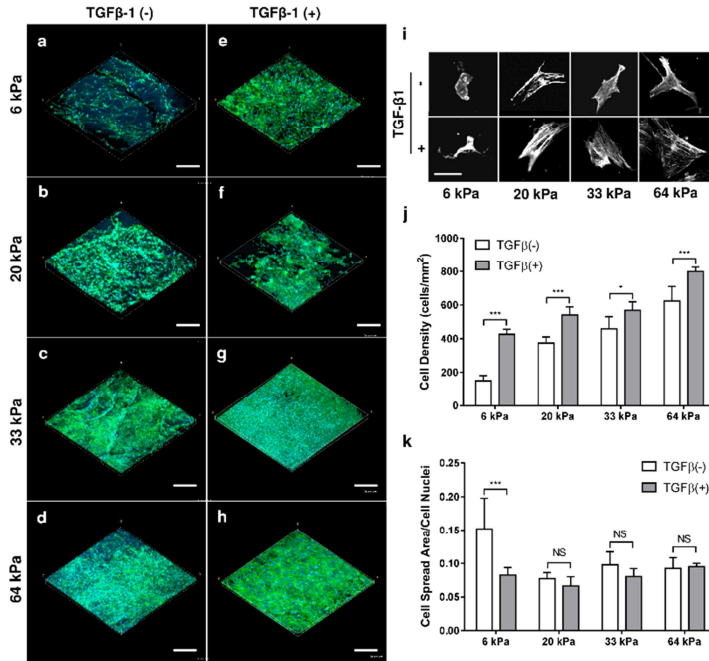


**Figure IV – 5.** Effects of SF hydrogel stiffness and TGF- $\beta$ 1 on attachment and spreading of hMSCs. (a-h) Confocal stack renderings of hMSCs with (e-h) or without (a-d) TGF-  $\beta$ 1 at various SF hydrogel elasticities (SF1.5-6kPa, SF2-20kPa, SF3-33kPa, SF4-64kPa). Cells were stained for cell nuclei (DAPI, blue) and F-actin (phalloidin, green), scale bar 300  $\mu$ m. (i) Individual hMSC morphologies imaged and presented in grayscale with respect to SF hydrogel stiffness and TGF-  $\beta$ 1 administration; scale bar 50  $\mu$ m. Cell density (j) and attachment (k) of hMSCs for all the hydrogel matrices shown in images a-h were quantified and tabulated. \*  $P < 0.05$ , \*\*\*  $P < 0.001$ , NS  $P > 0.05$ .

#### 4.3.5. Effect of SF Hydrogel Rigidity and TGF- $\beta$ 1 on Vascular SMC Commitment of hMSCs

Myogenic differentiation was evaluated by real time PCR and assessed for SMC-specific marker expression of smooth muscle  $\alpha$ -actin ( $\alpha$ SMA), calponin, and smooth muscle myosin heavy chain (MYH11) as shown in Figure 6a-c. Human MSCs cultured without TGF- $\beta$ 1 for 72 h on SF hydrogels displayed non-significant ( $p > 0.05$ ) variation in  $\alpha$ SMA and calponin gene expression for all elasticities investigated when compared to the culture plate control (Figure 6a-b). In contrast, in the absence of TGF- $\beta$ 1 administration the gene expression of the mature SMC

marker, MYH11, was significantly ( $p < 0.05$ ) upregulated on 33 kPa (SF3) substrate compared to the culture plate condition (Fig 6c).

Interestingly, the inclusion of 10 ng/ml of TGF- $\beta$ 1 did not result in significant variation of  $\alpha$ SMA transcription levels for all SF hydrogels investigated, Figure 6a. However, a significant ( $p < 0.05$ ) variation in calponin gene expression was recorded on 6 kPa soft hydrogel (SF1.5) with and without TGF- $\beta$ 1 as shown in Figure 6b. By comparison, the administration of TGF- $\beta$ 1 significantly ( $p < 0.001$ ) upregulated MYH11 gene expression on 33 kPa (SF3) over all others, 6 kPa (SF1.5), 20 kPa (SF2), 64 kPa (SF4) and culture plate (Fig 6c). Further, a significant ( $p < 0.05$ ) difference was also observed on 33 kPa (SF3) among TGF- $\beta$ 1 (+) and TGF- $\beta$ 1 (-) conditions. The greater variation of MYH11 gene expression for hMSCs cultured on SF hydrogels with TGF- $\beta$ 1 compared to TGF- $\beta$ 1 (-) conditions indicates that a crosstalk exists between physical cues (stiffness) and chemical stimuli (TGF- $\beta$ 1), which regulate hMSC fate decisions.

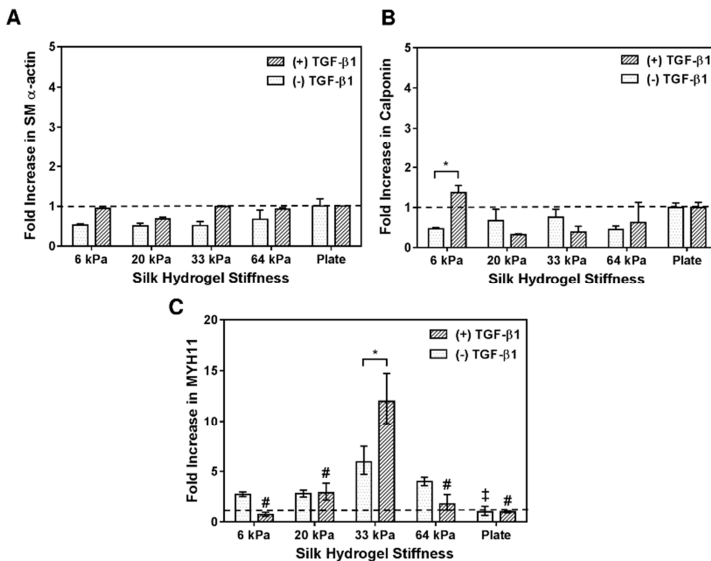


**Figure IV - 6.** PCR assessment of selected vascular markers of hMSCs cultured on silk hydrogels of different stiffness for 72 h: (a) smooth muscle  $\alpha$ -actin, (B) calponin, and (C) MYH11. \* indicates significant difference between groups ( $p < 0.05$ ). † indicates significant ( $p < 0.05$ ) difference from the gene expression for hMSCs cultured without TGF- $\beta$ 1 on SF hydrogels compared to 33 kPa (SF3) condition. # indicates significant ( $p < 0.001$ ) difference in gene

expression for hMSCs cultured with TGF- $\beta$ 1 on SF hydrogels compared to 33 kPa (SF3) condition.

We further confirmed stem cell lineage commitment using the protein level expression of calponin and MYH11 for hMSCs cultured on SF hydrogels with TGF- $\beta$ 1 for 72 h (Figure 7). High levels of calponin were detected for SF1.5, SF2, SF3 hydrogels 6, 20, and 33 kPa stiffness respectively, Figure 7. Consistent with reported gene expression, MYH11 protein expression was detected for all SF hydrogel conditions with greatest expression on 33 kPa (SF3) substrate. Compared to softer SF hydrogels, calponin and MYH11 expression were absent on stiff condition (SF4). Altogether, these results suggest that appropriate substrate stiffness and growth factor presentation can achieve mature and directed differentiation of hMSCs, specifically in the context of vascular SMCs.

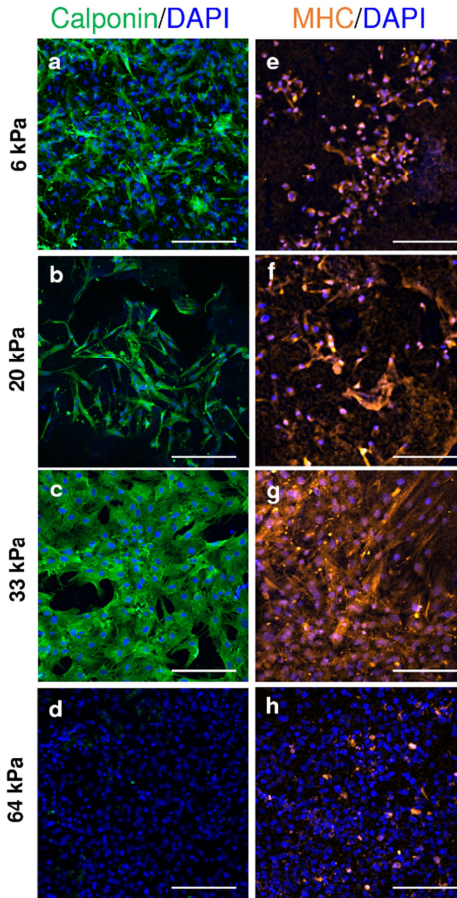


**Figure IV – 7.** Immunostaining of hMSCs cultured with TGF- $\beta$ 1 on SF hydrogels of different stiffness for 72 h for select vascular SMC markers: calponin (a-d) (green), MYH11 (e-h) (orange). Scale bar 200  $\mu$ m.

#### **4.4. Discussion:**

Stem cells develop an exquisite relationship with their surroundings which elicit an ensemble of cellular events influenced not only by the physical environment, such as rigidity (Engler, 2006) and geometry (Huebsch, 2010), but also the chemical makeup of their milieu through growth factors (Narita, 2008) and cytokines (Discher, 2009), amongst others (Phillips, 2010). Recent evidence suggests a complex

interplay whereby matrix physical and chemical stimuli may work synergistically to direct highly specialized cellular events and fate outcomes (Park, 2011; Wingate, 2014). Therefore, resolving the effects associated with the crosstalk of physicochemical stimuli within the *in vivo* microenvironment may provide a template for the rational design of specialized and directed stem cell differentiation platforms. We chose to address these queries by examining the vascular fate commitment of hMSCs cultured on SF hydrogels of different stiffness in the presence of growth factor (TGF- $\beta$ 1) administration.

To minimize the compounding effects of other biological stimuli, we selected a substrate material that allowed for cellular attachment in the absence of defined biological ligands or serum proteins. The tunable properties of SF allow for the regulation of format and substrate mechanical properties with high fidelity, meanwhile highly biocompatible. In our hands, we find SF hydrogels prepared from a simple CO<sub>2</sub> processing technique to be a promising biomaterial platform for probing the effects of substrate stiffness and cell maintenance and fate commitment. Here we report tunable stiffness of our SF hydrogels by simple adjustment of the starting silk protein in water concentration. This observation is complimentary to previous studies using SF protein concentration to modulate substrate mechanical properties (Kundu, 2013; Floren, 2012). When cultured with serum-starved media upon our SF hydrogels hMSCs attached and spread for up to 72 h (Supplementary Figure 1). This data suggests that SF is permissive to stem cell adhesion and maintenance irrespective to the presentation of adsorbed serum proteins or other biological ligands. The exact mechanism of hMSC adhesion and maintenance in low serum media demonstrated here on SF hydrogels is not immediately understood. Sengupta et al demonstrated an upregulation of integrin alpha-5 (ITGA5) in hMSCs cultured on SF patterned films (Sengupta, 2010), which may be a result of sparse RGY and RGV sequences previously identified in SF (Zhou, 2001). Recent reports have also demonstrated a potential CD44 interaction for fibroblasts (Yang, 2010) and rat MSCs (Yang, 2014) cultured on SF constructs. From the cited literature, it is likely that hMSC-SF interactions are a result of the unique material chemistry of SF. Future studies are needed to elucidate the distinct cellular interactions of specific cell lines, particularly stem cells, upon SF-based materials.

The TGF- $\beta$  family regulates a diversity of cellular functions during development and tissue homeostasis through their effects on cell proliferation, differentiation, apoptosis and ECM production (Derynck, 1997; Roelen, 2003). Several reports have implicated TGF- $\beta$ 1 promoting MSC differentiation into SMC lineage (Narita, 2008; Kinner, 2002), and further evidence suggests that these TGF- $\beta$ 1 pathways may form a crosstalk with other signaling events elicited through mechanosensing stimuli such as substrate rigidity (Park, 2011). However, the role that these different micro-environmental factors play independently and in concert towards mature vascular SMC differentiation has yet to be studied in a relevant platform for potential tissue engineering scaffolds such as SF hydrogel matrices.

The inclusion of 10 ng/ml of TGF- $\beta$ 1 to our cell culture regiment significantly ( $p < 0.05$ ) increased cell density of hMSCs upon the SF hydrogels irrespective of stiffness. This is consistent with other studies that have reported on the cell attachment and proliferation of hMSCs on substrates of variable stiffness (Engler, 2006). Interestingly, we did not find significant differences of hMSC spreading between groups (stiffness and TGF-beta) with the exception of the low stiffness condition (6 kPa). Cell spreading and morphology in two dimensions are strongly correlated to stem cell differentiation and lineage commitment (Engler, 2006); whereas, recent evidence suggests this phenomenon is less pronounced in three dimensions (Huebsch, 2010). We note that while our porous SF hydrogels do not allow deep penetration of cells into the matrices, our system still mimics a three dimensional environment which may impart analogous geometrical cues as observed in other defined three dimensional substrates; thereby, resulting in similar cellular morphologies between groups.

Strikingly, we demonstrated a significant increase in both the gene and protein expression of the mature vascular SMC marker MYH11 for hMSCs cultured on SF hydrogel with TGF- $\beta$ 1 within 72 h. We observed a strong correlation of SF substrate stiffness to upregulate MYH11 expression both with and without TGF- $\beta$ . For instance, MYH11 expression was detected both on the gene and protein level for soft (6 kPa, SF1.5) to mid-range stiff (33 kPa, SF3) SF hydrogels. In particular, we observed an approximate 12 and 6 fold increase in MYH11 gene expression for 33 kPa (SF3) hydrogel with and without TGF- $\beta$  regiment. In contrast, early SMC

markers ( $\alpha$ SMA) and (calponin) transcription levels were not significantly upregulated for all conditions, with the exception of 6 kPa (SF1.5) soft hydrogel, TGF- $\beta$ 1 (+) and TGF- $\beta$ 1 (-) groups. Consistent with our findings, Park et al. reported transcription levels for  $\alpha$ SMA and calponin in hMSCs cultured with 10 ng/ml TGF- $\beta$  on soft (15 kPa), two-dimensional gelatin substrates were comparable to transcription levels of the culture plate control (Park, 2011).

Previously, authors have reported on directed hMSC differentiation towards myogenic lineage by regulating substrate stiffness (Engler, 2011) or combining with TGF- $\beta$ 1 administration (Park, 2011). However, these studies only investigated early ( $\alpha$ SMA, calponin) myogenic markers, but often achieving directed stem cell differentiation towards a mature status is desired (Andreadis, 2013). Stem cell differentiation into SMC-like populations is repeatedly evaluated by identifying the expression of several candidates involved in the contractile apparatus such as  $\alpha$ SMA, h1-calponin, MYH11 and desmin (Liu, 2013). However, recent evidence suggests that some SMC markers are potentially expressed at measurable levels in multipotent MSCs. For instance, MSCs cultured without differentiation media expressed mRNA levels for several SMC markers at levels comparable to primary SMCs, with the exception being the mature SMC marker MYH11 (Tamama, 2008). Indeed, MYH11 is only expressed late in myogenesis and displays the highest specificity of SMC differentiation compared to any other known marker (Owens, 2004). Collectively, these recent findings suggest that mature markers such as MYH11 logically serve as a reliable indication of mature SMC phenotype in hMSCs as shown here.

Our results support the hypothesis that the convergence of physical and chemical environmental cues can lead to specific and directed differentiation of hMSCs into matured vascular SMCs. Our data suggests that proper substrate stiffness and growth factor (TGF- $\beta$ ) can significantly upregulate SMC genes and protein expression. We note that one limitation of our method is the potential differences of SF hydrogel water content or network density among the different hydrogel formulations. Recently, Wen et al. systematically modulated the porosity, ligand density and stiffness of polyacrylamide (PA) hydrogels and observed how these properties affect stem cell fate processes (Wen, 2014). Here the author's

concluded that stiffness rather than porosity or ligand density was the primary impetus driving stem cell differentiation. In line with this, while it is difficult to decouple certain physical parameters (i.e. porosity, network density) from our SF hydrogel formulations presented here, evidence suggests that substrate stiffness is the dominant physical parameter in directing stem cell fate, as demonstrated here.

Previous studies have highlighted a significant crosstalk between substrate rigidity and growth factor activity. Regulation of MSC commitment into chondrogenic or myogenic phenotypes on two dimensional matrices can be modulated based on substrate stiffness and TGF- $\beta$ 1 administration (Park, 2010). Recently, soft (2 kPa), three dimensional matrices combined with vascular endothelial growth factor (VEGF) were revealed to act synergistically to guide MSC differentiation into mature endothelial phenotype while enhancing paracrine signaling (Wingate, 2014). Indeed, there is growing evidence that a tight interplay exists between ECM mechanical properties and the activity and availability of several growth factors. It is well established that ECMs provide not only physical support for cellular processes but also act as a repository for a plethora of chemical signals (Martino, 2014). For instance, TGF- $\beta$ 1 is believed to form a physical association with numerous ECM proteins and only through matrix straining, via cell contractile forces transmitted through integrins, is it liberated and active (Hinz, 2015). In line with this, Wipff et al. demonstrated a positive correlation between TGF- $\beta$ 1 activation and polyacrylamide hydrogel stiffness for cultured fibroblast and epithelial cells (Wipff, 2007). Here the authors proposed a contraction-mediated activation of TGF- $\beta$ 1 whereby increasing ECM stiffness (i.e. polymer stiffness) resulted in increased levels of active TGF- $\beta$ 1. Nonetheless, it remains to be resolved how mechanical activation of TGF- $\beta$ 1 is achieved using our current SF hydrogel system. From the cited literature, there is evidence to suggest that ECM mechanics play a critical role in the deployment and activation of chemical signals in the cellular microenvironment. Our results are complementary to these findings, whereby stem cell behavior can be regulated based on the integration of substrate physical and chemical properties.

Although others have reported on the differentiation of stem cells towards mature SMC lineage, our study advances these previous results in several ways. First, we explored the potential to direct specialized hMSC differentiation by

modulating stiffness and growth factor using a well-defined biomaterial scaffold platform. In contrast to previous studies, our methodology employs SF, a well-tolerated biomaterial with an impressive portfolio of tissue engineering applications. Secondly, we demonstrate the expression of a mature SMC marker (MYH11) within the span of 72 h with appropriate substrate stiffness 33 kPa (SF3) and growth factor (10 ng/ml TGF- $\beta$ 1). By comparison, El-Mounayri et al. derived mature and functional human coronary-like vSMCs from embryonic stem cells (ESCs) using a complex growth factor regiment across 28 d (El-Mounayri, 2013). We acknowledge the limitation that our study did not show the functional behavior of the SMC line derived here from hMSCs; however, our methodology suggests that complex differentiation protocols may be simplified by engineering the cellular microenvironment on multiple scales, i.e. matrix stiffness with growth factor. Third, it highlights the significance of designing multifaceted biomaterial matrices, culminating physical and chemical cues, to direct stem cell differentiation in a highly controlled and specialized approach.

#### **4.5. Conclusion:**

There is a growing consensus that the next generation of biomaterial platforms must adopt a biomimetic approach whereby the integration of physical and chemical environmental cues becomes necessary to direct highly specialized cellular processes, including stem cell fate decisions. This study demonstrates the potential utility of SF hydrogels as a tunable platform, integrating physical (stiffness) and chemical (TGF- $\beta$ 1) stimuli, for directed and specialized differentiation of hMSCs. Our results demonstrate that SF hydrogels provide a permissive environment for hMSCs in the absence of serum media, meanwhile tunable in stiffness by simple adjustment of SF protein content. Further, we report on the ability to augment hMSC differentiation into mature SMCs within modest culture periods (72 h) by combining appropriate SF hydrogel stiffness (33 kPa) with growth factor (TGF- $\beta$ 1). This study advances our understanding of how complex multicomponent biomaterials, whereby mimicking the intricacy of natural tissue environments, can play a significant role in developing optimal stem cell differentiation protocols. Ultimately, such an understanding of how engineered cellular niche environments interact with stem cell

fate processes will be instrumental in the design of future tissue engineering platforms.

## Chapter V

# Three-Dimensional, Soft Neotissue Arrays as High Throughput Platforms for the Interrogation of Engineered Tissue Environments

*Part of this chapter has been published in: Biomaterials*

Michael Floren, Wei Tan. "Three-Dimensional, Soft Neotissue Arrays as High Throughput Platforms for the Interrogation of Engineered Tissue Environments". *Biomaterials*, 59 (2015) 39-52.

**Abstract:** Local signals from tissue-specific extracellular matrix (ECM) microenvironments, including matrix adhesive ligand, mechanical elasticity and micro-scale geometry, are known to instruct a variety of stem cell differentiation processes. Likewise, these signals converge to provide multifaceted, mechanochemical cues for highly-specific tissue morphogenesis or regeneration. Despite accumulated knowledge about the individual and combined roles of various mechanochemical ECM signals in stem cell activities on 2-dimensional matrices, the understandings of morphogenetic or regenerative 3-dimensional tissue microenvironments remain very limited. To that end, we established high-throughput platforms based on soft, fibrous matrices with various combinatorial ECM proteins meanwhile highly-tunable in elasticity and 3-dimensional geometry. To demonstrate the utility of our platform, we evaluated 64 unique combinations of 6 ECM proteins (collagen I, collagen III, collagen IV, laminin, fibronectin, and elastin) on the adhesion, spreading and fate commitment of mesenchymal stem cell (MSCs) under two substrate stiffness (4.6 kPa, 20 kPa). Using this technique, we identified several neotissue microenvironments supporting MSC adhesion, spreading and differentiation toward early vascular lineages. Manipulation of the matrix properties, such as elasticity and geometry, in concert with ECM proteins will permit the

investigation of multiple and distinct MSC environments. This paper demonstrates the practical application of high through-put technology to facilitate the screening of a variety of engineered microenvironments with the aim to instruct stem cell differentiation.

## **5.1. Introduction**

There is abundant evidence suggesting that local signals from tissue-specific extracellular matrix microenvironments significantly affect cellular differentiation, phenotypic expression and maintenance (Reilly, 2010; da Silva Meirelles, 2008; Bajpai, 2012). Substrate biophysical signals, such as soluble factors (Bajpai, 2012), cell-ligand interactions (Suzuki, 2010), matrix elasticity (Engler, 2006; Discher, 2005) and geometry (Huebsch, 2010) play critical roles in a diversity of biological events including cell adhesion, growth, differentiation, and apoptosis (Huebsch, 2010; Wingate, 2012). Together these signals converge to provide a multifaceted, complex mechanochemical signaling environment for highly-specific tissue morphogenesis and regeneration. Despite accumulated knowledge regarding individual and combined roles of various mechanochemical ECM signals in stem cell activities, the intricacy exhibited by cellular microenvironments poses a considerable challenge in resolving the mechanisms ascribed to stem cell behavior and fate determination processes. This complexity mandates a systemic approach whereby integrative studies must be expanded to capture a more comprehensive understanding of the determinants which direct stem cell differentiation toward desired cell type and function. Conventional methods to elucidate these mechanisms have traditionally been executed in large scale, two-dimensional tissue culture platforms which are often limited by combinatorial brevity, substrate production, and reagent supply. Furthermore, these signals, matrix and biophysical, are often observed independently to differentiate cells on 2-dimensional substrates, an environment vastly different from the way cells are presented naturally in vivo, i.e. a 3-dimensional tissue context which elicits multiple signal inputs to regulate cell fate.

High through-put approaches have emerged in recent years to circumvent the limitations of traditional low through-put techniques (i.e. conventional cultureware), with the promise to develop complex platforms for combined

biomolecule/substrate discovery. The salient features of microarray technology include the reproducibility and screening of multiple microenvironments with significantly less reagent and substrate requirements than traditional methods, while lending improved deconstruction of complex multivariable studies (Titmarsh, 2013). Several reports have demonstrated ECM protein microarrays (Flaim, 2005), soluble factor screening (Ghaedi, 2011), biomaterial chemistry screening (Anderson, 2004; Mei, 2010), and multiple signal integration arrays (i.e. elasticity and chemical factor) with encouraging results (Gobaa, 2011; Wingate, 2014). However, despite the versatility afforded by current microarray technologies, the incorporation of multiple signals within engineered microarrays remain limited. Meanwhile the integration of current combinatorial microarray technologies in three-dimensions, coupled with other biophysical properties, such as tunable stiffness and geometry, have yet to reach fruition. Capturing complex, multifaceted 3-dimensional environments in high-throughput with combinatorial signaling will likely prove instrumental towards the design of future tissue regeneration biomaterial platforms.

To resolve the mechanisms associated with complex matrix signals and stem cell behavior and fate decisions, we established a high-throughput ECM platform based on soft, fibrous matrices meanwhile highly-tunable in elasticity and 3-dimensional geometry. The technology we demonstrate here is amenable to manipulation of several matrix properties, such as elasticity and geometry, in concert with customizable ECM protein micro-dot combination. Furthermore, selective cellular adhesion and isolation afforded by ECM microarrays permits the investigation of multiple and distinct cellular microenvironments in the presence of specific ECM signaling. Altogether, we demonstrate the practical adaptation of high-throughput technology to facilitate the screening of various tunable mechano-ligand microenvironments in three dimensions with the aim to optimize stem cell fate decisions.

## **5.2. *Materials & Methods***

### **5.2.1. *Materials***

Polyethylene glycol dimethacrylate (PEGDM) with a molecular weight of 750 kDa and polyethylene oxide (PEO) (MW 400 kDa) were purchased from Sigma (St. Louis, MO). The photoinitiator Irgacure ® 2959 was purchased through Ciba Specialty Chemicals Corp. (Tarrytown, NY). (3-trimethoxysilyl)propyl methacrylate (TMPMA) was purchased through Sigma. Rhodamine-methacrylate was supplied by Polysciences, Inc. (Warrington, PA). Albumin-Cy3 and streptavidin-Cy5 protein conjugates were acquired through Life Technologies (Grand Island, NY). Microarray print buffer components, glycerol, triton X-100, were purchased through Sigma. Collagen I extracted from rat tail was supplied by Sigma. Collagen III and collagen IV were extracted by human placenta and provided by Sigma. Laminin from Engelbreth-Holm-Swarm murine sarcoma basement membrane was acquired through Sigma. Fibronectin purified from human plasma was obtained through EMD Millipore Corp. (Temecula, CA.).  $\alpha$ -elastin extracted from bovine ligament was purchased from Elastin Products Co (Owensville, Missouri). Anti-collagen I, anti-collagen III, anti-collagen IV, anti-laminin, anti-fibronectin and anti-elastin primary antibodies were obtained from EMD Millipore Corp. Secondary antibody Cy3 conjugate was purchased through EMD Millipore Corp. Primary rat pulmonary arterial smooth muscle cells (PASMCs) were maintained in DME-F12 (Hyclone, Logan, UT), with 10% fetal bovine serum (FBS, Atlanta Biologicals, Flowery Branch, GA) and 1% Pen/Strep (Hyclone, Logan, Ut). Rat mesenchymal stem cells were maintained in DMEM (Corning, Corning, New York) with 10% defined FBS (Hyclone) for MSCs and 1% Penn/Strep (Hyclone). Bovine serum albumin (BSA) was obtained from Sigma. (4',6-diamidino-2-phenylindole) DAPI nuclear stain and Alexa488-phalloidin cytoskeleton stain were purchased through Invitrogen, Inc. (Eugene, OR). Primary anti-PECAM antibody was supplied through Novus Biologicals (Littleton, CO). Secondary anti-rabbit IgG antibody conjugated with Alexa 555 was acquired through Invitrogen, Inc. Vectashield hard mount mounting media was obtained through Vector Laboratories, Inc. (Burlingame, CA).

### **5.2.2 Fabrication of PEGDM Soft Matrices**

An electrospinning solution composed of 3.2% wt PEGDM 750, 3.4% wt PEO, 0.4 % wt of Irgacure 2959 and 93% DI H<sub>2</sub>O was mixed for 30 minutes with magnetic

stir bar. PEGDM 750 photopolymerizable soft matrices were fabricated by electrospinning on a custom setup comprised of a high voltage power supply (Gamma High Voltage Research, Ormond Beach, FL), grounded collecting surface, motorized syringe pump (NE-300 New Era Pump Systems, Farmingdale, NY), and a 14mm syringe. The solution (2 ml) was spun at a distance of 26 cm from the stationary collecting surface, at the voltage of 30 kV, and a flow rate of 1.10 ml/hr. Electrospun matrices were deposited onto standard glass slides (25mm X 75mm, Fischer Scientific Inc.) that were pretreated with TMPMA to present methacrylate groups that can bond the matrices to the glass. PEGDM matrices were subsequently introduced into an inert argon environment to remove oxygen, and then were stabilized with polymerization under UV exposure (352 nm light) with an average intensity of 5 mW/cm<sup>2</sup> for predetermined time durations.

### **5.2.3. Characterization of PEGDM Soft Matrices**

#### **5.2.3.1. FTIR Analysis**

PEGDM electrospun samples were first loaded into a sealed liquid-cell (Sigma), in the presence of an inert argon environment to prevent oxygen contamination during IR acquisition. The double bond conversion in PEGDM was evaluated using a real-time mid-range Fourier transform infrared spectroscopy (FTIR) (Nicolet 4700, Thermo Fisher Scientific, Waltham, MA) by examining the disappearance of the C=C peak within the methacrylate group (at ~1635cm<sup>-1</sup>) over time during polymerization under UV light (5 mW/cm<sup>2</sup>). To account for sample and background variation, data were normalized with the C=O peak located in the range from 1650 to 1726 cm<sup>-1</sup>.

#### **5.2.3.2. Scanning Electron Microscopy Imaging**

Scanning electron microscopy (FESEM, JSM-7401F, Jeol Ltd, Tokyo, Japan) was used to examine the microstructure of the electrospun PEGDM substrates in both dry and hydrated states. For hydrated samples, substrates were photopolymerized for 15 min and rinsed in DI H<sub>2</sub>O for 24 hr. To prepare for imaging, rinsed samples were shock frozen in liquid nitrogen (-195°C), and lyophilized for

approximately 24 hr. ImageJ was used to analyze changes in fiber diameter and porosity.

### **5.2.3.3. Fluorescent Imaging**

To image the structure of PEGDM soft matrices in their hydrated state, rhodamine-methacrylate was introduced into the electrospun fibers and subsequently stabilized with UV exposure to provide fluorescence of the fibrous structure. Matrices with PEGDM-rhodamine conjugates were then visualized using either a fluorescent microscope or a confocal laser scanning microscope.

### **5.2.3.4. Rheology**

Changes in the storage modulus ( $G'$ ) of PEGDM substrates with respect to photopolymerization time were characterized using a rheometer, (ARES TA rheometer, TA Instruments, New Castle, DE). PEGDM matrices, with approximately 0.3mm in thickness, were deposited onto TMPMA-modified circular coverslips (18mm in diameter) and photopolymerized for 2, 5, 10, or 15 min, and then rinsed in DI H<sub>2</sub>O for 24 hr. PEGDM soft matrices were tested with a parallel plate configuration. A vertical load of 5 grams was applied to all samples to prevent slippage. A strain sweep at a frequency of 1 rad/s and a frequency sweep at a strain of 5% were run on each sample. Specimen were inspected for slippage or tearing after shearing, and data collected from the linear viscoelastic region in the strain sweep were used to determine the storage modulus  $G'$ . Elastic modulus was calculated using the following relationship:  $E = G'(1+\nu)$  where E is elastic modulus,  $G'$  is storage modulus measured in shear and  $\nu$  is the Poisson's ratio taken as approximately zero (Fozdar, 2011).

### **5.2.4. ECM Protein Array Preparation**

Protein printing efficiency and optimization was developed using control proteins albumin-Cy3 and streptavidin-Cy5 conjugates. A printing buffer consisting of 1% glycerol and 0.2% Triton X-100 was utilized for all protein depositions. To prepare ECM arrays, stock solutions of collagen I, collagen III, collagen IV, fibronectin, laminin, and elastin were suspended at a concentration of 250  $\mu\text{g}/\mu\text{l}$  in

printing buffer. For combinatorial arrays, collagen I is denoted as C1, collagen III as C3, collagen IV as C4, fibronectin as Fn, laminin as L, and elastin as E. Samples were deposited on the fibrous PEGDM matrix using Aushon 2470 arrayer with 185 micron pins (Aushon BioSystems, Billerica, MA), to achieve dots with a nominal diameter of 250 microns. Individual spots with 7 replicates (total of 8) of each protein combination were deposited with a 500  $\mu\text{m}$  pitch distance onto the PEGDM matrices. Between different sample depositions, the print needles were cleaned by sonication in cleaning solution before use. Approximately twenty ECM microarrays could be deposited simultaneously in this method within  $\sim 1\text{hr}$ . Prepared ECM microarrays were stored at  $4^\circ\text{C}$  in a humid environment for 24 h before use.

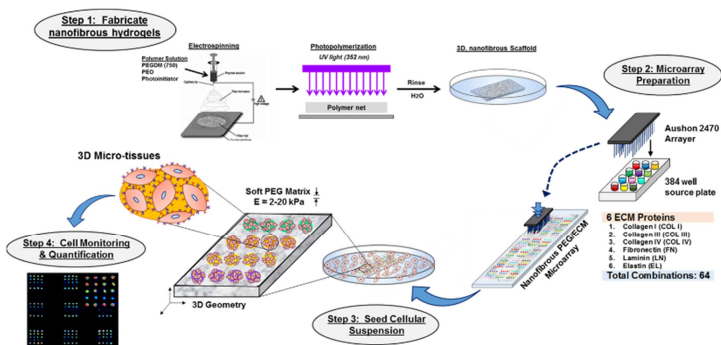


**Figure V - VI.** Illustration of ECM Neotissue Fabrication and Utility for Multivariate Cell Culture Platforms.

### 5.2.5. Cell Seeding and Cell Culture

The microarray slides of fibrous PEGDM matrix containing ECM proteins were rinsed in DI  $\text{H}_2\text{O}$  for 1 h, followed by sterilization with 70% ethanol for 1hr prior to cell seeding. Matrix microarray slides were equipped with 16mm x 16mm silicone multiwall chamber (Grace Bio-Labs) to partition individual microarray replicates. Cell seeding protocols were optimized using rat mesenchymal stem cells (MSCs) and primary cell rat pulmonary arterial smooth muscle cells (PASCs) obtained from rat vascular pulmonary arteries (Figure S1, Supplement Information). Cells with passages of 3-8 were used for all experiments. PASCs were detached from culture flask and suspended at a concentration of  $10^6$  cells per ml in serum free media. The

cell suspension was dispensed onto the 3-dimensional matrix microarray within the gasket region at a cell density of  $10^5$  cells per array and incubated for 2 hours. The arrays were then gently aspirated by submerging into a large chamber filled with pre-warmed media. Culture media was changed daily. Rat MSCs were extracted from femurs of 10 week old Sprague-Dawley rats weighing approximately 200g each. Metaphyseal heads of the femurs were removed and marrow was flushed out with ice-cold MSC culture media using 25g needles. Clumps in the marrow were dissociated by repeated aspiration with 18g needles and marrow suspension was filtered through 40 $\mu$ m nylon strainer. After a brief centrifugation, cells were re-suspended in warm culture media and seeded. Media was completely replaced after 24h to remove any unattached cells. For neotissue cell seeding, a cell suspension of passages 2-5 with concentration of  $10^6$  cells per ml in serum free media was prepared. The cell suspension was dispensed onto the 3-dimensional matrix microarray within the gasket region at a cell density of  $10^5$  cells per neotissue array and incubated for 4 hours. The arrays were then gently aspirated into a large chamber filled with prewarmed media. Following aspiration, culture media (10% serum) was introduced into the microarray wells. For cell culture lasting longer than 24 h, the culture media was changed daily.

### **5.2.6. Immunofluorescent Staining**

Following cell culture, neotissue arrays were samples were fixed with 3.7% formaldehyde at room temperature, permeated with 0.1% Triton X-100 and blocked with 3% BSA. Immunofluorescent staining of cells for cell nuclei (DAPI) and cellular cytoskeleton (Alexa488-phalloidin) were utilized to observe cell adhesion and spreading respectively. Platelet endothelial cell adhesion molecule (PECAM-1) antigenic staining was performed to characterize vascular differentiation. For vascular marker immunostaining, samples were first incubated with primary anti-PECAM in 1% BSA overnight at 4° C. Following primary antibody coupling, samples were washed 3X in PBS and incubated with secondary antibody anti-rabbit IgG antibody conjugated with Alexa 555 for 2 h at room temperature. All samples were

finally mounted with Vectashield Hard Set mounting media and stored at 4° C for imaging.

### **5.2.7. Confocal Imaging**

Confocal images were acquired using a Nikon A1R laser scanning confocal microscope piloted by NIS-Elements 4.0 and equipped with 405 nm, 488 nm, 561 nm, and 640 nm laser lines. Typically, the relative z position of the focal plane was ensured by using an equipped Nikon Perfect Focus System. Unless otherwise stated, a 10x 0.5NA objective with the pinhole set to 1.2 Airy Units (AU) was used. Neotissue array large images were obtained using a motorized XY stage with piezo Z-Drive insert for rapid multidimensional (XYZ) imaging. The image overlap was set to 5% and the resulting digital montage was generated using the same NIS-Elements 4.0 software. When needed, multiple z planes were acquired in order to capture all of the cells within each micro printed well. A maximum intensity projection image was then generated using the piloting software.

### **5.2.8. Image & Statistical Analysis**

Neotissue image intensities were obtained using National Institute of Health (NIH) ImageJ software (v.1.4). For each neotissue array condition, a minimum of 3 replicate arrays were imaged for statistical significance. Replicate dots per a single array (8 per condition) were averaged and reported with standard error for each intensity evaluated respectively. Nuclear intensities were normalized to the max adhesion values on each array. F-actin and PECAM intensities were further normalized to their respective nuclear intensities to observe cellular spreading and vascular differentiation independent to cell number. To evaluate significant differences between the different protein and stiffness conditions, a 2<sup>7</sup> (6 proteins + elasticity) full factorial design was performed on all normalized 24 h data using Minitab statistical software (Minitab, State College, PA) to determine the magnitudes of main and interaction effects and their statistical significance respectively. A minimum of 3 arrays for each experimental parameter investigated were used for all factorial analysis.

### **5.3. Results**

#### **5.3.1. Characterization of 3-dimensional Fibrous Soft Hydrogel Matrix**

Fibrous hydrogels were prepared by electrospinning a photopolymerizable polymer (PEGDM) onto a TMSPSA-functionalized glass surface, followed by UV stabilization (Figure 1). The presence of methacrylate groups on the glass surface allows firm attachment of fibrous hydrogels for substrate stability and longevity after multiple rinses in aqueous solution, facilitating unbridged function for extended biological assays. PEGDM (MW 750) was selected for its biocompatibility, ease of manipulation, elasticity, anti-fouling, and commercial availability (Zhu, 2009). The stabilization of PEGDM substrates is achieved via radical chain photopolymerization between the methacrylate groups in the presence of a photoinitiator and UV light (352nm). We employed mid-range FTIR to characterize the degree of PEGDM conversion by monitoring the disappearance of the reactive methacrylate peak at  $1637\text{ cm}^{-1}$  for samples over the course of 15 minutes UV exposure (Figure 2A). Results showed the attenuation of the methacrylate peak with up to 46% reduction after 15 minutes of UV exposure. The lack of efficient methacrylate conversion is likely due to the occurrence of polymerization in the dry state, reducing chain mobility and active crosslinking domains for polymerization.

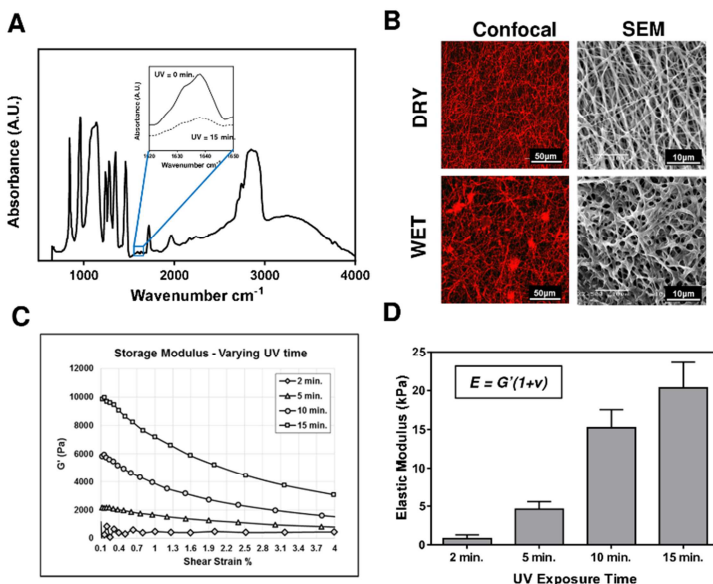


**Figure V – 2.** Electrospun PEGDM fibrous hydrogel characterization. (A) Mid-range IR identifies methacrylate conversion with UV exposure. (B) Fibrous architecture was investigated using confocal laser microscopy and scanning electron microscopy in both wet and dry states. (C) Shear stress vs. shear strain relationships for several PEGDM substrates prepared under different UV exposures. (D) Translation of shear-strain relationships into elastic modulus using a Poisson ratio  $\nu \sim 0$  [16].

The fibrous architecture of electrospun PEGDM substrates was examined using different microscopy techniques (Figure 2B) in both hydrated and dry states. Copolymerizing the PEGDM fibrous hydrogels with rhodamine-methacrylate permitted the visualization of individual fiber diameter and geometry under confocal microscopy. Employing scanning electron microscopy, higher magnification images were obtained of the fibrous substrates in dry and wet states. Both imaging methods demonstrate the fiber diameter increased after hydration to approximately 0.5 -1 $\mu\text{m}$ . Lack of beading or webbing of the electrospun nets indicates optimal spinning parameters with minimal artifacts.

To evaluate our capability to regulate the elastic properties of these fibrous substrates, mechanical properties were evaluated under shear using a parallel plate rheometer for PEGDM specimens prepared under different UV exposures at 2, 5, 10 or 15 minutes. Results are presented in Figures 2C-2D. The storage modulus

increased with the UV exposure time from 400 Pa to 10 kPa after 2- and 15- minute UV exposure, respectively. The elastic modulus determined with the shear modulus measured here (Figure 2D) are in good agreement with compressive modulus determined in our previous work (Wingate, 2012).

### **5.3.2. Design and Optimization of 3-dimensional Protein Microarray**

The deposition of protein microdots is illustrated in Figure 3. Array deposition produces repeatable distinct microdots of  $240 \pm 11.4 \mu\text{m}$  in diameter and  $580 \pm 16.8 \mu\text{m}$  in pitch to pitch distance (Figure 3A). To optimize the presentation, homogeneity and longevity of protein dots in the 3-dimensional fibrous PEGDM substrates, we have performed iterations with a number of printing buffers using a quality control protein, albumin (Figure 3B). The glycerol content in the buffer was found to influence printing parameters significantly. With increasing glycerol content, protein dot circularity increased whereas the fluorescent intensity of dots decreased. The glycerol content of 1% (v/v) was sufficient in retaining dot circularity without markedly reducing protein intensity after incubation, and thus was used for all studies here. Serial dilutions of quality control proteins, cy3-albumin and cy5-streptavidin, revealed strong protein uptake by the fibrous PEGDM hydrogels, with proteins detected at a deposition concentration as low as  $15 \mu\text{g/ml}$  (Figure 3C). The fluorescent intensity of microdots is correlated well with the deposition concentration. Figure 3D demonstrates 3-dimensional presentation of protein microdots with approximately  $200\mu\text{m}$  in diameter and  $50\mu\text{m}$  in depth penetration of PEGDM fibrous substrates. Finally, optimized printing conditions are applied to produce 3-dimensional protein array with global deposition over a large area ( $10\text{mm} \times 20\text{mm}$ ); results show minimal perturbations occur in the array organization and layout (Figure 3E).

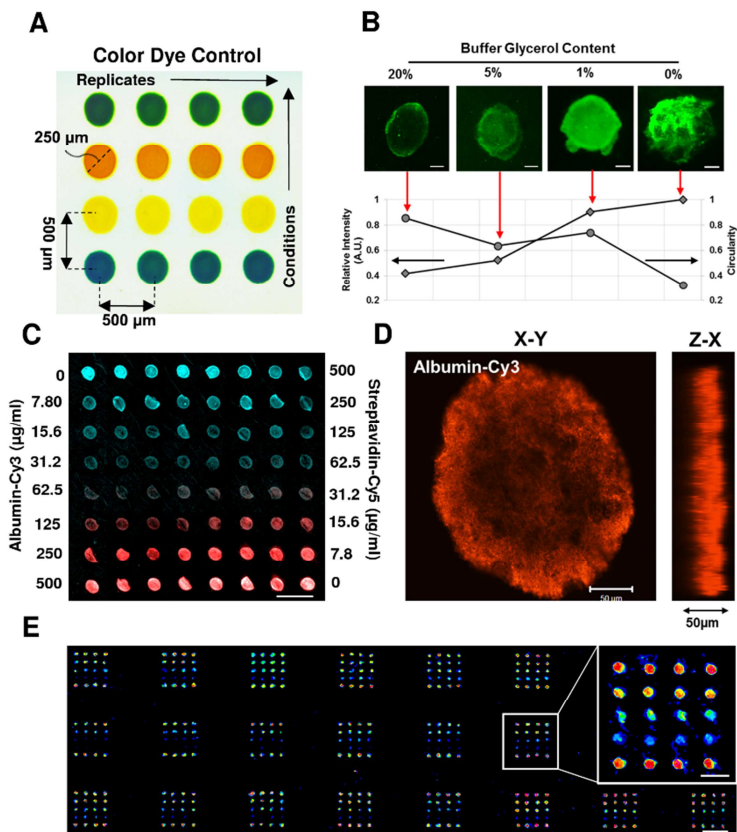


**Figure V – 3. Protein Microdot Optimization.** (A) Array layout depicted through color dye control. (B) Optimization of buffer glycerol content achieves ideal spotting. Inset images scale bar 50 μm. (C) Serial dilution of two model proteins (Albumin-Cy3, Streptavidin-Cy5) demonstrating distinct dot deposition and periodicity. Scale bar 500 μm. (D) Confocal microscopy rendering of albumin-Cy3 deposition illustrating 3-dimensional dot presentation. Scale bar 50 μm. (E) Printing optimization techniques allow for global array deposition onto PEGDM substrates. Scale bar 1 mm. Inset image scale bar 500 μm.

To further assess printing efficiency, we used six types of ECM proteins and their combinations. Imaging results demonstrate that collagen I microdots could be detected at the same resolution – concentrations similar to the quality control proteins (i.e. 15-250 μg/ml), which was stable after several days of continuous rinsing in PBS (Figure 4A). Figure 4B represents the design of a combinatorial ECM protein microarray comprised of 6 ECM proteins, resulting in a total of 64 protein conditions (rows) and replicates of eight (columns) for each condition. To ensure the

protein retention for all ECM proteins, antigenic immunostaining was performed, with immunofluorescence results on collagen I and collagen IV shown in Figures 4C and 4D (note: all other protein data not shown for brevity). For all proteins investigated, we found that the immunofluorescence intensity correlated well with expected protein distribution and density. Nevertheless, it should be noted that some detectable fluorescence was observed on the protein combinations absent of the immunostained protein, for example, as shown on the slide stained with collagen IV antibody (Figure 4D). We attributed this phenomenon to the cross reactivity (<10% for collagen I and III) of the collagen IV primary antibody used, as reported by the manufacturer (EMD Millipore). To prevent potential for protein carryover between depositions, we performed consecutive rinsing and sonication of the array tips between each deposition, ameliorating deposition artifacts between replicate dots. Therefore, distinct immunofluorescent detection of specific ECM proteins demonstrate successful deposition of combinatorial designs without condition carryover or contamination.

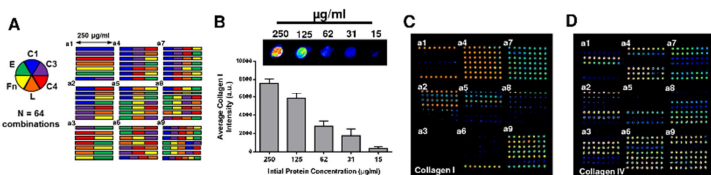


**Figure 4.** Design and Characterization of Combinatorial Protein Neotissue Array. (A) Design of a combinatorial ECM matrix with 6 proteins yielding 64 unique spotting combinations: C1 (collagen I), C3 (collagen III), C4 (collagen IV), L (Laminin), Fn (Fibronectin), E (Elastin). (B) Serial dilutions of Collagen I are retained after several rinsing stages and detectable at concentrations as low as 15 µg/ml (n=8). Immunostaining of combinatorial ECM matrix for collagen I (C) and collagen IV (D) after deposition and rinsing. Scale bar 1 mm.

### 5.3.3. Stem Cell Adhesion and Spreading within 3-dimensional Neotissue Arrays

To demonstrate the feasibility of our matrix hydrogel arrays to support cell adhesion and spreading for the formation of 3-dimensional engineered microenvironments, we developed seeding protocols for MSCs (progenitor/stem cells) and PASCs (primary cells). Images of PASC arrays were shown in Figure

S1 (supplemental information). MSCs were seeded onto the soft hydrogel arrays ( $E = 4.6$  kPa) in serum-free media for 4 hours at 37°C, followed by gentle aspiration and extended culture in serum-containing media for an additional 20 hr. The MSCs attached preferentially to the protein deposited regions with little to no cell attachment observed on the neat PEGDM fibrous matrix (Figures 5A-5B). Upon closer inspection, distinct cellular islands formed 3-dimensional engineered neotissue microdomains within specialized matrix microenvironments, showing a tissue thickness of approximately 50-100  $\mu\text{m}$  (Figures 5C-5D). MSC attachment and spreading are analyzed with fluorescent microscopy imaging, after stained with DAPI (nucleus) and phalloidin-488 (F-actin). Staining for cell nuclei identified distinct cell populations associated with the ECM protein depositions (Figure 5E). Results on quantification of MSC adhesion are illustrated in Figures 5F-5G, which show preferential matrix conditions for 3-dimensional cell adhesion. For instance, a mixture of collagen I and collagen III yielded approximately 3-fold increase in DAPI intensity compared to elastin alone. High-resolution micrographs of the cells in relevant protein matrix environments taken from the DAPI intensity images, confirmed the affinity of certain protein conditions that support cell adhesion over others. To evaluate matrix effects on cellular spreading and morphology, fluorescently labeling of cell F-actin was performed and analyzed with normalization to the respective DAPI intensity measurement for each protein condition. Figure 5H demonstrates the strong dependence of MSC spreading on protein environments of the matrix. Several protein conditions were identified to significantly influence MSC spreading in the neotissue array. The spreading for MSCs cultured on collagen I microdots showed nearly 2-fold increase when compared to MSCs cultured on elastin microdots. Notably, eight combinations of a total of 63 combinatorial matrix environments exhibited F-actin intensity of less than 1 relative to the DAPI intensity, which indicates minimal spreading. Overall, these results highlight the potential of using our fabricated neotissue array platform to capture cellular phenomenon in precisely-defined microenvironments and to determine cause-effect relationship of matrix environments on cells.

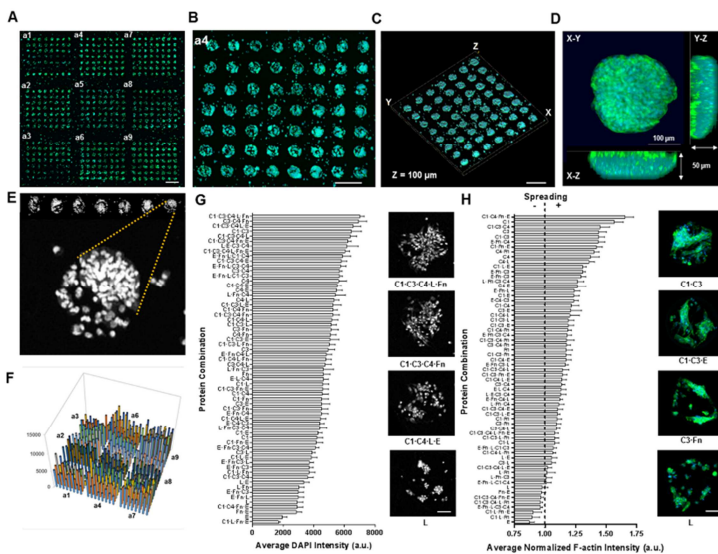


**Figure V – 5.** Rat mesenchymal stem cells (MSCs) adhered on neotissue slides ( $E = 4.6$  kPa substrate). (A) Confocal montage image of neotissue array after 24 h cell culture with distinct cellular islands visible for all protein spotting conditions (scale bar 1 mm)(green, f-actin; blue, DAPI). (B) Magnification of a4 subarray depicting cellular dot circular geometry and periodicity (scale bar 500  $\mu\text{m}$ ). (C,D) Confocal 3-dimensional rendering of cell loaded subarray (C)(scale bar 250  $\mu\text{m}$ ) and of a single cellular dot (D). (E) Nuclear staining of MSCs seeded on the neotissue arrays for image analysis and quantification. (F) 3-dimensional bar graph representing the average nuclear pixel intensities for all protein combinations for image (A). (G,H) Sorted average pixel intensities for adhesion (G) and spreading (H) for all protein combinations after 24 h cell culture ( $n = 3$  neotissue arrays); Insets depict cellular dot images for adhesion and spreading of representative protein conditions (scale bars 100  $\mu\text{m}$ ).

### 5.3.4. Effect of Protein Environment and Matrix Elasticity on MSC Adhesion and Spreading

To investigate the effects of matrix elasticity and ECM protein environment on MSC adhesion and spreading, we evaluated MSCs on the 3-dimensional fibrous matrix arrays prepared with two UV exposure times, 5 and 15 minutes, which produce substrates with different elasticity, 4.6 and 20 kPa, respectively. Figure 6 shows the distinct patterns of 3-dimensional adhesion and spreading of MSCs on soft (4.6 kPa) and stiff (20 kPa) matrix arrays after 24-hour cell culture. Cell attachment and spreading on both arrays were confirmed, as illustrated in Figure 6A. Statistical analysis of the MSC adhesion and spreading profiles highlighted a diverse set of protein combinations that are correlated to either positive or negative influence with

respect to different matrix elasticity conditions (Figure 6B). In an effort to delineate the regulatory mechanisms underlying the effects of elasticity, protein environment, and their interaction on cell activity, we compared the variations of average MSC adhesion and spreading for each protein environment on the 4.6 kPa array with those on the 20 kPa array (Figures 6C-6D). Comparison of the average MSC adhesion profiles on 4.6 kPa and 20 kPa matrices revealed a nearly linear relationship with the exception of few outliers, suggesting cell adhesion in most protein environments is independent of matrix elasticity. Among the few outliers, MSC adhesion on C1·C4·L was favored in the 20 kPa matrix, whereas C3·C4·Fn was favored in the 4.6 kPa matrix. These trends are further illustrated with corresponding images which depict distinct adhesion profiles in various elasticity and protein environments. MSC spreading was found to be strongly influenced by the matrix elasticity (Figure 6D). Compared to the 20 kPa array, MSC spreading on the 4.6 kPa array significantly increased. Compared to cell adhesion, MSC spreading was more synergistically regulated by matrix elasticity and adhesive protein environments. Cell spreading in several protein environments (i.e. C1·C4·Fn·E and L) favored the 4.6 kPa array and others (i.e. C3·E, Fn·E) favored 20 kPa array. Several distinct cell spreading conditions existential to elasticity and protein combinations are also illustrated with corresponding images (Figures 6D-6F).

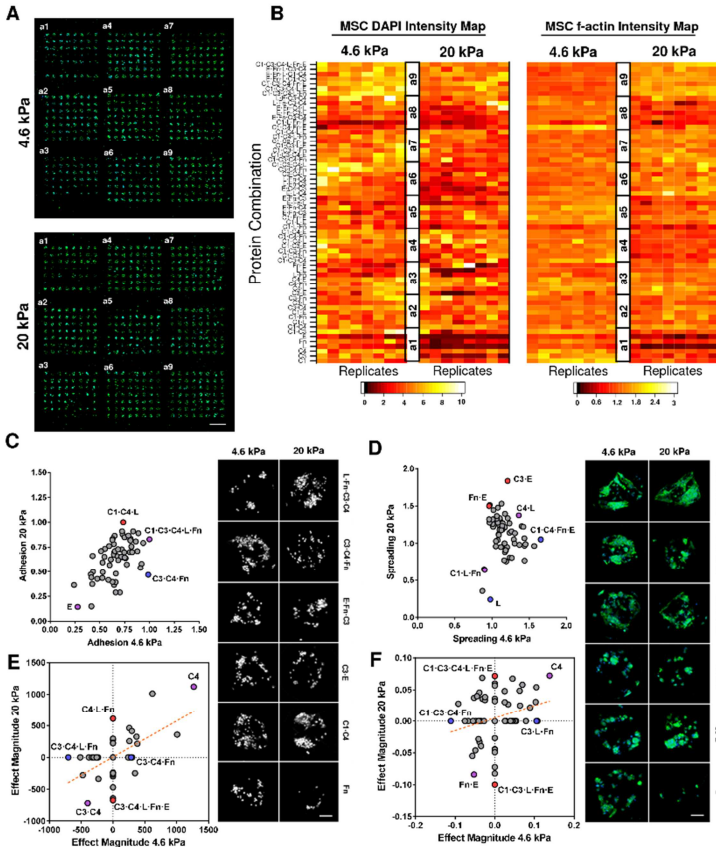


**Figure 5 – 6.** Cultured MSCs display differential adhesion and spreading characteristics in response to protein combination and matrix elasticity. (A,B) Cellular structures, nuclei and f-actin, are stained, imaged (A) and quantified using software to produce an average intensity map (B) for distinct elastic environments (4.6 kPa;20 kPa). (C,D) Comparison of average adhesion (C) and spreading (D) of MSCs on each protein condition for soft (4.6 kPa) and stiff (20 kPa) neotissue substrates. Conditions denoted by blue or red significantly favor adhesion or spreading for soft (4.6 kPa) or stiff (20 kPa) matrix elasticity respectively, purple denotes both. Insets depict adhesion and spreading of representative protein conditions screened from the arrays in (A) (scale bars 100  $\mu$ m). (E,F) Results of  $2^7$  full factorial ANOVA of significant ( $p < 0.01$ ) main and interaction effects for DAPI (E) and f-actin (F) intensities supporting either soft (4.6 kPa) or stiff (20 kPa) matrix conditions ( $n = 3$  neotissue arrays). Blue and red dots represent prominent protein conditions supporting significant effects only on soft (4.6 kPa) or stiff (20 kPa) or both (purple dot) substrates respectively.

The equivocal activity of several protein combinations and their effects on MSCs under different elastic substrates inspired us to perform full factorial design and subsequent analysis of variance (ANOVA) for main (1-factor) and interaction ( $2^7$ -

factor) effects with a significance level of  $p < 0.05$ . Results are shown in Figures 6E-6F, which respectively demonstrate the effect magnitude for matrix elasticity on cell adhesion (Figure 6E) and cell spreading (Figure 6F) in all protein environments (see Supplementary Figure S2 for enumeration of all effects). Our results revealed that the protein environment exhibiting the most significant upregulation on cell adhesion was C4 for both stiffness environments (20 kPa and 4.6 kPa), while few protein environments were found to decrease (e.g. C3·C4) cell adhesion on both arrays, with protein-regulated variations independent of elasticity. Finally, cell adhesion variations for other protein environments were differentially regulated by the matrix elasticity. For example, C1 promoted cell adhesion on the 20 kPa array but weakened adhesion on 4.6 kPa. Interestingly, we revealed an inverse adhesive profile for C1·C3·E condition, whereby enhanced attachment was observed for soft substrate when compared to stiff substrate which had reduced adhesion. Similar to adhesion, we estimated the contribution of matrix elasticity, protein environment and their interaction on MSC spreading variation using factorial ANOVA (Figure 6F). Cell spreading was markedly enhanced by C4 but reduced by Fn·E on both 20 kPa and 4.6 kPa arrays. Several protein environments, however, significantly influence cell spreading only under one matrix elasticity: C3·L·Fn enhanced spreading on 4.6 kPa alone, while C1·C3·C4·L·Fn·E enhanced spreading on 20 kPa alone. In contrast, reduced spreading conditions were revealed to be C1·C3·C4·Fn and C1·C3·L·Fn·E for 4.6 kPa and 20 kPa, respectively. Overall, performing linear regression (Figures 6E-6F) revealed positive trends for MSC adhesion and spreading on softer substrates (4.6 kPa) compared to stiff (20 kPa). Furthermore, both adhesion and spreading array analyses revealed a tendency to support similar significant effects on attachment and spreading potential (positive slope) of all protein environments on these matrices.VII

### **5.3.5. Effects of Matrix Elasticity and Adhesive Protein Environment on MSC Fate Commitment in 3-dimensional Engineered Neotissues**

To explore effects of neotissue microenvironments on stem cell differentiation, we cultured MSCs within our neotissue arrays for 24 h under two

different elasticities and then stained cells for the vascular marker PECAM. Representative MSC cultures within neotissue arrays are depicted in Figure 7A, stained for cell nuclei (blue), F-actin (green), and PECAM (red). Immunostaining for the differentiation marker PECAM resulted in detectable levels after 24 h culture on both elastic arrays (Figure 7B). Cell images on several relevant protein conditions and as per elasticity are illustrated in Figure 7C. Interestingly, PECAM expression intensity was notably greater on stiff (20 kPa) vs. soft (4.6 kPa) matrix (Figure 7D). On each elastic array, several protein environments were identified to significantly influence PECAM expression. Notably, C1·C4·Fn·E and C1 provided the greatest difference in PECAM intensity for 4.6 kPa matrix when compared to 20 kPa matrix. Likewise, C3·E, C3·L·E, and C4·L·Fn resulted in upregulated PECAM expression on 20 kPa matrix and much lower expression on 4.6 kPa. Of the top ten protein environments that enhanced PECAM expression on 4.6 kPa matrix, 2 conditions contained laminin; however, comparison to the bottom ten environments, 7 conditions contained laminin, while all other types of proteins see nominal fluctuation between the top ten and bottom ten protein environments for PECAM. Further, of those 7 conditions, 5 represented combinations of laminin and fibronectin. This suggests laminin reduces PECAM expression on 4.6 kPa substrate. Comparably, the ten highest PECAM intensities for 20 kPa matrices all lacked collagen I, with laminin and elastin constituting the greatest frequency at 6 and 5 conditions out of 10 respectively. Interestingly, the ten lowest PECAM intensities for 20 kPa matrices showed a considerable increase in collagen I content (5 out of 10) and a significant decrease (2 of 10) in elastin frequency. Altogether, these results suggest that elastin and collagen I play important but opposite roles in determining overall PECAM expression on stiff matrices, while laminin, in particular laminin mixed with fibronectin, play a role in reducing PECAM on soft matrices.

We estimated the contribution of matrix elasticity, protein environment and their interaction on PECAM expression variation using factorial ANOVA for each of 128 neotissues assayed Figures 7E-G. Detecting significant effects of those factors on PECAM expression level represent PECAM variation for elasticity regulation (E), protein environmental effect (P), and elasticity-regulated variation

for protein environmental effect ( $E \times P$ , elasticity-by-environment interaction). A total of 67 conditions varied in PECAM expression level between two elasticity matrices independently of the protein environment ( $pE < 0.05$ ,  $pE \times P > 0.05$ ). This is a set of conditions whose PECAM level is regulated by the matrix elasticity but this variation is not protein-dependent. The PECAM level of 20 conditions was affected by the protein environments independently of the matrix elasticity ( $pP < 0.05$ ,  $pE \times P > 0.05$ ), which represent roughly 15% of the conditions surveyed. Finally, 27 conditions showed significant interaction between the stiffness and the environments on PECAM expression ( $pE \times P < 0.05$ ). This latter group represents MSC expression of PECAM that responds differently to the protein environments examined, depending on the matrix elasticity, and therefore represent engineered neotissues with MSC differentiation synergistically regulated by matrix elasticity and protein environments. Notably, C4·L·Fn·E significantly enhanced PECAM expression on stiff matrices (20 kPa) alone, while C3·L·Fn on soft matrices (4.6 kPa) alone. Further, C1·C3·L·Fn·E significantly reduced PECAM expression on stiff matrices alone, while C3·Fn on soft matrices alone. Unlike analysis results for cell adhesion, no protein condition resulted in inverse PECAM expression on the different elastic matrices. Some of the prominent protein conditions that significantly influenced PECAM expression positively and negatively, irrespective of elasticity, include C3·L·Fn·E and C3·C4·L·Fn, respectively. Linear regression of all significant PECAM effects revealed a positive regression slope suggesting significant PECAM expression conditions generally followed similar trends between both elastic matrices.

To further decouple the stiffness effect on cell differentiation from protein effects, comparison of the general effects obtained through 2<sup>7</sup> full factorial ANOVA of substrate elasticity over all cellular phenomenon is presented in Figure 7F. In agreement with our previous findings, MSC adhesion and spreading significantly ( $p < 0.001$ ) correlated negatively for all protein conditions on stiff (20 kPa) matrix compared to soft (4.6 kPa). Interestingly, despite negative influences on adhesion and spreading, stiff matrices significantly ( $p < 0.05$ ) upregulated PECAM expression irrespective of protein condition, when compared to soft matrices. Of the significant ( $p < 0.05$ ) effects leading to reduced PECAM

expression, thirteen conditions were found on 20 kPa substrate versus eighteen conditions on 4.6 kPa substrate. We note that of the eighteen significantly negative effects on PECAM expression for soft substrate, eight were not shared with the stiff substrate (20 kPa). Investigating the average PECAM intensities for both substrates we find the maximum intensity reported for 20 kPa to be approximately 15% greater than that measured on 4.6 kPa (data not shown). Collectively, these trends suggest that matrix elasticity may have a more significant role in PECAM expression of MSCs cultured on our neotissue arrays than any of the protein environments presented.

#### **5.4. Discussion**

The need for engineered stem cell niches integrating several extrinsic stimuli has become a significant challenge within the research community. Recent evidence suggests that cells react to a complex mechanosensing apparatus whereby the interaction of ligand tethering and ECM stiffness can impart differential cellular functions (Seo, 2013), including differentiation (Trappmann, 2012). Indeed, emerging reports have highlighted the significance of protein conformational status which is influenced by the underlying matrix stiffness (Anita, 2008), or chemistry (Klotzsch, 2014) effectively modulating the presentation of binding sites for cell receptors and/or growth factors (Hynes, 2009), the entirety of which can significantly influence cellular processes (Cole, 2009). Due to the lack of existing methods to accurately and efficiently capture these complex microenvironments, we created a high throughput method whereby 3-dimensional matrix physical properties and biological ligand could be modulated. The design of a multivariate protein array for screening of stem cell microenvironments required the fabrication of an appropriate platform incorporating 3-dimensional substrate with fiber architecture and tunable elasticity and finally the integration of a combinatorial ECM protein library upon our engineered substrates.

The choice of neotissue substrate was an important requisite of our design which necessitated: 1) tunable elasticity, 2) 3-dimensional architecture, 3) reproducible fabrication, and 4) ease of sample production. For this work, we chose

a soft, fibrous hydrogel platform prepared from an electrospinning method as previously described (Wingate, 2012; Wingate 2014). Recent studies have highlighted the importance of 3-dimensional, fibrous matrices to optimize stem cell niche environments (Carlson, 2012; Lim, 2009), as well as their candidacy as platforms for MSC differentiation into vascular lineages (Wingate, 2012; Wingate, 2014). We find electrospinning, followed by UV polymerization to represent a highly versatile technique whereby stiffness and microstructure can be reproduced with high fidelity. The electrospun matrices produced here require facile production techniques, meanwhile providing reproducible elastic moduli of ~3–20 kPa which represent biologically relevant stiffness range for native vasculature (Wingate, 2012), while avoiding disparity in substrate architecture and geometry.

We chose a contact style arrayer for the protein deposition which is capable of depositing up to 3200 distinct protein dots, of ~240 $\mu$ m diameter and pitch 500 $\mu$ m, onto a standard 25mm x 75mm microscope slide. Protein deposition volume is on the order of picoliters (MacBeath, 2000), which represents several orders of magnitude less reagent required for traditional-scale cultures. Tailoring of the printing buffer for ECM proteins was found to significantly affect dotting efficiency upon our unique substrates. Others have reported buffer reformulations for 2-dimensional microarray technologies (Flaim, 2005; Soen, 2006). We found significantly less glycerol content was necessary to retain our protein deposits on our 3-dimensional substrates. Our methodology requires printing upon a dry electrospun surface, whereby the lack of substrate moisture likely assists in dot uptake and retention, removing the necessity for increased glycerol concentration.

The neotissue arrays we prepared here revealed a robust biological response of MSCs cultured within these substrates. MSCs were found to attach preferentially to protein deposited microdots, retaining the array structure and periodicity. In the absence of protein spotting, lack of cellular attachment and spreading was ostensible due to the inert and anti-fouling properties (Zhu, 2009) of the neat PEGDM electrospun matrices. Furthermore, evidence of 3-dimensional cellular organization was detected over a diversity of protein and substrate conditions. Using both stem cell and matured cells in our study, we showed the method described here could be amenable to virtually any cell line of interest, with minor modification to current

protocols. For this work, we only investigated the cellular response on MSCs over 24 h and 72hr (Figure S1, Supplemental Information); however, preliminary extended cell culture experiments demonstrated that these neotissue arrays retained their structure and functionality up to 7 days continuous culture. Therefore, we suspect these neotissue arrays can easily be adapted for longer cell culture regimens, with the potential to integrate spatiotemporal signals.

Our focus on vascular regeneration inspired the choice of proteins employed: collagen I, collagen III, collagen IV, laminin, fibronectin and elastin; all of which are amply represented in the native vasculature (Davis, 2005) and have distinct roles in development and vasculogenesis (Davis, 2005; Wagenseil, 2009). However, we note that our developed technique is adaptable to virtually any protein combination or formulation of interest for the end user. The choice of protein concentration utilized for cell culture was another important design consideration for our neotissue arrays. We found cellular attachment with as little as 15  $\mu\text{g/ml}$  spotting concentration of pure collagen I could be achieved on our PEGDM electrospun substrates (data not shown). Therefore, we chose a protein dot concentration of 250  $\mu\text{g/ml}$  for our experiments in order to ensure sufficient representation of each protein mixture.

The ability to deposit complex protein combinations onto our engineered soft matrices with high reproducibility and accuracy encouraged us to adapt this technology towards a high-throughput neotissue platform. Current cellular microarray technologies lack the amenity to observe substrate parameters such as elasticity, geometry and biological ligand in synergy. Attempts to integrate multiple signals into microarray technologies have been reported previously. Gobaa et al. successfully coupled tunable elastic microwells with array spotting technology to investigate the effects of cell density, substrate elasticity and protein on the adipogenic or osteogenic differentiation of MSCs in 2-dimensions (Gobaa, 2011). However, emerging evidence suggests a drastically different ensemble of biological signals exists for stem cells when cultured in 3-dimensions (Huebsch, 2010; Battista, 2005). Recent attempts at 3-dimensional microarray platforms have emerged with promising results (Fernandes, 2010; Dolatshahi-Pirouz, 2014), but the integration and independent modulation of several mechano-chemical factors in 3-dimensional formats is still a considerable challenge in the microarray community (Ranga, 2012).

A key aspect of our neotissue arrays is their ability to incorporate significant matrix parameters, including 3-dimensional geometry, elasticity and biological ligand, and investigate their effects in synergy or independently on cellular phenomenon in high-throughput fashion. However, one limitation of our neotissue arrays, compared to other micro-engineered niche environments (Hui, 2007), is that it's comprised of a single medium chamber, thereby allowing cellular crosstalk events among different conditions. Adaption of our technology to a multiwell format (Khetani, 2007) or proper spotting randomization (Gobaa, 2011) could obviate this problem.

Our interest in vascular regeneration prompted us to evaluate the potential of our neotissue arrays to instruct vascular commitment of MSCs. Several reports have observed the differentiation of MSCs into vascular lineages in vitro (Oswald, 2004; Pittenger, 1999). The majority of literature regarding stem cell differentiation into vascular lineages involves precise soluble factor regiment (Oswald, 2004), application of shear (Ahsan, 2010), matrix rigidity (Engler, 2006; Wingate, 2014), composition of the ECM (Kniazeva, 2011; Lozito, 2009; Wang, 2013), or multiple factors (Wingate, 2014; Portalska, 2012). For example, it has been shown that the administration of vascular endothelial growth factor (VEGF) (Oswald, 2004) or combination with shear stress (Wu, 2008) or matrix elasticity (Wingate, 2014) instructs MSC differentiation into vascular lineages. Wang et al demonstrated the significance of ECM proteins in determining the vascular commitment of MSCs (Wang, 2013). Others have reported on specific ECM environments for improved vascular differentiation of MSCs (Yang, 2010). However, few studies have investigated the role of insoluble matrix factors combined with elasticity in modulating vascular commitment of MSCs. Abdeen et al demonstrated a positive correlation between 2-dimensional fibronectin-modified hydrogels and stiffness towards proangiogenic signaling of MSCs (Abdeen, 2014). Despite significant progress in defining MSC to vascular differentiation protocols, a fundamental understanding of how matrix ligand, in concert with tunable elasticity in 3-dimensional environments, as presented in this study, is largely missing.

We postulated that the merging of biological ligand with appropriate elasticity in 3-dimensional environment could augment or repress the fate commitment of stem cells into specific lineages. Our work revealed a strong dependence of matrix protein

composition and elasticity on MSC cellular processes including adhesion, spreading and differentiation toward early vascular lineages. Interestingly, we observed a negative correlation between MSC adhesion and spreading with substrate stiffness. Though stiffer 2D substrates generally increase receptor-ligand activity leading to increased F-actin expression and thus cell spreading, our results showed a different trend with 3D matrices which might be caused by different focal adhesion mechanisms employed by 3D cell-matrix interaction compared to 2D cell-substrate (Cukierman, 2002). In fact, evidence suggests that the creation of cellular focal adhesions on compliant 3-dimensional substrates is abrogated preventing cell traction forces, whereas rigid substrate analogs prevent cells from exerting sufficient force to deform their matrix (Huebsch, 2010); with these events directly influence cellular spreading upon substrates. In contrast, the inclusion of biological ligands at specific densities can result in differential spreading of cells regardless of substrate stiffness. Trappmann and colleagues observed similar spreading of cells on stiff substrates with a 5-fold reduction in active ligand binding sites compared to neat soft substrates (Trappmann, 2012). The mechanism by which ECM protein and substrate elasticity effects MSC adhesion and spreading here is not fully understood. From the cited literature, it is likely protein-elasticity crosstalk influences MSC attachment and spreading observed here. Probing the ability to activate and deactivate certain integrin signaling events via protein interaction with substrate stiffness may help elucidate these complex phenomena (Chaudhuri, 2014).

We evaluated the efficacy of our neotissue arrays to instruct MSC differentiation towards vascular lineage. Our data revealed a strong dependence of matrix protein composition and elasticity on MSC differentiation toward vascular lineages. Indeed, several combinatorial environments were arrived at that significantly up- or down- regulate expression of PECAM. For instance, we observed a negative correlation for PECAM expression for laminin on soft matrix, when compared to stiff which was comparably positive. Likewise, we found an inverse relationship between collagen I and elastin protein to down and upregulate PECAM expression on stiff but not soft substrate respectively. These findings are in agreement with previous observations that report the capacity of MSC differentiation in vascular lineages by individual stimuli such as elasticity (Engler, 2006) or

biological ligand (Suzuki, 2010; Kniazeva, 2011; Lozito, 2009; Wang, 2013). For instance, the PECAM level affected by collagen I-related environments independently of the matrix elasticity may be explained by the lack of collagen I in normal endothelium (PECAM+) and increased collagen I content (Dean, 2005) in damaged endothelium to promote trans-differentiation of endothelial cells to mesenchymal cells (Breitbach, 2007). We note that unlike previous studies, our data revealed the potential to augment or suppress cellular functions by coupling discrete protein combinations with appropriate matrix elasticity. Recent evidence suggests a significant crosstalk between ECM protein and underlying matrix elasticity. Fibronectin exhibits greater unfolding on stiffer substrates (Antia, 2008), improving expression of cell binding domains and cellular attachment of fibroblasts (Seo, 2013). Further, it has recently been recognized that focal-adhesion kinase (FAK), a mechano-sensing integrin signal important for cellular differentiation (Liao, 2013), can be differentially activated based on ECM protein combined with substrate stiffness (Seong, 2013). In line with that, ECM stiffness alone was found to induce malignant phenotypes in normal mammary epithelial cells, but this effect could be abrogated when accompanied by an increase in basement-membrane ligands (Chaudhuri, 2014). These led to a mechanism whereby substrate stiffness coupled with ECM composition can modulate cellular phenotype, suggesting that substrate mechanical cues may instruct diverse effects on cell behavior depending on the presence and type of integrins presented. Our study reinforces the fact that distinct protein environments signal cellular phenomenon diversely when presented on matrices of different stiffness. This group represents MSC expression of PECAM that responds differently to the protein environments examined, depending on the matrix elasticity, and therefore MSC differentiation can be synergistically or antagonistically regulated by matrix elasticity and protein environments.

While different protein combinations induced differential cellular processes, we also demonstrated a significant dependence of matrix elasticity on the up-regulation of PECAM independent of the protein combination. It is widely accepted that matrix elasticity directs MSC differentiation and commitment into different lineages (Engler, 2006; Wingate, 2012). These findings have been further validated with recent observations that stem cell differentiation is predominantly driven by the underlying

substrate stiffness even in the presence of protein tethering (Wen, 2014). Our data revealed a significant ( $p < 0.05$ ) up-regulation of vascular marker PECAM on stiff substrate (20 kPa) in comparison to soft substrate (4.6 kPa). The stiffness we report here for optimal vascular commitment of MSCs is in agreement with recent studies. For instance, Kshitiz et al linked optimum levels of PECAM expression of cardiac progenitor cells cultured in 3-dimensional-matrices approaching an elasticity of 16 kPa (Kshitiz, 2015). The authors suggested a mechanism by which the expression of VEGF receptor (VEGFR2) was enhanced under the effective elasticity observed, a mechanosensing pathway previously described for human microvascular endothelial (HMVE) cells (Mammoto, 2009). Another recent study reported a pro-angiogenic secretome for MSCs cultured on substrates of 20 kPa stiffness when compared to softer substrates (2 kPa) (Seib, 2009). These studies are complimentary to the findings we report here, whereby appropriate stiffness is likely crucial in the fate decisions afforded by stem cells in response to their ECM environment and specifically in the context of vascular regeneration.

## **5.5. Conclusion**

We developed a high throughput method that allows for the rapid screening of a diversity of engineered microenvironments with tunable matrix elasticity and geometry, combined with specific ECM protein combination. This work highlights the importance and necessity of employing a systemic approach, whereby incorporating several environmental signals becomes necessary to establish optimal MSC differentiation protocols. Collectively, our data suggests that a complex milieu exists coupling protein functional behavior with substrate elasticity and that this phenomenon may potentially be exploited through proper application of high-throughput screening methodologies. Future studies will be focused on adapting this technology to instruct specific MSC differentiation processes by expanding the library of ECM proteins and experimental parameters employed.

## Chapter VI

# Nanofibrous Photoclickable Hydrogel Microarrays for High-Throughput Screening of Cellular Microenvironments

**Abstract:** Stem cell (SC) therapy promises to revolutionize the treatment of various diseases with the potential to regenerate functional tissues in vitro or in vivo. Several recent studies have demonstrated that cellular microenvironments such as ligand-activated cell-matrix interactions and/or matrix physical properties such as elasticity and geometry have significant role in directing the differentiation processes in stem cells (Lutolf, 2009; Wingate, 2012). Microarrays have emerged as an important tool for studying stem cell processes in a high-throughput manner (Gupta, 2010; Gobba, 2011). Nevertheless, most of the existing ECM arrays being either 2-D or shallow 3-D are not able to capture the effects of biophysical and chemical cues on stem-cell fate completely. Here, we report the development of a microarray platform based on electrospun nanofibrous hydrogels of photoclickable thiol-ene poly(ethylene glycol) (PEG) hydrogels. Thiol-ene polymerizations proceed by an orthogonal, step-growth mechanism where one thiol reacts with one ene leading to a highly homogenous distribution in crosslinks, thus imparting tunable substrate stiffness with high fidelity (Hoyle, 2010). Furthermore, it allows for the subsequent covalent post-modification of PEG thiol-ene hydrogel substrates with small engineered peptides with high reactivity and specificity. Taken together, the manipulation of the matrix properties, such as stiffness and geometry, in concert with engineered peptides will facilitate the interrogation of multiple and distinct SC microenvironments. To this end, we demonstrate the potential application of this high-throughput technology for

screening of a variety of engineered 3D microenvironments for stem cell fate optimization.

## **6.1. Introduction**

Stem cells are intrinsically influenced by their microenvironment through ligand-activated cell-matrix interactions and/or matrix physical properties such as stiffness and geometry, collectively eliciting a significant role in directing the differentiation processes in stem cells. The utility of high-throughput microarrays for screening various libraries of biomolecules, such as proteins and peptides, has increasingly become a popular interrogation platform to study the effects of various molecules (biological or synthetic) on cellular behavior (Anderson, 2005; Flaim, 2015; Gobaa, 2011). Cellular microenvironments represent a diverse myriad of signaling events through soluble (growth factors) and insoluble (matrix proteins) factors; together directing highly specialized tissue homeostasis, morphogenesis and differentiation (Floren, 2015; Flaim, 2005). Thus, the ability to screen these matrix cues both individually or with interaction against relevant cellular models is of considerable interest in tissue engineering and regenerative medicine. Nevertheless, most of the existing cellular microarrays being either 2-D or shallow 3-D are not able to capture the effects of biophysical and chemical cues on stem cell fate decisions completely.

Extracellular matrix (ECM) proteins are comprised of a myriad of physical and chemical signaling motifs. Small engineered peptides (SEPs), based off of recognized signaling motifs, have been developed to investigate the effects of individual peptide sequences on cellular activity in a highly specific manner. For instance, RGD sequence, widely accepted to participate in integrin-mediated adhesion of cells to surfaces (Ruoslahti, 1987), is ubiquitous in nature and found in several ECM proteins such as fibronectin, vitronectin, laminin, and collagen (Pierschbacher, 1984). Consequently, several studies have incorporated RGD and other adhesive ligands into tissue engineered scaffolds with the aim to tailor the biological response of cells (Shu, 2004; Hersel, 2003; Nuttelman, 2005).

Microarrays have emerged as an important tool for studying stem cell processes in a high-throughput manner (Gupta, 2010; Gobba, 2011). Nevertheless, most of the existing ECM arrays being either 2-D or shallow 3-D are not able to capture the effects of biophysical and chemical cues on stem-cell fate completely. Further, it is often difficult to decouple the compounding effects of multiple integrin motifs present in full ECM proteins with regard to stem cell fate decision processes. However, combinatorial studies investigating the individual and synergistic role of several SEPs on stem cell differentiation in a relevant model, i.e. soft, fibrous matrix, are absent.

To address these issues, we developed soft, fibrous hydrogels based on PEG thiol-ene substrates. The utility of thiol-ene chemistry allows for the incorporation of orthogonal reactive groups by exploiting the reactivity of thiols (cysteine residues) and therefore offers a diverse library of molecules for functionalization. We further demonstrate the novelty of our technique by developing high-throughput microarrays with various thiol-functional molecules or peptides to direct cellular adhesion and spreading. This technique is amenable to a variety of analytes, meanwhile presented on a highly tunable hydrogel, via stiffness or geometry, allowing for the screening of a wealth of engineered microenvironments correlating to directed cellular processes.

## **6.2. *Materials & Methods***

### **6.2.1. *Macromer synthesis***

Four-arm poly(ethylene glycol) norbornene (PEGNB) was synthesized as described in detail elsewhere (Roberts, 2013). Briefly, first 5-norbornene-2-carboxylic acid (Sigma) (8x molar excess compared to amine-terminated PEG arms) in dimethylformamide (DMF) was pre-reacted for 5 minutes under argon with 2-(1H-7-Azabenzotriazol-1-yl)-1,1,3,3-tetramethyl uronium hexafluorophosphate methanaminium (HATU, 4x molar excess, Chem Impex INT'L, Inc) and N,N-diisopropylethylamine (DIEA, 4x excess, Sigma) at room temperature. The pre-reacted mixture was then added to 4-arm PEG amine in DMF, and allowed to react for 24-48 hours under argon at room temperature. After that, 4-armPEG-NB was

precipitated in ice-cold ethyl ether, purified by dialyzing against DI H<sub>2</sub>O for 2-3 days, sterile filtered (0.2  $\mu$ m) and then lyophilized. Using <sup>1</sup>H-NMR spectroscopy, norbornene conjugation ( $\delta$  = 5.9 - 6.3 ppm) per 4-arm PEG molecule ( $\delta$  = 3.4 – 3.9 ppm) was determined to be 100%.

### **6.2.2. Electrospinning**

Nanofibrous hydrogel platforms were prepared by electrospinning an aqueous solution of 4-armPEGNB (5 kDa, 10 wt%), poly(ethylene glycol dithiol, Sigma) (1 kDa, thiol: ene = 0.9), poly(ethylene oxide) (5 wt%, MW: 400 kDa), and photoinitiator Irgacure 2959 using a custom set up equipped with a 14-mm syringe and a high voltage power supply (Gamma High Voltage, Inc). Electrospinning was conducted at +16 kV, 0.8 ml/hr, and needle-to-collector distance of 20 cm. Electrospun fibers were collected on a glass slide (25mm X 75mm) previously modified with 3-(mercaptopropyl) triethoxysilane. Substrates were subsequently exposed to UV (352 nm light) with an average intensity of 5 mW/cm<sup>2</sup> for specific time points.

### **6.2.3. Scanning electron microscopy**

Scanning electron microscopy was used to examine the microstructure of the electrospun hydrogel substrates in both dry and hydrated states using JEOL JSM 6480-LV at the Nanomaterials Characterization Facility (NCF) at CU-Boulder. For hydrating, samples were soaked in deionized water for 1 or 24 hours. Hydrated samples were shock frozen in liquid nitrogen and lyophilized for 48 hours. All the samples were coated with a thin Au layer prior to imaging to prevent charging. Image J was used to measure fiber diameter (two images, 15 fibers per image).

### **6.2.4. Peptide Synthesis**

All the peptides used in this study (CRGDS, CRGES, YRGDS) were synthesized via standard Fmoc solid-phase methodology, rink-amide resin, and HBTU/HATU activation using PS3 peptide synthesizer (Protein Technologies, Inc). After completion of peptide synthesis, simultaneous cleavage from resin and side chain deprotection was achieved by treatment with a trifluoroacetic acid (TFA) cocktail for 5 hours. Peptides containing Cys(Trt) were cleaved using 92.5% TFA,

2.5% Ethanedithiol (EDT), 2.5% water and 2.5% triisopropylsilane (TIS). For other peptides, a cleavage solution of 95% TFA, 2.5% water and 2.5% TIS was used. Crude peptide was precipitated and washed (3 times) with ice-cold diethyl ether, and then allowed to dry overnight. The dry peptide powder so obtained was then dissolved in Milli Q water, filtered using 0.2  $\mu\text{m}$  filter, and then lyophilized. This lyophilized powder was used for the experiments without further purification. The molecular mass of all the peptides was confirmed by matrix-assisted laser desorption, ionization time-of-light (MALDI-TOF) mass spectrometry (Applied Biosystems DE Voyager) using  $\alpha$ -cyano-4-hydroxycinnamic acid matrix (Sigma). MALDI-TOF-MS:  $[\text{M} + 1\text{H}]^+$ : CRGDS: Calculated (536.58), Observed (536.34); CRGES: Calculated (550.60), Observed (551.10); YRGDS: Calculated (596.61), Observed (596.72).

### **6.2.5. Fluorescent Peptide Synthesis**

CDGEAK peptide was synthesized via standard Fmoc solid-phase methodology, rink-amide resin, and HBTU/HATU activation. Further, N-terminal of the peptide was capped with acetic anhydride (Ac-CDGEAK), cleaved from the resin and processed as described earlier. MALDI-TOF-MS:  $[\text{M} + 1\text{H}]^+$ : Calculated (663.72), Observed (663.49). Ac-CDGEAK peptide (12.5 mg) was dissolved in DMF (2.45 mL) containing Alexa Fluor® 488 carboxylic acid, 2,3,5,6-tetrafluorophenyl ester (1 mg) or Alexa Fluor® 568 carboxylic acid, succinimidyl ester (1 mg) with N,N-Diisopropylethylamine (DIEA, 50  $\mu\text{L}$ ) and reacted overnight protected from light. The samples were concentrated using rotovap, dissolved in Milli Q water, and lyophilized. These fluorescently labeled peptides (Ac-CDGEAK(AF488) and Ac-CDGEAK(AF568)) were used for the experiments without further purification.

### **6.2.4. Engineered Peptide Array Preparation**

Printing efficiency and optimization was developed using a control compound maleamide-488/586 conjugate. A printing buffer consisting of 1% glycerol and 0.2% Triton X-100 was utilized for all protein depositions. To prepare peptide arrays, pre-weighed powders of CRGDS, CRGES, YRGDS and CDGEAK-568 were suspended into printing buffer to reach the desired concentration. Subsequently, photoinitiator

I2959 was added to each peptide solution at a dilution of 0.05% v/v. Peptides were deposited on the fibrous PEG thiol-ene matrices using Aushon 2470 arrayer with 185 micron pins (Aushon BioSystems, Billerica, MA), to achieve dots with a nominal diameter of 250 microns with a 500 $\mu$ m pitch distance. Between different sample depositions, the print needles were cleaned by sonication in cleaning solution before use. Following array printing, PEG thiol-ene peptide arrays were subsequently exposed to 5 mW cm<sup>2</sup> UV light for 5 minutes under inert atmosphere (Argon). Following UV peptide stabilization, prepared PEG thiol-ene peptide arrays were stored at 4°C in a humid environment for 24 h before use.

### **6.2.5. Cell Seeding and Cell Culture**

Electrospun PEG thiol-ene matrices containing various peptides were rinsed in DI H<sub>2</sub>O for 1 h, followed by sterilization with 70% ethanol for 1hr prior to cell seeding. Matrix microarray slides were equipped with 16mm x 16mm silicone multiwall chamber (Grace Bio-Labs) to partition individual microarray replicates. Cell seeding protocols were optimized using primary bovine pulmonary arterial smooth muscle cells (PASCs) obtained from bovine vascular pulmonary arteries. Cells with passages of 3-8 were used for all experiments. PASCs were detached from culture flask and suspended at a concentration of 10<sup>6</sup> cells per ml in serum free media. The cell suspension was dispensed onto the 3-dimensional matrix microarray within the gasket region at a cell density of 10<sup>5</sup> cells per array and incubated for 2 hours. The arrays were then gently aspirated by submerging into a large chamber filled with pre-warmed media. Culture media was changed daily.

### **6.2.6. Immunofluorescent Staining**

Following cell culture, PEG thiol-ene peptide arrays were fixed with 3.7% formaldehyde at room temperature, permeated with 0.1% Triton X-100 and blocked with 3% BSA. Immunofluorescent staining of cells for cell nuclei (DAPI) and cellular cytoskeleton (Alexa488-phalloidin) were utilized to observe cell adhesion and spreading respectively. All samples were finally mounted with Vectashield Hard Set mounting media and stored at 4°C for imaging.

### **6.2.7. Confocal Imaging**

Confocal images were acquired using a Nikon A1R laser scanning confocal microscope piloted by NIS-Elements 4.0 and equipped with 405 nm, 488 nm, 561 nm, and 640 nm laser lines. Typically, the relative z position of the focal plane was ensured by using an equipped Nikon Perfect Focus System. Unless otherwise stated, a 10x 0.5NA objective with the pinhole set to 1.2 Airy Units (AU) was used. PEG thiol-ene peptide array large images were obtained using a motorized XY stage with piezo Z-Drive insert for rapid multidimensional (XYZ) imaging. The image overlap was set to 5% and the resulting digital montage was generated using the same NIS-Elements 4.0 software. When needed, multiple z planes were acquired in order to capture all of the cells within each micro printed well. A maximum intensity projection image was then generated using the piloting software.

### **6.2.5. Statistical analysis**

All tests were performed in triplicate. Statistical significance of collected data was determined at each condition using an independent Student's t-test. Data are presented as mean  $\pm$  standard deviation (SD) and was considered statistically significant at 95% confidence ( $p < 0.05$ ).

## **6.3. Results**

### **6.3.1. Characterization of 3-dimensional fibrous PEG thiol-ene hydrogel matrix**

Fibrous, PEG thiol-ene hydrogels were prepared by an electrospinning process (Figure 1A) similar to our previous method (Wingate 2012; Floren, 2015). We thiolated conventional glass slides to allow covalent attachment of the PEG thiol-ene matrices which improves sample handling and longevity for cell studies. PEG thiol-ene was selected for its biocompatibility, ease of manipulation, soft mechanical properties, anti-fouling, commercial availability and selectivity of thiol-radicals (Reddy, 2006; Hoyle, 2010; Zhu, 2009). Thiol-ene polymerizations proceed by an orthogonal, step-growth mechanism where one thiol reacts with one ene leading to a

highly homogenous distribution in crosslinks (Figure 1B), thus engendering tunable substrate stiffness (Figure 1E,F) with high fidelity.

We examined the fibrous architecture of electrospun PEG thiol-ene substrates using SEM (Figure 1C,D) in both hydrated and dry states. Microscopy revealed a highly fibrous hydrogel structure with average fiber diameter of  $647.6 \pm 81.4$  nm. The absence beading or webbing of the electrospun matrices indicates optimal spinning parameters with minimal artifacts.

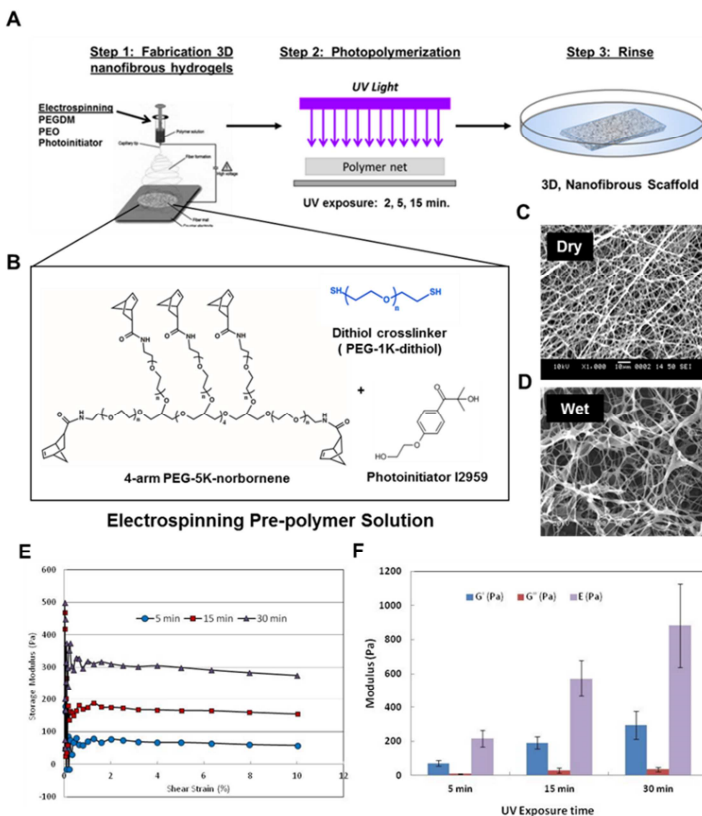


**Figure VI – 1.** Fabrication of nanofibrous PEG-thiol-ene hydrogels. (A) Schematic of electrospinning of PEG-thiol-ene pre-polymer solution (B) followed by UV polymerization. Dry (C) and wet (D) SEM imaging of electrospun PEG-thiol-ene nanofibrous matrices. (C) Rheological measurements of shear stress vs. shear strain for several PEG-thiol-ene substrates prepared under different UV exposures. (D) Translation of shear-strain relationships into elastic modulus using a Poisson ratio  $\nu \sim 0$  [16].

### 6.3.2. Engineered Peptide Synthesis and Array Fabrication

The deposition of peptide microdots is illustrated in Figure 2(A). Following the preparation of PEG thiol-ene matrices, peptide printing is achieved using a contact style arrayer (Ashon 2470) and subsequently post stabilized via a second UV step. Post functionalization of our PEG thiol-ene matrices allows for the covalent incorporation of a diversity of biological ligands or other engineered biomolecules. To illustrate this, printing optimization strategies employing a fluorescently labelled control (maleamide 488/568) are depicted in Figure 2(B-D). Deposition size was found to be approximately 200 $\mu\text{m}$  in diameter which is in agreement with our previous work utilizing ECM proteins (Floren, 2015). Figure 2 (C) represents a serial dilution of eight concentrations of maleamide-488 (green) and eight concentrations of maleamide-568 (red) resulting in sixty-four unique depositions. Full randomization of these sixty-four conditions can be achieved via arraying software as seen in Figure 2(D).

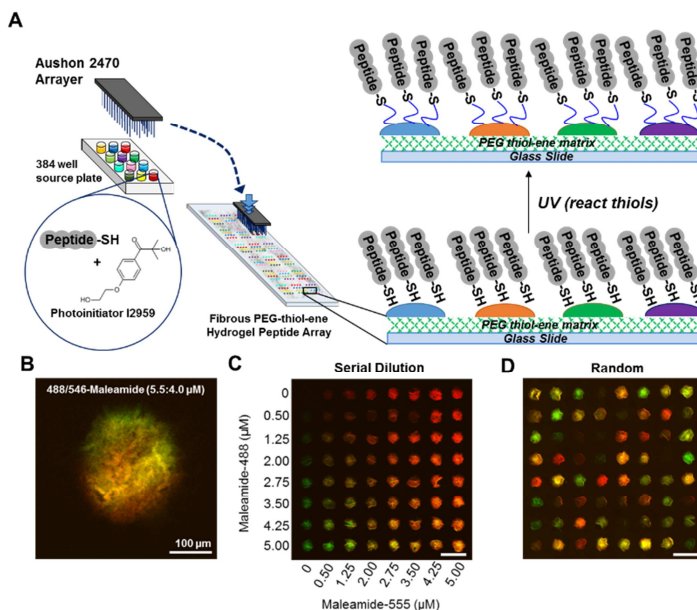


**Figure VI – 2.** Fibrous PEG-thiol-ene hydrogel peptide array fabrication. (A) Schematic of microarray contact printer used to spot different peptide solutions onto electrospun PEG-thiol-ene coated glass slide. Crosslinking is achieved via UV light initiated thiol-ene reactions of di-thiol and norbornene groups on 4-armPEGNB. (B-D) Representative example of two

fluorescently labeled model compounds (maleamide). (B) Depiction of a single deposition of maleamide-488/546 (green/red), ratio 5.5:4.0  $\mu\text{M}$ , illustrating dot circularity and homogeneity. (C) Sixty-four unique concentrations of maleamide-488 (green) and maleamide-546. (D) Complete randomization of the sixty-four unique conditions from (C). Scale bars 500  $\mu\text{m}$  (C,D).

### **6.3.3. Primary Cell Adhesion and Spreading within Peptide Functionalized PEG thiol-ene Matrices**

Following peptide array printing and UV stabilization, PEG thiol-ene peptide arrays were rinsed in water for a minimum of one hour and subsequently sterilized using 70% alcohol (EtOH) prior to cell culture with PSMCs for 24 h. As depicted from the confocal microscope images in Figure 3, the cells only attached to RGD deposited spots with no attachment outside the printing deposition, i.e. neat PEG thiol-ene substrate. We observed cell attachment on YRGDS spots (Figure 3(C); however, the cellular density was considerably less when compared to the covalently stabilized CRGDS spots (Figure 3A). This indicates that covalent stabilization of RGD (CRGDS) permits greater cellular adhesion than surface adsorbed RGD (YRGDS). In contrast, while CRGES peptide was covalently attached to the PEG thiol-ene matrices, the scrambled sequence did not facilitate cell adhesion (Figure 3B), similar to the neat PEG thiol-ene controls (not shown). To further confirm the covalent stabilization of our engineered peptides, we observed a fluorescently-labeled peptide (CDGEAK-568) after UV stabilization and shown in Figure 3(D). The fluorescent intensity of the CDGEAK-568 dots correlate well with the deposition concentration. Together, these results imply that post functionalization of PEG thiol-ene matrices with thiol-ene reactive compounds leads to the fabrication of stable and defined peptide arrays.

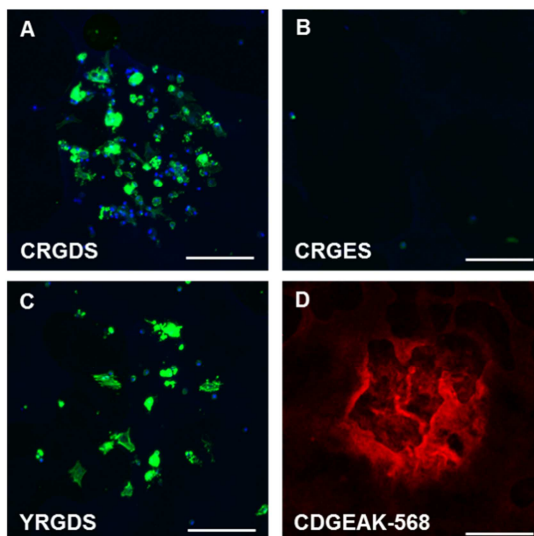


**Figure VI – 3.** Confocal images of PSMCs cultured for 24 h on fibrous PEG thiol-ene hydrogels functionalized with CRGDS (A), CRGES (scramble) (B), YRGDS (C) and CDGEAK-568 (D). Scale bar 100  $\mu\text{m}$ . Cells only attach and spread in the presence of RGD adhesive peptide and is inhibited on RGE (scramble) peptide.

#### 6.3.4. Primary Cell Adhesion and Spreading within PEG thiol-ene Peptide Functionalized Arrays

To further demonstrate the utility of our peptide arrays, we investigated the influence of the adhesive ligand (RGD) post functionalized at several dilutions within the PEG thiol-ene matrices, as shown in Figure 4(A-C). We varied CRGD dilution range from 0.1 to 15 mM and observed cell attachment of PSMCs after 24 h (Figure 4B-C). Cell attachment positively correlated with CRGDS printing concentration. Similar trends were observed for PSMCs seeded onto randomized CRGDS dilutions (Figure 4D-F), indicating that cell-cell paracrine signaling was not a significant factor in cell adhesion. The precision of robotic array spotting allows for complex array layout and design over large areas (Figure 4G). The utility of these complex depositions are further supported by localized cellular attachment as shown in Figure 4H,I. We can conclude from these results that advanced peptide array designs can be prepared, with cellular recognition at modest peptide concentrations (< 1 mM), as well as potential for more complex combinatorial array designs.

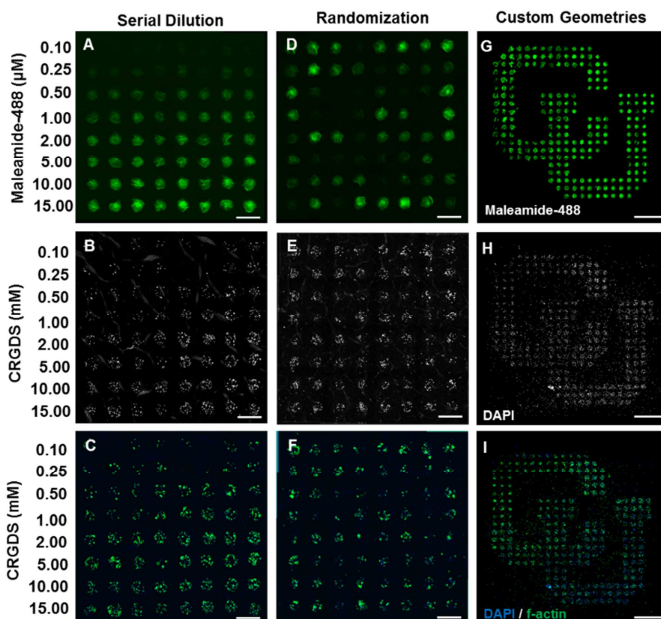


**Figure VI – 4.** Confocal images of primary aortic PSMCs cultured on fibrous PEG thiol-ene hydrogels functionalized with CRGDS at several dilutions (A-C). Complete randomization of CRGDS dilution range depicted in A-C (D-F). Advanced spotting geometry for CRGDS (10 mM). (B-H) Cell nuclear staining (DAPI) in greyscale. (C-I) Merging of cell nuclei stain DAPI (blue) with f-actin stain (green). Scale bars: 500  $\mu$ m (A-F), 2 mm (G-H).

## 6.4. Discussion:

The need for engineered stem cell niches with increased complexity has become a significant challenge within the research community. Due to the lack of current traditional methods to accurately and efficiently capture these complex microenvironments we developed a simple strategy to fabricate high-throughput engineered peptide microarrays using thiol-ene chemistry. This facile method provides a platform for the covalent functionalization of PEG thiol-ene substrates with either engineered peptides or dye-conjugated compounds with high reactivity and specificity. Further, thiol-ene polymerizations proceed by an orthogonal, step-growth mechanism where one thiol reacts with one ene leading to a highly homogenous distribution in crosslinks, thus imparting tunable substrate stiffness with high fidelity (Hoyle, 2010).

Similar to our previous work using ECM proteins (Floren, 2015), we find contact-style array technology to represent a reliable and reproducible method to prepare complex array designs using engineered peptides, which may be further functionalized via UV stabilization post array printing. Engineered peptides are advantageous over conventionally utilized ECM proteins in that the specificity of the desired biological ligands can be highly tuned by the end user. Here we demonstrated the potential to exploit the adhesive ligand (RGD) to influence cell attachment and spreading of PSMCs within 24 h. We observed cellular attachment at modest RGD concentrations ( $< 1$  mM), with absence of cells on the negative controls (RGE and neat PEG thiol-ene matrix). While we only investigated the role of RGD ligand on cell behavior, we note that post functionalization of our PEG thiol-ene matrices can be achieved with any molecule with thiol-ene reactivity, i.e. cysteine residues. Collectively, these results highlight the diverse properties of our substrates, whereby stiffness, geometry, and functionalized molecules (biological or chemical) can be tuned with high specificity.

The preparation of multivariate microenvironments to direct cellular processes is of considerable interest to the research community. Here, we demonstrate the ability to control primary cell adhesion to soft, fibrous hydrogels functionalized with RGD peptide. However, future work will be focused on designing combinatorial peptide studies, whereby, the integration of several biological ligands of interest with tunable physical properties can instruct stem cell differentiation in a highly specific manner. The ability to design such microenvironments with tunable physical properties, stiffness and geometry, as well as biological affinity, through engineered peptides, would conceivably be of great value towards the preparation of future tissue engineering platforms.

## **6.5. Conclusion:**

We have developed a highly tunable platform with 3-D nanofibrous hydrogels based off of thiol-ene coupling chemistry to facilitate high-throughput combinatorial screening of engineered microenvironments for optimizing stem cell differentiation. Microarray depositions of approximately 250  $\mu\text{m}$  and 500  $\mu\text{m}$  were achieved using conventional contact arraying technology. We further specialized our matrices by

post-functionalizing our PEG thiol-ene substrates with biomolecules with thiol-ene reactivity. Collectively, the manipulation of the matrix properties, such as stiffness and geometry, in concert with engineered peptides will facilitate the interrogation of multiple and distinct SC microenvironments.

## **Chapter VII**

### **Conclusion and Future perspectives**

#### **7.1. Conclusions**

This thesis advances the understanding of how different microenvironmental cues effect cell function, particularly in the context of stem cell differentiation, establishes a foundation for the development of future biomaterials combining physical and chemical signals for highly specialized tissue regeneration outcomes, provides a rationale for improved stem cell differentiation protocols via multiple signal integration, and positions hydrogels based on natural (silk fibroin) or synthetic (PEG) polymers as viable candidates, incorporating both physical and chemical stimuli, to direct stem cell fate decisions in a relevant platform.

The first part of this thesis demonstrated a technique to fabricate silk fibroin hydrogels using high pressure CO<sub>2</sub> as a volatile acid without the need for chemical crosslinking agents or surfactants. The advantage to this fabrication technique resides in the remarkably clean production method, simple and efficient recovery of CO<sub>2</sub> post processing, at gelation times shorter than other reported gelation schemes. Further, we demonstrate that this processing method imparts unique structural geometry and porosity throughout the prepared hydrogels. Hydrogel porosity and pore structure represent important design criteria for utility as tissue engineering substrates; we reveal through our novel technique that these features are improved over conventional gelation methods. Lastly, we observed a significant improvement in the mechanical properties of silk hydrogels prepared under high pressure CO<sub>2</sub>. We further detail a mechanistic model whereby the rate of silk protein gelation is believed to be a function of the kinetics of solution acidification from absorbed CO<sub>2</sub> as well as potentially accelerated by high pressure effects.

We next chose to exploit the salient properties of silk hydrogels prepared under CO<sub>2</sub> to investigate the effects of tunable substrate properties on stem cell lineage commitment. The transforming growth factor  $\beta$  (TGF- $\beta$ ) family is a potent regulator of several cell functions such as proliferation, spreading (Hui, 2007) and is strongly associated with vascular smooth muscle cell (vSMC) differentiation of stem cells (Mei, 2010). Therefore, the focus of this part of the thesis was on exploiting the combined use of substrate stiffness and growth factor (TGF-  $\beta$ 1) on SF matrices, with the aim of correlating the effects on the vascular commitment of human mesenchymal stem cells (hMSCs). One advantage to employing silk fibroin as the hydrogel material choice was the inherent biocompatibility and biorecognition imparted by silks. When cultured with serum-starved media upon our SF hydrogels hMSCs attached and spread for up to 72 h. This data suggests that SF is permissive to stem cell adhesion and maintenance irrespective to the presentation of adsorbed serum proteins or other biological ligands. This observation was critical towards our experimental design as previous reports often examine the effects of matrix physical properties on stem cells in the presence of serum-media, an ambiguous cocktail of chemical factors and proteins. The ability to culture stem cells on our silk hydrogels without serum proteins allowed us to investigate the roles of

physical and chemical stimuli independently of one another. The results we present here reveal that hMSC differentiation into mature SMCs can be achieved within modest culture periods (72 h) by combining appropriate SF hydrogel stiffness (33 kPa) with growth factor (TGF- $\beta$ 1). These findings advance our understanding of how complex multicomponent biomaterials, whereby mimicking the intricacy of natural tissue environments, can play a significant role in developing optimal stem cell differentiation protocols.

In addition to soluble factors, insoluble microenvironmental cues such as matrix proteins play a critical role in how cells interact and 'observe' their environment. Recent evidence suggests that cells react to a complex mechanosensing apparatus whereby the interaction of ligand tethering and ECM stiffness can impart differential cellular functions (Seo, 2013), including differentiation (Trappmann, 2012). To this end, we developed a high throughput method that allows for the rapid screening of a diversity of engineered microenvironments with tunable matrix elasticity and geometry, combined with specific ECM protein combination. By adopting a combinatorial approach, we observed the effects of substrate stiffness and unique ECM protein combination on the adhesion, spreading and fate commitment of mesenchymal stem cell (MSCs) under two substrate. Using this technique, we identified several microenvironments supporting MSC adhesion, spreading and differentiation toward early vascular lineages. One advantage to our platform is the ability to manipulate matrix properties, such as stiffness and geometry, in concert with ECM protein presentation in a high-throughput manner. Our data revealed a strong dependence of matrix protein composition and stiffness on MSC differentiation toward vascular lineages. Indeed, several combinatorial environments were arrived at that significantly up- or down- regulate expression of PECAM, an early marker for endothelial phenotype. Collectively, this portion of the thesis supports the hypothesis that a complex milieu exists coupling protein functional behavior with substrate elasticity and that this phenomenon may potentially be exploited through proper application of high-throughput screening methodologies.

Our study investigating the interplay of ECM protein and substrate stiffness advanced our understanding of how cells interact with the various components of

the cellular microenvironments. Nevertheless, most of the existing ECM arrays are not able to capture the effects of biophysical and chemical cues on stem-cell fate completely. For instance, ECM proteins are comprised of a myriad of physical and chemical signaling motifs. Meanwhile, small engineered peptides (SEPs), based off of recognized signaling motifs, have emerged to investigate the effects of individual peptide sequences on cellular activity in a highly specific manner. Further, it is often difficult to decouple the compounding effects of multiple integrin motifs present in full ECM proteins with regard to stem cell fate decision processes. However, combinatorial studies investigating the individual and synergistic role of several SEPs on stem cell differentiation in a relevant model, i.e. soft, fibrous matrix, are absent. The final portion of this thesis developed a microarray platform based on electrospun nanofibrous hydrogels of photoclickable thiol-ene poly(ethylene glycol) (PEG) hydrogels. Thiol-ene polymerizations proceed by an orthogonal, step-growth mechanism where one thiol reacts with one ene leading to a highly homogenous distribution in crosslinks, thus imparting tunable substrate stiffness with high fidelity (Hoyle, 2010). Furthermore, it allows for the subsequent covalent post-modification of PEG thiol-ene hydrogel substrates with small engineered peptides with high reactivity and specificity. Here, we demonstrated the ability to control primary cell adhesion to soft, fibrous hydrogels functionalized with RGD peptide. However, future work will be focused on designing combinatorial peptide studies, whereby, the integration of several biological ligands of interest with tunable physical properties can instruct stem cell differentiation in a highly specific manner. The ability to design such microenvironments with tunable physical properties, stiffness and geometry, as well as biological affinity, through engineered peptides, would conceivably be of great value towards the preparation of future tissue engineering platforms.

## **7.2. Future Directions**

There is supporting evidence that stem cells develop an intimate relationship with their surroundings, whereby cellular events influenced not only by the physical environment, such as rigidity (Engler, 2006) and geometry (Huebsch, 2010), but also the chemical makeup of their milieu through soluble (growth factors) (Mei, 2010;) and

insoluble (ECM proteins, peptides) cues (Flaim, 2005; Floren 2015),. The work presented in this thesis advances our knowledge on how the tight interplay of spatial cues elicited through matrix physical and chemical stimuli may influence cellular events and fate outcomes. There is, however, a practical shift amongst the research community in which both spatial and temporal control of biomimetic scaffolds is likely critical in recapitulating the complex nature of the stem cell niche. Indeed, recent reports have highlighted a significant regulatory role of stem cell fate commitment based off of the temporal expression of matrix physical cues such as rigidity (Lee, 2014; Yang, 2014). Yang et al. concluded that stem cells possess mechanical memory, in which temporal shifting of cellular substrate rigidity, i.e. soft to stiff and vis versa, can result in differential stem cell fate processes. The concept that past physical environments may be 'stored' within the cell as a repository of information guiding the cells' fate lends further investigation into the fourth dimension (temporal control) of biomaterial design. The substrates developed in this thesis could serve as excellent platforms for this achievement. In particular, the chemical specificity and fidelity imparted by the PEG thiol-ene hydrogel substrates detailed earlier (Chapter VI) are amendable to various tunable platforms as well as a myriad of post functionalization pathways. The ability to design complex microenvironments tailored with high spatial and temporal resolution in high throughput would constitute a break through in the research community.

We demonstrated through progression of this thesis a logical approach to design complex microenvironments with an emphasis on high throughput capability. While we revealed this technology to several cell model systems (primary and stem cells), we have certainly promoted the potential to study regenerative systems. However, we would be ingenious to not recognize the potential to explore disease model systems using our current approach. The ability to screen pharmaceuticals or other small molecular systems on disease-induced tissue models is an area of active interest and expansion in research. This can be demonstrated by the recent findings of Chaudhuri et al. in which malignant phenotype in mammary epithelial cells can be rescued by adjusting substrate stiffness in concert with biological ligand presentation (Chaudhuri, 2014). Further, the ability to study multiple disease-state 'micro' tissues, particularly in case of hepatocyte functionality, is under active

development with promising outcomes (Khetani, 2007). There is considerable evidence to suggest that the cellular microenvironment may progressively stiffen (Antia, 2008) or change their protein expression (Dean, 2005) with the progression of disease. The ability for our high throughput systems to integrate tunable rigidity, both healthy and disease level stiffness, equally matched with biochemical modulation suggests these platforms may provide an ideal foundation for exploratory studies in which several microenvironments may be interrogated against their ability to promote or disuade disease progression in relevant tissue models.

A final note on the translation of complex microenvironments into relevant biomaterial platforms for *in vivo* and clinical validation. Here we demonstrated the potential to design complex microenvironments to direct stem cell fate decision in both a synthetic or natural polymer setting. In particular, natural polymers represent an exciting portfolio of biomaterials for potential clinical applications, in part due to their improved biocompatibility and biodegradation kinetics. The ability to design biomaterials with both spatial and/or temporal control of various stimuli in the context of well-tolerated material sources, such as silk fibroin, could represent a paramount achievement in tissue engineering. Indeed, many current clinical-level therapies are lacking due to the disconnect between benchscale observation to clinical level proof of concept. These limitations can foreseeably be alleviated through judicious material selection, via natural polymer approaches, the result being a cohort of biomaterials capable of controlling the regeneration, or repair, of tissues on the patient-level.

### ***List of abbreviation and acronyms***

(CVD) Cardiovascular Disease

(ECM) Extracellular Matrix

(MSC) Mesenchymal Stem Cell

(iPSC) Induced Pluripotent Stem Cell

(SMC) Smooth Muscle Cell

(PEG) Poly ethylene glycol

(2D) Two dimensional

(3D) Three dimensional

(TGF- $\beta$ ) Transforming Growth Factor Beta

(VEGF) Vascular Endothelial Growth Factor

(BMP-2) Bone Morphogenic Protein 2  
(PDGF) Platelet-Derived Growth Factor  
(bFGF) basic Fibroblast Growth Factor  
(SC) Stem Cell  
(EC) Endothelial Cell  
(CO<sub>2</sub>) Carbon Dioxide  
(PBS) Phosphat Buffer Solution  
(SEM) Scanning Electron Microscopy  
(ESEM) Environemntal Scanning Electron Microscopy  
(FTIR) Fourier-Transform Infrared Spectroscopy

## **References**

1. Abdeen, A.A., J.B. Weiss, J. Lee, and K.A. Kilian, *Matrix composition and mechanics direct proangiogenic signaling from mesenchymal stem cells*. Tissue Engineering Part A, **2014**. 20: p. 2737-2745.
2. Ahsan, T., and R.M. Nerem, *Fluid shear stress promotes an endothelial-like phenotype during the early differentiation of embryonic stem cells*. Tissue Engineering Part A, **2010**. (16): p. 3547–3553.

3. Altman, G. H., R. L. Horan, H. H. Lu, et al., *Silk matrix for tissue engineered anterior cruciate ligaments*. *Biomaterials* **2002**. (23) p. 4131-4141.
4. Altman, G.H., F. Diaz, C. Jakuba, T. Calabro, R. Horan, J. Chen, H. Lu, J. Richmond, and D. Kaplan, *Silk-based biomaterials*. *Biomaterials* **2003**. (24) p. 401-416.
5. Anderson, D., D. Putnam, E. Lavik, T. Mahmooda, and R. Langer, *Biomaterial microarrays: rapid, microscale screening of polymer–cell interaction*. *Biomaterials* **2005**. (26) p. 4892–4897
6. Anderson D., S. Levenberg, and R. Langer. *Nanoliter-scale synthesis of arrayed biomaterials and application to human embryonic stem cells*. *Nat. Biotechnol* **2004**. (22) p. 863–866.
7. Andreadis S.T., *Give your heart a chance: match the muscle to the vessel*. *Cardiovascular Research* **2013**. (98) p. 1-2.
8. Annabi, N., S.M. Mithieux, A.S. Weiss, and F. Dehghani, *The fabrication of elastin-based hydrogels using high pressure CO<sub>2</sub>*. *Biomaterials* **2009**. (30) p. 1–7.
9. Annabi, N., S.M. Mithieux, A.S. Weiss, and F. Dehghani, *Cross-linked open-pore elastic hydrogels based on tropoelastin, elastin and high pressure CO<sub>2</sub>*. *Biomaterials* **2010**. (31) p. 1655–1665.
10. Annabi, N., S.M. Mithieux, E.A. Boughton, A.J. Ruys, A.S. Weiss, and F. Dehghani, *Synthesis of highly porous crosslinked elastin hydrogels and their interaction with fibroblasts in vitro*. *Biomaterials* **2009**. (30) p. 4550-4557.

11. Anseth, K. S., C.N. Bowman, and L. Brannon-Peppas, *Mechanical properties of hydrogels and their experimental determination*. *Biomaterials* **1996**. (17) p. 1647– 1657.
12. Antia, M., G. Baneyx, K.E. Kubow, and V. Vogel. *Fibronectin in aging extracellular matrix fibrils is progressively unfolded by cells and elicits an enhanced rigidity response*. *Faraday Discuss* **2008**. (139) p. 229–249.
13. Ayub, Z., M. Arai, and K. Hirabayashi, *Biosci.*, *Mechanism of the gelation of fibroin solution*. *Biosci Biotechnol Biochem* **1993**. (57) p. 1910–1912.
14. Bajpai, V.K., and S.T. Andreadis, *Stem Cell Sources for Vascular Tissue Engineering and Regeneration*. *Tissue Engineering Part B* **2012**. (18) p. 405-425.
15. Bajpai, V.K., P. Mistriotis, Y.H. Loh, G.Q. Daley, and S.T. Andreadis, *Functional vascular smooth muscle cells derived from human induced pluripotent stem cells via mesenchymal stem cell intermediates*. *Cardiovasc Res* **2012**. (96) p. 391-400.
16. Battista, S., D. Guarnieri, C. Borselli, S. Zeppetelli, A. Borzacchiello, L. Mayol, D. Gerbasio, D.R. Keene, L. Ambrosio, and P.A. Netti. *The effect of matrix composition of 3D constructs on embryonic stem cell differentiation*. *Biomaterials* **2005**. (26) p. 6194–6207.
17. Bini, E., D.P. Knight, and D.L. Kaplan, *Mapping domain structures in silks from insects and spiders related to protein assembly*. *J. Mol. Biol.* **2004**. (335) p. 27–40.
18. Bonani, W., D. Maniglio, A. Motta, W. Tan, and C. Migliaresi. *Biohybrid nanofiber constructs with anisotropic biomechanical properties*. *J. Biomed. Mater. Res.: Part B Appl. Biomat* **2011**. (96) p. 276-86.

19. Bondar, B., S. Fuchs, A. Motta, C. Migliaresi, and C.J. Kirkpatrick. *Functionality of endothelial cells on silk fibroin nets: Comparative study of micro- and nanometric fibre size*. *Biomaterials* **2008** (29) p. 561–572.
20. Bortoluzzi, D., C. Cinquemani, E. Torresani, and S. Spilimbergo, *Pressure-induced pH changes in aqueous solutions – On-line measurement and semi-empirical modelling approach*. *S. J. Supercrit. Fluids* **2011**. (56) p. 6–13.
21. Bouten, C.V.C., P.Y.W. Dankers, A. Driessen-Mol, S. Pedron, A.M.A. Brizard, and F.P.T. Baaijens, *Substrates for cardiovascular tissue engineering*. *Adv. Drug. Deliver. Rev.* **2011** (63) p. 221-241.
22. Breitbach, M., T. Bostani, W. Roell, Y. Xia, O. Dewald, J.M. Nygren, et al. *Potential risks of bone marrow cell transplantation into infarcted hearts*. *Blood* **2007**. (110) p. 1362-1369.
23. Bryant, J.S., and K.S. Anseth. *The effects of scaffold thickness on tissue engineered cartilage in photocrosslinked poly(ethylene oxide) hydrogels*. *Biomaterials* 2001. (22) p. 619–626.
24. Carlson, A.L., C.A. Florek, J.J. Kim, T. Neubauer, J.C. Moore, C. Cohen et al. *Microfibrous substrate geometry as a critical trigger for organization, self-renewal, and differentiation of human embryonic stem cells within synthetic 3-dimensional microenvironments*. *FASEB* **2012**. (26) p. 3240–3251
25. Carmeliet, P., *Mechanisms of angiogenesis and arteriogenesis*. *Nature Med.* **2000**. (6) p. 389–395.

26. Chaudhuri, O., S.T. Koshy, C. Branco da Cunha, J. Shin, C.S. Verbeke, K.H. Allison, et al. *Extracellular matrix stiffness and composition jointly regulate the induction of malignant phenotypes in mammary epithelium*. *Nature Mater* **2014**. (13) p. 970–978.
27. Chen, X., Z. Shao, D.P. Knight, and F. Vollrath, *Conformation transition kinetics of Bombyx mori silk protein*. *Proteins: Struct., Funct., Bioinf.* **2007**. (68) p. 223–231.
28. Chiarini, A., P. Petrini, S. Bozzini, I. Pra, and U. Armato, *Silk fibroin/poly(carbonate)-urethane as a substrate for cell growth: in vitro interactions with human cells*. *Biomaterials* **2003**. (24) p. 789-799.
29. Chomczynski, P., and N. Sacchi. *Single-step method of RNA isolation by acid guanidinium thiocyanate-phenol-chloroform extraction*. *Anal. Biochem.* **1987**. (162) p. 156–159.
30. Chua, C., *Review The Design of Scaffolds for Use in Tissue Engineering. Part I. Traditional Factors*. *Tissue Engineering* 2001. 7(6) p. 679-689.
31. Cleary et al. *Vascular Tissue Engineering: The Next Generation*. *Trends in Molecular Medicine* **2012**. (7) p. 394-404.
32. Cole, M.A., N.H. Voelcker, H. Thissen, H.J. Griesser. *Stimuli-responsive interfaces and systems for the control of protein-surface and cell-surface interactions*. *Biomaterials* **2009**. (30) p. 1827–1850.
33. Coleman, D., and F.O. Howitt, *Studies on Silk Proteins. I. The Properties and Constitution of Fibroin. The Conversion of Fibroin into a Water-Soluble Form and Its Bearing on the Phenomenon of Denaturation*. *Proc. R. Soc. Lond. A* **1947** (190) p. 145-169.

34. Cruise, G.M, D.S. Scharp, and J.A. Hubbell, *Characterization of permeability and network structure of interfacially photopolymerized poly(ethylene glycol) diacrylate hydrogels*. *Biomaterials* **1998**. (19) p. 1287–1294.
35. Cukierman, E., R. Pankov, and K.M. Yamada. *Cell interactions with three-dimensional matrices*. *Curr. Opin. Cell Biol.* **2002**. (14) p. 633–639.
36. Cukierman, E., R. Pankov, D.R. Stevens, and K.M. Yamada. *Taking cell-matrix adhesions to the third dimension*. *Science* **2001**. (294) p. 1708–1712.
37. da Silva Meirelles, L., A.I. Caplan, and N.B. Nardi. *In search of the in vivo identity of mesenchymal stem cells*. *Stem Cells* **2008**. (26) p. 2287-2299.
38. Davis, G.E., and D.R. Senger. *Endothelial extracellular matrix: Biosynthesis, remodeling, and functions during vascular morphogenesis and neovessel stabilization*. *Circ. Res.* **2005**. (97) p. 1093–1107.
39. Dean, R.G., L.C. Balding, R. Candido, W.C. Burns, Z. Cao, S.M. Twigg, et al. *Connective tissue growth factor and cardiac fibrosis after myocardial infarction*. *J. Histochem. Cytochem.* **2005**. (53) p. 1245-1256.
40. Dehghani, F., N. Annabi, P. Valtchev, S. Mithieux, A. Weiss, S. Kazarian, and F. Tay, *Effect of Dense Gas CO<sub>2</sub> on the Coacervation of Elastin*. *Biomacromolecules* **2008**. (9) p. 1100-1105.
41. Derynck, R., and X-H. Feng, *TGF- $\beta$  receptor signaling*. *Biochim Biophys Acta* **1997**. (1333) p. 105–150.

42. Discher, D.E., Discher, D.J. Mooney, and P.W. Zandstra. *Growth factors, matrices, and forces combine and control stem cells*. Science 2009. (324) p. 1673–1677.
43. Discher, D.E., P. Janmey, and Y.L. Wang. *Tissue cells feel and respond to the stiffness of their substrate*. Science **2005**. (310) p. 1139-1143.
44. Dolatshahi-Pirouz, A., M. Nikkhah, A.K. Gaharwar, B. Hashmi, E. Guermani, H. Aliabadi, et al. *A combinatorial cell-laden gel microarray for inducing osteogenic differentiation of human mesenchymal stem cells*. Sci. Rep. **2014**. (4) p. 3896.
45. Drury, J.L., and D.J. Mooney. *Hydrogels for tissue engineering: scaffold design variables and applications*. Biomaterials **2003**. (24) p. 4337-4351.
46. Duan, Z., R. Sun, C. Zhu, and I.M. Chou, *An improved model for the calculation of CO<sub>2</sub> solubility in aqueous solutions containing Na<sup>+</sup>, K<sup>+</sup>, Ca<sup>2+</sup>, Mg<sup>2+</sup>, Cl<sup>-</sup>, and SO<sub>4</sub><sup>2-</sup>*. Mar. Chem. **2006**. (98) p. 131–139.
47. Edsall, J.T., H.A. McKenzie, *Water and proteins. II. The location and dynamics of water in protein systems and its relation to their stability and properties*. Adv. Biophys. **1983**. (16) p. 53-183.
48. Edwards, T.J., G. Maurer, J. Newman, and J.M. Prausnitz, *Vapor-liquid equilibria in multicomponent aqueous solutions of volatile weak electrolytes*. AIChE J. **1978**. (24) p. 966–976.
49. Elliot, W.H., W. Bonani, D. Maniglio, A. Motta, W. Tan, and C. Migliaresi. *Silk Hydrogels of Tunable Structure and Viscoelastic Properties Using Different Chronological Orders of Genipin and Physical Cross-Linking*. Applied Materials & Interfaces **2015**. (22) p. 12099-12108.

50. El-Mounaryi, O., A. Mihic, E.A. Shikatani, M. Gagliardi, S.K. Steinbach, N. Dubois, R. Dacosta, R.K. Li, G. Keller, and M. Husain. *Serum-free differentiation of functional human coronary-like vascular smooth muscle cells from embryonic stem cells*. *Cardiovasc Res* **2013**. (98) p. 125–135.
51. Engler, J.A., S. Sen, H.L. Sweeney, and D.E. Discher. *Matrix Elasticity Directs Stem Cell Lineage Specification*. *Cell* **2006**. (126) p. 677–689.
52. Fernandes, T.G., S.J. Kwon, S.S. Bale, M.Y. Lee, M.M. Diogo, D.S. Clark et al. *Three-Dimensional Cell Culture Microarray for High Throughput Studies of Stem Cell Fate*. *Biotechnol Bioeng* **2010**. (106) p. 106–118.
53. Fini, M., A. Motta, P. Torricelli, G. Giavaresi, N. Nicoli Aldini, M. Tschon, R. Giardino, and C. Migliaresi. *The healing of confined critical size cancellous defects in the presence of silk fibroin hydrogel*. *Biomaterials* **2005**. (26) p. 3527-3536.
54. Flaim, C.J., S. Chien, and S.N. Bhatia. *An extracellular matrix microarray for probing cellular differentiation*. *Nat. Methods* **2005**. (2) p. 119–125
55. Floren, M.L., S. Spilimbergo, A. Motta, and C. Migliaresi. *Carbon Dioxide Induced Silk Protein Gelation for Biomedical applications*. *Biomacromolecules* **2012**. (13) p. 2060– 2072.
56. Floren, M.L., S. Spilimbergo, A. Motta, and C. Migliaresi, *Porous poly(D,L-lactic acid) foams with tunable structure and mechanical anisotropy prepared by supercritical carbon dioxide*. *J Biomed Mater Res Part B* **2011**. (99B) p. 338-349.
57. Fozdar, D.Y., P. Soman, J.W. Lee, L.H Han, and S. Chen. *Three-dimensional polymer constructs exhibiting a tunable negative Poisson's ratio*. *Adv Funct Mater* **2011**. (21) p. 2712–2720.

58. Fratzl, P., and R. Weinkamer. *Nature's hierarchical materials*. *Progress in Materials Science* **2007** (52) p. 1263-1334.
59. Frith, J.E., R.J. Mills, J.E. Hudson, and J.J. Cooper-White. *Tailored integrin-extracellular matrix interactions to direct human mesenchymal stem cell differentiation*. *Stem Cells Dev* **2012**. 21(13) p. 2442-2456.
60. Gebhardt, R., C. Vendrely, M. Hanfland, C. Riekel, *Silk Fiber Formation after High-Pressure Treatment of Fibroin Solution in a Diamond Anvil Cell*. *Macromolecules* **2008**. (41) p. 9934–9936.
61. Ghaedi, M., N. Tuleuova, M.A. Zern, J. Wu, A. Revzin. *Bottom-up signaling from HGF-containing surfaces promotes hepatic differentiation of mesenchymal stem cells*. *Biochem. Biophys. Res. Commun* **2011**. (407) p. 295–300.
62. Gibson, L.J., and M.F. Ashby. *The Mechanics of Three-Dimensional Cellular Materials*. *Proc. R. Soc. Lond. A* **1982**. (382) p. 43-59.
63. Gobaa, S., S. Hoehnel, M. Roccio, A. Negro, S. Kobel, and M.P. Lutolf. *Artificial niche microarrays for probing single stem cell fate in high throughput*. *Nat Meth* **2011**. (8) p. 949-955.
64. Gong, Z., and L.E. Niklason. *Small-diameter human vessel wall engineered from bone marrow-derived mesenchymal stem cells (hMSCs)*. *FASEB J* **2008**. (22) p. 1635–1648.
65. Gotoh, Y., S. Niimi, T. Hayakawa, and T. Miyashita. *Preparation of lactose-silk fibroin conjugates and their application as a scaffold for hepatocyte attachment*. *Biomaterials* **2004**. (25) p. 1131–1140.

66. Gross, M., and R. Jaenicke. *Proteins under pressure: The influence of high hydrostatic pressure on structure, function and assembly of proteins and protein complexes*. Eur. J. Biochem. **1994**. (221) p. 617–630.
67. Gunatillak, P.A., and R. Adhikari. *Biodegradable synthetic polymers for tissue engineering*. Eur Cells Mater J **2003**. (5) p. 1–16.
68. Han, H., T. Wecker, F. Grehn, G. Schlunck. *Elasticity-dependent modulation of TGF-beta responses in human trabecular meshwork cells*. Invest Ophthalmol Vis Sci **2011**. 52(6) p. 2889-2896.
69. Han, J., J.Y. Liu, D.D. Swartz, and S.T. Andreadis. *Molecular and functional effects of organismal ageing on smooth muscle cells derived from bone marrow mesenchymal stem cells*. Cardiovasc Res **2010**. (87) p. 147–155.
70. Hanawa, T., A. Watanabe, T. Tsuchiya, R. Ikoma, M. Hidaka, and M. Sugihara. *New oral dosage form for elderly patients: preparation and characterization of silk fibroin gel*. Chem. Pharm. Bull. **1995**. (43) p. 284-288.
71. Hersel, U., C. Dahmen, and H. Kessler. *RGD modified polymers biomaterials for stimulated cell adhesion and beyond*. Biomaterials, **2003**. (24) p. 4385–4415
72. Hinz, B., *The matrix and the transforming growth factor: tale of a strained relationship*. Matrix Biol. **2015**. [e-pub ahead of print]
73. Hofland, G., M. Es, L.A.M. Wielen, G. Witkamp, *Isoelectric Precipitation of Casein Using High-Pressure CO<sub>2</sub>*. Ind. Eng. Chem. Res. **1999**. (38) p. 4919-4927.

74. Hofland, G., A. Rijke, R. Thiering, L.A.M. Wielen, G. Witkamp, *Isoelectric precipitation of soybean protein using carbon dioxide as a volatile acid*. J. Chromatogr., B: Biomed. Sci. Appl. **2000**. (743) p. 357–368.
75. Hofland, G.M., M. Berkhoff, G.J. Witkamp, L.A.M. Wielen, *Dynamics of precipitation of casein with carbon dioxide*. Int. Dairy J. **2003**. (13) p. 685–697.
76. Howdle, S.M., M.S. Watson, M.J. Whitaker, V.K. Popov, M.C. Davies, F.S. Mandel, J.D. Wang, and K.M. Shakesheff, *Supercritical fluid mixing: preparation of thermally sensitive polymer composites containing bioactive materials*. Chem. Commun. **2001** (1) p. 109-110.
77. Hoyle, C.E., and C. N. Bowman, *Thiol–Ene Click Chemistry*. Angew. Chem. Int. Ed. **2010**. (49) p. 1540-1573
78. Hu, X., D. Kaplan, and P. Cebe. *Determining Beta-Sheet Crystallinity in Fibrous Proteins by Thermal Analysis and Infrared Spectroscopy*. Macromolecules **2006** (39) p. 6161–6170.
79. Hu, X., K. Shmelev, L. Sun, E. Gil, S. Park, P. Cebe, D. Kaplan, *Regulation of Silk Material Structure by Temperature-Controlled Water Vapor Annealing*. Biomacromolecules **2011**. (12) p. 1686-1696.
80. Huebsch, N., P.R. Arany, A.S. Mao, D. Shvartsman, O.A. Ali, S.A. Bencherif et al. *Harnessing traction-mediated manipulation of the cell/matrix interface to control stem-cell fate*. Nat Mater **2010**. 9(6) p. 518-526.
81. Hui, E.E., and S.N. Bhatia. *Micromechanical control of cell–cell interactions*. Proc. Natl. Acad. Sci. **2007**. (104) p. 5722-5726.

82. Hynes, R.O., *The extracellular matrix: Not just pretty fibrils*. Science **2009**. (326) p. 1216–1219.
83. Jayakrishnan, A., and S.R. Jameela, *Glutaraldehyde as a fixative in bioprostheses and drug delivery matrices*. Biomaterials **1996**. (17) p. 471-484.
84. Ji, C., N. Annabi, A. Khademhosseini, F. Dehghani, *Fabrication of porous chitosan scaffolds for soft tissue engineering using dense gas CO<sub>2</sub>*. Acta Biomater. **2011**. (7) p. 1653–1664.
85. Jin, H., S.V. Fridrikh, G.C. Rutledge, D.L. Kaplan, *Electrospinning Bombyx mori Silk with Poly(ethylene oxide)*. Biomacromolecules **2002**. (3) p. 1233-1239.
86. Kan, I., E. Melamed, and D. Offen. *Integral therapeutic potential of bone marrow mesenchymal stem cells*. Curr. Drug Targets **2005**. 6(1) p. 31–41.
87. Kanie, K., Y. Narita, Y. Zhao, F. Kuwabara, M. Satake, S. Honda, H. Kaneko, T. Yoshioka, M. Okochi, H. Honda, and R. Kato, *Collagen type IV-specific tripeptides for selective adhesion of endothelial and smooth muscle cells*. Biotechnol. Bioeng. **2012** (109) p. 1808–1816.
88. Kazarian S. G. *Polymer processing with supercritical fluids*. Polym. Sci., Ser. C **2000**. (42) p. 78-101.
89. Khetani, S.R., and S.N. *Microscale Human Liver Tissue for Drug Development*. Nature Biotechnology **2007**. (26) p. 120-126.
90. Kim, T.G., H. Shin, D.W. Lim. *Biomimetic scaffolds for tissue engineering*. Adv. Funct. Mater. **2012**. (22) p. 2446–2468.

91. Kim, S.H., Y.S. Nam, T.S. Lee, W.H. Park, *Silk Fibroin Nanofiber. Electrospinning, Properties, and Structure*. Polym. J. **2003**. (35) p. 185–190.
92. Kim, U., J. Park, H.J. Kim, M. Wada, D.L. Kaplan, *Three-dimensional aqueous-derived biomaterial scaffolds from silk fibroin*. Biomaterials **2005**. (26) p. 2775-2785.
93. Kim, U., J. Park, C. Li, H. Jin, R. Valluzzi, D.L. Kaplan, *Structure and Properties of Silk Hydrogels*. Biomacromolecules **2004** (5) p. 786-792.
94. Kinner, B., J.M. Zaleskas, and M. Spector. *Regulation of smooth muscle actin expression and contraction in adult human mesenchymal stem cells*. Exp Cell Res, **2002** (278) p. 72–83.
95. Kitchen, D. B., L.H. Reed, R.M. Levy, *Molecular Dynamics Simulation of Solvated Protein at High Pressure*. Biochemistry **1992** (31) p. 10083–10093.
96. Klotzsch, E., I. Schoen, J. Ries, A. Renn, V. Sandoghdare, V. Vogel. *Conformational distribution of surface-adsorbed fibronectin molecules explored by single molecule localization microscopy*. Biomater. Sci. **2014** (2) p. 883-892.
97. Kniazeva, E., S. Kachgal, A.J. Putnam. *Effects of extracellular matrix density and mesenchymal stem cells on neovascularization in vivo*. Tissue Engineering Part A **2011** (17) p. 905–914.
98. Kochanek, K.D., J.Q. Xu, S.L. Murphy, A.M. Miniño, and H.C. Kung. *Deaths: final data for 2009*. National vital statistics reports. **2011** 60(3).

99. Krawiec, J.T., D.A. Vorp. *Adult stem cell-based tissue engineered blood vessels: A review*. *Biomaterials* **2012**. (33) p. 3388-3400
100. Kshitiz, M.E., E.H. Hubbi, J. Ahn, J. Downey, A. Kim, et al. *Matrix rigidity controls endothelial differentiation and morphogenesis of cardiac precursors*. *Sci Signal* **2015** (5) p. ra41
101. Kundu, B., R. Rajkhowa, S.C. Kundu, X. Wang. *Silk fibroin biomaterials for tissue regenerations*. *Adv. Drug. Deliv. Rev.* **2013**. (65) p. 457-470.
102. Kuraitis, D., C. Giordano, M. Ruel, A. Musarò, E.J. Suuronen. *Exploiting extracellular matrix-stem cell interactions: a review of natural materials for therapeutic muscle regeneration*. *Biomaterials* 2012 (33) p. 428–443.
103. Kweon, H., J.-h. Yeo, K.-gill Lee, H. C. Lee, H. S. Na, Y. H. Won, et al. *Semi-interpenetrating polymer networks composed of silk fibroin and poly(ethylene glycol) for wound dressing*. *Biomedical Materials* **2008**. (3) p. 034115.
104. Lachaud, C.C., D. Pezzolla, A. Dominguez-Rodríguez, T. Smani, B. Soria, A. Hmadcha. *Functional Vascular Smooth Muscle-like Cells Derived from Adult Mouse Uterine Mesothelial Cells*. *PLoS ONE* **2013**. 8(2) p. e55181.
105. Laflamme, M.A., C.E. Murry. *Heart regeneration*. *Nature* **2011**. (473) p. 326–335.
106. Langer, R., J.P. Vacanti. *Tissue Engineering*. *Science* **1993**. (260) p. 920-926.
107. Laslett, L.J., P. Alagona Jr., B.A. Clark 3rd, J.P. Drozda Jr., F. Saldivar, S.R. Wilson, C. Poe, M. Hart. *The worldwide environment of*

*cardiovascular disease: prevalence, diagnosis, therapy, and policy issues: a report from the American College of Cardiology.* J Am Coll Cardiol. **2012** (60) p. S1–49.

108. Lawrence B.D., J.K. Marchant, M.A. Pindrus, F.G. Omenetto, D.L. Kaplan. *Silk film biomaterials for cornea tissue engineering.* Biomaterials **2009**. (30) p. 1299–1308.
109. Lee, C.H., A. Singla, Y. Lee. *Biomedical applications of collagen.* Int. J. Pharm. **2001**. (221) p. 1–22.
110. Lee, K.Y., W.S. Ha, *DSC studies on bound water in silk fibroin/S-carboxymethyl kerateine blend films.* Polymer **1999**. (40) p. 4131–4134.
111. Li, D., and Z. Duan, *The speciation equilibrium coupling with phase equilibrium in the H<sub>2</sub>O–CO<sub>2</sub>–NaCl system from 0 to 250 °C, from 0 to 1000 bar, and from 0 to 5 molality of NaCl.* Chem. Geol. **2007**. (244) p. 730–751.
112. Li, M., Z. Wu, C. Zhang, S. Lu, H. Yan, D. Huang, H. Ye. *Study on porous silk fibroin materials. II. Preparation and characteristics of spongy porous silk fibroin materials.* J. Appl. Polym. Sci. **2001**. (79) p. 2192-2199.
113. Liao, X., S. Lu, Y. Wu, W. Xu, Y. Zhuo, Q. Peng, et al. *The effect of differentiation induction on FAK and Src activity in live HMSCs visualized by FRET.* PLoS One. **2013** (27) p. 8
114. Liao, X., S. Lu, Y. Zhuo, C. Winter, W. Xu, et al. *Visualization of Src and FAK Activity during the Differentiation Process from HMSCs to Osteoblasts.* PLoS ONE **2012**. 7(8) p. e42709

115. Lim, S.H., H.Q. Mao. *Electrospun scaffolds for stem cell engineering*. *Adv. Drug Deliv. Rev.* **2009** (61) p. 1084–1096
116. Liu, Y., B. Deng, Y. Zhao, S. Xie, R. Nie. *Differentiated markers in undifferentiated cells: Expression of smooth muscle contractile proteins in multipotent bone marrow mesenchymal stem cells*. *Dev Growth Differ.* **2013**. (55) p. 591-605.
117. Livak, K.J., T. D. Schmittgen. *Analysis of relative gene expression data using real-time quantitative PCR and the  $2^{-\Delta\Delta C_T}$  Method*. *Methods* **2001**. (25) p. 402–408.
118. Lozito, T.P., J.M. Taboas, C.K. Kuo, R.S. Tuan. *Mesenchymal stem cell modification of endothelial matrix regulates their vascular differentiation*. *J Cell Biochem* **2009**. (107) p. 706–713.
119. MacBeath, G., S.L. Schreiber. *Printing Proteins as Microarrays for High-Throughput Function Determination*. *Science* **2000**. (289) p. 1760
120. Mammoto, A., K.M. Connor, T. Mammoto, C.W. Yung, D. Huh, C.M. Aderman, et al. *A mechanosensitive transcriptional mechanism that controls angiogenesis*. *Nature* **2009**. (457) p. 1103–1108
121. Mandal, B.B., S. H. Park, E. S. Gil, D. L. Kaplan, *Multilayered silk scaffolds for meniscus tissue engineering*. *Biomaterials* **2011** (32) p. 639–651.
122. Mann B.K., A.S. Gobin, A.T. Tsai, R.H. Schmedlen, J.L. West. *Smooth muscle growth in photopolymerized hydrogels with cell adhesive and proteolytically degradable domains: synthetic ECM analogs for tissue engineering*. *Biomaterials* **2001**. (22) p. 3045–3051

123. Martino, M.M., P.S. Briquez, E. Guc, F. Tortelli, W.W. Kilarski, S. Metzger, J.J. Rice, G.A. Kuhn, R. Müller, M.A. Swartz, J.A. Hubbell. *Growth factors engineered for super-affinity to the extracellular matrix enhance tissue healing*. *Science* **2014** (343) p. 885–888.
124. Martino, M.M., M. Mochizuki, D.A. Rothenfluh, S.A. Rempel, J.A. Hubbell, T.H. Barker. *Controlling integrin specificity and stem cell differentiation in 2D and 3D environments through regulation of fibronectin domain stability*. *Biomaterials* **2009**. 30(6) p. 1089-1097.
125. Matsumoto, A., J. Chen, A.L. Collette, U.J. Kim, G.H. Altman, P. Cebe, D. Kaplan. *Mechanisms of silk fibroin sol-gel transitions*. *J. Phys. Chem. B*, **2006**. (110) p. 21630–21638.
126. Mei, Y., K. Saha, S.R. Bogatyrev, J. Yang. et al. *Combinatorial development of biomaterials for clonal growth of human pluripotent stem cells*. *Nat. Mater* **2010**. (9) p. 768–778
127. Meinel, L., R. Fajardo, S. Hofmann, R. Langer, J. Chen, B. Snyder, G. Vunjak-Novakovic, D. Kaplan. *Silk implants for the healing of critical size bone defects*. *Bone* 2005 (37) p. 688–698.
128. Meyssami, B.; Balaban, M.O.; Teixeira, A.A. *Prediction of pH in model systems pressurized with carbon dioxide*. *Biotechnol Prog.* **1992** (8) p. 149–154.
129. Yang, M., S. Yuan, T. Chung, et al., *Characterization of Silk Fibroin Modified Surface: A Proteomic View of Cellular Response Proteins Induced by Biomaterials*, *BioMed Research International*, **2014**. (vol. 2014) p. 13

130. Motta, A., M. Floren, C. Migliaresi. *Silk in Medicine in P. Aramwit's Silk: Properties, Production and Uses*. **2012**. Hauppauge, NY. USA: Nova Publishing Group.
131. Motta, A., B. Barbato, C. Foss, P. Torricelli, C. Migliaresi. *Stabilization of Bombyx mori silk fibroin/sericin films by crosslinking with PEG-DE 600 and genipin*. *J. Bioact. Compat. Polym.* **2011**. (26) p. 130-143.
132. Motta, A., L. Fambri, C. Migliaresi. *Regenerated silk fibroin films: Thermal and dynamic mechanical analysis*. *Macromol. Chem. Phys.* **2002**. (203) p. 1658-1665.
133. Motta, A., C. Migliaresi, F. Faccioni, P. Torricelli, M. Fini, R. Giardino. *Fibroin hydrogels for biomedical applications: Preparation, characterization and in vitro cell culture studies*. *J. Biomater. Sci., Polym. Ed.*. **2004**. (15) p. 851-864.
134. Moy, R.L., A. Lee and A. Zalka. *Commonly used suture materials in skin surgery*. *Am. Fam. Physician* **1991**. (44) p. 2123-2128.
135. Mozhaev, V., K. Heremans, J. Frank, P. Masson, C. Balny. *High pressure effects on protein structure and function*. *Proteins: Struct., Funct., Bioinf.* **1996**. (24) p. 81–91.
136. Mozhaev, V., K. Heremans, J. Frank, P. Masson, C. Balny. *Exploiting the effects of high hydrostatic pressure in biotechnological applications*. *Trends Biotechnol.* **1994**. (12) p. 493-501.
137. Murphy, A.R., D.L. Kaplan. *Biomedical applications of chemically-modified silk fibroin*. *J Mater Chem* **2009**. 19(36) p. 6443–6450

138. Narita, Y., A. Yamawaki, H. Kagami, M. Ueda, Y. Ueda. *Effects of transforming growth factor-beta 1 and ascorbic acid on differentiation of human bone-marrow-derived mesenchymal stem cells into smooth muscle cell lineage*. Cell Tissue Res **2008**. (333) p. 449-459.
139. Nazarov, R., H. Jin, D.L. Kaplan. *Porous 3-D Scaffolds from Regenerated Silk Fibroin*. Biomacromolecules **2004**. (5) p. 718-726.
140. Nuttelman, C.R., M.C. Tripodi, K.S. Anseth. *Synthetic hydrogel niches that promote hMSC viability*. Matrix Biol **2005**. 24(3) p. 208–218.
141. O'Shea, C.A., S.O. Hynes, G. Shaw, B.A. Coen, A.C. Hynes, J. McMahon, M. Murphy, F. Barry, T. O'Brien. *Bolus delivery of mesenchymal stem cells to injured vasculature in the rabbit carotid artery produces a dysfunctional endothelium*. Tissue Engineering Part A **2010**. (16) p. 1657-1665.
142. Oswald, J., S. Boxberger, B. Jørgensen, S. Feldmann, G. Ehninger, et al. *Mesenchymal stem cells can be differentiated into endothelial cells in vitro*. Stem Cells **2004**. (22) p. 377–384.
143. Owens, G.K., M.S. Kumar, B.R. Wamhoff. *Molecular regulation of vascular smooth muscle cell differentiation in development and disease*. Physiol. Rev. **2004**. (84) p. 767–801.
144. Palocci, C., A. Barbetta, A. Grotta, M. Dentini, *Porous Biomaterials Obtained Using Supercritical CO<sub>2</sub>-Water Emulsions*. Langmuir **2007**. (23) p. 8243–8251.
145. Park, J.S., J.S. Chu, A.D. Tsou, R. Diop, Z. Tang, A. Wang, S. Li. *The effect of matrix stiffness on the differentiation of mesenchymal stem cells in response to TGF- $\beta$* . Biomaterials **2011**. (32) p. 3921-3930.

146. Partap, S., I. Rehman, J.R. Jones, J.A. Darr. "Supercritical Carbon Dioxide in Water" Emulsion-Templated Synthesis of Porous Calcium Alginate Hydrogels. *Adv. Mater.* **2006**. (18) p. 501–504.
147. Peppas, N.A., J.Z. Hilt, A. Khademhosseini, R. Langer. *Hydrogels in Biology and Medicine: From Molecular Principles to Bionanotechnology*. *Adv. Mater.* **2006**. (18) p. 1345-1360.
148. Petrini, P., C. Parolari, M.C. Tanzi, *Silk fibroin-polyurethane scaffolds for tissue engineering*. *J Mater. Sci. Mater. Med.* **2001**. (12) p. 849-853.
149. Phillips, J.E., T.A. Petrie, F.P. Creighton, A.J. Garcia. *Human mesenchymal stem cell differentiation on self-assembled monolayers presenting different surface chemistries*. *Acta Biomater* **2010** (6) p. 12–20.
150. Philp, D., S.S. Chen, W. Fitzgerald, J. Orenstein, L. Margolis, H.K. Kleinman. Complex extracellular matrices promote tissue-specific stem cell differentiation. *Stem Cells* **2005**. (23) p. 288–296.
151. Pierschbacher, M. D. & Ruoslahti, E. Cell attachment activity of fibronectin can be duplicated by small synthetic fragments of the molecule. *Nature* 309, 30–33 (1984)
152. Pittenger, M.F., A.M. Mackay, S.C. Beck, R.K. Jaiswal, R. Douglas, J.D. Mosca, et al. *Multilineage potential of adult human mesenchymal stem cells*. *Science* **1999**. (284) p. 143–147
153. Place, E.S., N.C. Evans, M.M. Stevens, *Complexity in biomaterials for tissue engineering*. *Nature Mater.* 2009. (8) p. 457–470.

154. Portalska, K., A. Leferink, N. Groen, H. Fernandes, L. Moroni, C. van Blitterswijk, et al. *Endothelial differentiation of mesenchymal stromal cells*. PLoS One **2012**. (7) p. e46842
155. Ranga, A., M.P. Lutolf. *High-throughput approaches for the analysis of extrinsic regulators of stem cell fate*. Curr Opin Cell Biol **2012**. (24) p. 236–244
156. Reddy, S.K., N. B. Cramer , C. N. Bowman, *Thiol–Vinyl Mechanisms. 2. Kinetic Modeling of Ternary Thiol–Vinyl Photopolymerizations*. Macromolecules **2006**. (39) p. 3681-3687 .
157. Reilly, G.C., A.J. Engler. *Intrinsic extracellular matrix properties regulate stem cell differentiation*. Biomechanics **2010**. (43) p. 55–62.
158. Roelen, B.A., P. Dijke. *Controlling mesenchymal stem cell differentiation by TGF family members*. J Orthop Sci **2003** (8) p. 740–748.
159. Ruoslahti, E., M. D. Pierschbacher. *New perspectives in cell adhesion: RGD and integrins*. Science **1987** (238) p. 491-497.
160. Salt, D.J., R. Leslie, P.J. Lillford, P. Dunnill. *Factors influencing protein structure during acid precipitation: A study of soya proteins*. Appl. Microbiol. Biotechnol. **1982** (14) p. 144-148.
161. Schneider, A., X. Y. Wang, D. L. Kaplan, J. Garlick and C. Egles, *Biofunctionalized electrospun silk mats as a topical bioactive dressing for accelerated wound healing*. Acta Biomaterialia **2009**. (5) p. 2570-2578.
162. Seib, F.P., M. Prewitz, C. Werner, M. Bornhauser. *Matrix elasticity regulates the secretory profile of human bone marrow-derived multipotent*

*mesenchymal stromal cells (MSCs)*. *Biochem Biophys Res Commun* **2009**. p. 389-663

163. Sengupta, S., S.H. Park, G.E. Seok, A. Patel, K. Numata, C.L. Lu, D. Kaplan. *Quantifying osteogenic cell degradation of silk biomaterials*. *Biomacromolecules* **2010** (11) p. 3592–3599.
164. Seo, J.H., K. Sakai, N. Yui. *Adsorption state of fibronectin on poly(dimethylsiloxane) surfaces with varied stiffness can dominate adhesion density of fibroblasts*. *Acta Biomater* **2013**. (9) p. 5493–5501
165. Seong, J., A. Tajik, J. Sun, J.L. Guan, M.J. Humphries, S.E. Craig, et al. *Distinct biophysical mechanisms of focal adhesion kinase mechanoactivation by different extracellular matrix proteins*. *Proc. Natl. Acad. Sci.* **2013**. (110) p.19372–19377.
166. Servoli, E., D. Maniglio, A. Motta, A., C. Migliaresi. *Folding and Assembly of Fibroin Driven by an AC Electric Field: Effects on Film Properties*. *Macromol. Biosci.* **2008**. (8) p. 827–835.
167. Servoli, E., D. Maniglio, A. Motta, R. Predazzer, C. Migliaresi. *Surface Properties of Silk Fibroin Films and Their Interaction with Fibroblasts*. *Macromol. Biosci.* **2005**. (5) p. 1175-1183.
168. Shu, X.Z., K. Ghosh , Y. Liu , F. S. Palumbo , Y. Luo , R. A. Clark , G. D. Prestwich, *Attachment and spreading of fibroblasts on an RGD peptide-modified injectable hyaluronan hydrogel*. *J. Biomed. Mater. Res. A* **2004**. (68) p. 365-375.
169. Silva, S., A. Motta, M. Rodrigues, A. Pinheiro, M. Gomes, J. Mano, R. Reis, C. Migliaresi. *Novel Genipin-Cross-Linked Chitosan/Silk Fibroin*

*Sponges for Cartilage Engineering Strategies*. *Biomacromolecules* **2008** (9) p. 2764-2774.

170. Silva, S.S., D. Maniglio, A. Motta, J.F. Mano, R.L. Reis, C. Migliaresi. *Genipin-Modified Silk-Fibroin Nanometric Nets*. *Macromol. Biosci.* **2008**. (8) p. 766–774.
171. Soen, Y., A. Mori, T.D. Palmer, P.O. Brown. *Exploring the regulation of human neural precursor cell differentiation using arrays of signaling microenvironments*. *Mol. Syst. Biol.* **2006**. (2) p. 37
172. Soffer, L., X. Wang, X. Zhang, J. Kluge, L. Dorfmann, D.L. Kaplan, G. Leisk. *Silk-based electrospun tubular scaffolds for tissue-engineered vascular grafts*. *J. Biomater. Sci. Polym. Ed.* **2008**. (19) p. 653–664.
173. Stegemann, J.P., S.N. Kaszuba, S.L. Rowe. *Review: advances in vascular tissue engineering using protein-based biomaterials*. *Tissue Engineering*. **2007** (13) p. 2601–2613
174. Stevens, M.M., J.H. George. *Exploring and Engineering the Cell Surface Interface*. *Science* **2010**. (310) p. 1135-1138.
175. Stowers, R.S., C.T. Drinnan, E. Chunga, and L.J. Suggs. *Mesenchymal stem cell response to TGF- $\beta$ 1 in both 2D and 3D environments*. *Biomater. Sci.*, **2013** (1) p. 860-869
176. Suzuki, S., Y. Narita, A. Yamawaki, Y. Murase, M. Satake, M. Mutsuga, et al. *Effects of extracellular matrix on differentiation of human bone marrow-derived mesenchymal stem cells into smooth muscle cell lineage: utility for cardiovascular tissue engineering*. *Cells Tissues Organs* **2010**. 191(4) p. 269-280.

177. Tamama, K., C.K. Sen, A. Wells. *Differentiation of bone marrow mesenchymal stem cells into the smooth muscle lineage by blocking ERK/MAPK signaling pathway*. *Stem Cells Dev.* **2008**. (17) p. 897–908.
178. Thiering, R., G. Hofland, N. Foster, G. Witkamp, L.A.M. Wielen, *Fractionation of soybean proteins with pressurized carbon dioxide as a volatile electrolyte*. *Biotechnol. Prog.* **2001**. (17) p. 513-521
179. Titmarsh, D.M., H. Chen, E.J. Wolvetang, J. Cooper-White. *Arrayed cellular environments for stem cells and regenerative medicine*. *Biotechnol. J.* **2013**. (8) p. 167–179.
180. Toews, K.L., R.M. Shroll, C.M. Wai. *pH-Defining Equilibrium between Water and Supercritical CO<sub>2</sub>. Influence on SFE of Organics and Metal Chelates*. *Anal. Chem.* **1995** (67) p. 4040–4043.
181. Trappmann B. et al. *Extracellular-matrix tethering regulates stem-cell fate*. *Nature Mater.* **2012**. (11) p. 742–749
182. Um, I., H. Kweon, Y. Park, S. Hudson. *Structural characteristics and properties of the regenerated silk fibroin prepared from formic acid*. *Int. J. Biol. Macromol.* **2001**. (29) p. 91–97.
183. Unger R.E., M. Unger, M. Wolf, K. Peters, A. Motta, C. Migliaresi, C. J. Kirkpatrick. *Growth of human cells on a non-woven silk fibroin net: a potential for use in tissue engineering*. *Biomaterials* **2004**. (25) p. 1069-1075.
184. Unger, R.E., M. Wolf, K. Peters, A. Motta, C. Migliaresi, C.J. Kirkpatrick. *Endothelialization of a non-woven silk fibroin net for use in tissue engineering: growth and gene regulation of human endothelial cells*. *Biomaterials* **2004** (25) p. 5137-5146.

185. Urry, D. W., *Molecular Machines: How Motion and Other Functions of Living Organisms Can Result from Reversible Chemical Changes*. Angew. Chem., Int. Ed. Engl. **1993**. (32) p. 819–841.
186. Vazao, H., R. P. das Neves, M. Graos, L. Ferreira. *Towards the maturation and characterization of smooth muscle cells derived from human embryonic stem cells*. PLoS One **2011**. (6) p. 17771.
187. Verheul, M., S.P.F.M. Roefs, J. Mellema, K.G. Kruif. *Power Law Behavior of Structural Properties of Protein Gels*. Langmuir **1998**. (14) p. 2263–2268.
188. Wagenseil, J.E., R.P. Mecham. *Vascular extracellular matrix and arterial mechanics*. Physiol. Rev. **2009**. (89) p. 957–989
189. Walas, S.M. *Chapter 11 Diffusion of Matter in Modeling with Differential Equations in Chemical Engineering*. Butterworth-Heinemann **1991**. USA
190. Wang, C.H., T.M. Wang, T.H. Young, Y.K. Lai, M.L. Yen. *The critical role of ECM proteins within the human MSC niche in endothelial differentiation*. Biomaterials **2013**. (34) p. 4223–4234.
191. Wang, Y., J.Y. Shyy, S. Chien. *Fluorescence proteins, live-cell imaging, and mechanobiology: seeing is believing*. Annu Rev Biomed Eng **2008**. (10) p. 1–38.
192. Wang, Y., E. Bella, C.S.D. Lee, C. Migliaresi, L. Pelcater, Z. Schwartz, B.D. Boyan, A. Motta. *The synergistic effects of 3-D porous silk fibroin matrix scaffold properties and hydrodynamic environment in cartilage tissue regeneration*. Biomaterials **2010**. (31) p. 4672–4681.

193. Wang, X., J.A. Kluge, G.G. Leisk, D.L. Kaplan. *Sonication-induced gelation of silk fibroin for cell encapsulation*. *Biomaterials* **2008**. (29) p. 1054– 1064
194. Wang, X., E. Wenk, A. Matsumoto, L. Meinel, C. Li, D.L. Kaplan, D.L. *Silk microspheres for encapsulation and controlled release*. *J. Controlled Release*. **2007**. (117) p. 360–370.
195. Weast, R.C., M.J. Astle. *Section 6: Fluid Properties*. **2010**. Chemistry and Physics, 86th Edition, USA: CRC Press
196. Weintraub, W.S., E.L. Jones, J.M. Craver, R.A. Guyton. *Frequency of repeat coronary-bypass or coronary angioplasty after coronary-artery bypasssurgery using saphenous venous grafts*. *Am J Cardiol* **1994**. 73(2) p. 103.
197. Wen, J.H., L.G. Vincent, A. Fuhrmann, Y.S. Choi, K.C. Hribar, H. Taylor-Weiner, et al. *Interplay of matrix stiffness and protein tethering in stem cell differentiation*. *Nature Mater.* **2014**. (13) p. 979–987
198. West, J.L., S.M. Chowdhury, A.S. Sawhney, C.P. Pathak, R.C. Dunn, J.A. Hubbell. *Efficacy of adhesion barriers: resorbable hydrogel, oxidized regenerated cellulose and hyaluronic acid*. *J Reprod Med* **1996**. (41) p. 149–154
199. West, J.L., J.A. Hubbell. *Separation of the arterial wall from blood contact using hydrogel barriers reduces intimal thickening after balloon injury in the rat: the roles of medial and luminal factors in arterial healing*. *Proc Natl Acad Sci.* **1996** (93) p. 13188–13193
200. West, J.L., J.A. Hubbell. *Polymeric biomaterials with degradation sites for proteases involved in cell migration*. *Macromolecules* **1999** (32) p. 241–244

201. Wingate, K., W. Bonani, Y. Tan, S. Bryant, W. Tan. *Compressive elasticity of threedimensional nanofiber matrix directs mesenchymal stem cell differentiation to vascular cells with endothelial or smooth muscle cell markers*. *Acta Biomater* **2012**. (8) p. 1440.
202. Wingate, K., M. Floren, Y. Tan, P.O.N. Tseng, W. Tan. *Synergism of Matrix Stiffness and Vascular Endothelial Growth Factor on Mesenchymal Stem Cells for Vascular Endothelial Regeneration*. *Tissue Engineering Part A* **2014** (20) p. 2503–2512.
203. Wipff, P.J., D.B. Rifkin, J.J. Meister, B. Hinz. *Myofibroblast contraction activates latent TGF-beta1 from the extracellular matrix*. *J. Cell Biol.* **2007**. (179) p. 1311–1323.
204. Wu, C.C., Y.C. Chao, C.N. Chen, S. Chien, Y.C. Chen, C.C. Chien, et al. *Synergism of biochemical and mechanical stimuli in the differentiation of human placenta-derived multipotent cells into endothelial cells*. *J Biomech.* **2008**. (41) p.813
205. Yang, F., S.W. Cho, S.M. Son, S.P. Hudson, S. Bogatyrev, L. Keung, et al. *Combinatorial extracellular matrices for human embryonic stem cell differentiation in 3D*. *Biomacromolecules* **2010** (11) p. 1909–1914
206. Yang, H., S.S. Yuan, T.W. Chung, S.B. Jong, C.Y.Lu, W.C. Tsai, W.C. Chen, P.C. Lin, P.W. Chiang, Y.C. Tyan. *Characterization of silk fibroin modified surface: A proteomic view of cellular response proteins induced by biomaterials*. *BioMed. Res. Int.* **2014**. p. 209469
207. Yang, M.C., N.H. Chi, N.K. Chou, Y.Y. Huang, T.W. Chung, Y.L. Chang, H.C. Liu, M.J. Shieh, S.S. Wang. *The influence of rat mesenchymal stem cell CD44 surface markers on cell growth, fibronectin expression, and*

- cardiomyogenic differentiation on silk fibroin - Hyaluronic acid cardiac patches*. *Biomaterials* **2010** (31) p. 854–862.
208. Yang, Y., X. Chen, F. Ding, P. Zhang, J. Liu, X. Gu. *Biocompatibility evaluation of silk fibroin with peripheral nerve tissues and cells in vitro*. *Biomaterials* **2007**. (28) p. 1643–1652.
209. Yang, Y., F. Ding, J. Wu, W. Hu, W. Liu, J. Liu and X. Gu, *Development and evaluation of silk fibroin-based nerve grafts used for peripheral nerve regeneration*. *Biomaterials* **2007**. (28) p. 5526-5535.
210. Young, T., L. Chen. *Pore formation mechanism of membranes from phase inversion process*. *Desalination* **1995**. (103) p. 233-247.
211. Yucel, T., P. Cebe, D.L. Kaplan. *Vortex-Induced Injectable Silk Fibroin Hydrogels*. *Biophys. J.* **2009**. (97) p. 2044–2050.
212. Zhang, W., X. Wang, S. Wang, J. Zhao, L. Xu, C. Zhu, D. Zeng, J. Chen, Z. Zhang, D. Kaplan, X. Jiang. *The use of injectable sonication-induced silk hydrogel for VEGF165 and BMP-2 delivery for elevation of the maxillary sinus floor*. *Biomaterials* **2011** (32) p. 9415-9424.
213. Zhou, C., F. Confalonieri, M. Jacquet, R. Perasso, Z. Li, J. Janin. *Silk fibroin: Structural implications of a remarkable amino acid sequence*. *Proteins* **2001** (44) p. 119– 122.
214. Zhu, J., C. Tang, K. Kottke-Marchant, R.E. Marchant. *Design and synthesis of biomimetic hydrogel scaffolds with controlled organization of cyclic RGD peptides*. *Bioconjug Chem.* **2009** 20(2) p. 333-339.

## Scientific Production

1. **Floren M.**, Bonani W., Dharmarajan A., Motta, A., Migliaresi C., Tan W. Human MSCs Cultured on Silk Hydrogels with Variable Stiffness and Growth Factor Differentiate into Mature SMC Phenotype. – Under Review Acta Biomaterialia (August 2015)
2. **Floren M.**, Tan W. Three-dimensional, soft neotissue arrays as high throughput platforms for the interrogation of engineered tissue environments. Biomaterials 59 (2015) 39-52.
3. Wingate K., **Floren M.**, Tan Y., Tseng Pi Ou N., and Tan W. Synergism of Matrix Stiffness and Vascular Endothelial Growth Factor on

Mesenchymal Stem Cells for Vascular Endothelial Regeneration. *Tissue Engineering Part A* 2014, 20(17-18): 2503-2512.

4. **Floren M.**, Spilimbergo S., Motta A., Migliaresi C. Carbon Dioxide Induced Silk Protein Gelation for Biomedical Applications. *Biomacromolecules* 2012, 13, 2060-2072.
5. Motta A., **Floren M.**, Migliaresi C. "Silk in Medicine" in P. Aramwit's *Silk: Properties, Production and Uses* – Nova publishing group 2012
6. Belfiore L., **Floren M.**, Belfiore C. Electric-field-enhanced nutrient consumption in dielectric biomaterials that contain anchorage-dependent cells. *Biophysical Chemistry* 2012, 161, 8-16.
7. **Floren M.**, Spilimbergo S., Motta A., Migliaresi C. Porous Poly(D,L lactic acid) Foams with Tunable Structure and Morphology Prepared by Supercritical Carbon Dioxide. *Journal of Biomedical Materials Research Part B: Applied Biomaterials*. 2011, 99, 338-349
8. Belfiore L., **Floren M.**, Paulino A., Belfiore C. Stress-sensitive tissue regeneration in viscoelastic biomaterials subjected to modulated tensile strain. *Biophysical Chemistry* 2011, 158, 1-8
9. Belfiore L., **Floren M.**, Volpato F., Paulino A., Belfiore C. Nutrient diffusion and simple nth-order consumption in regenerative tissue and biocatalytic sensors. *Biophysical Chemistry* 2011, 155, 65–73

### **Participation to *Congresses, Schools and Workshops***

1. **M Floren**, W Tan. "Soft 3-Dimensional Neotissue Microarrays as High-throughput Platforms for Interrogating Stem Cell Instructional Microenvironments". SB3C, Snowbird, UT, June 2015
2. **M. Floren**, W Tan. "Soft 3-Dimensional ECM Microarrays as High-Throughput Platforms". St. John, USVI, January 2015
3. for Optimizing Tissue Regenerative Microenvironments

4. **M Floren**, S. Bryant, W Tan. “*Protein Laden Soft Matrices as High-Throughput Platforms to Engineer Stem Cell Microenvironments*”, BMES Annual Meeting, San Antonio, TX, October 2014
5. A Dharmarajan, **M Floren**, W Tan. “High Spatio-temporal ERK Activity in Response to Mechano-chemical Stimuli in Rat Mesenchymal Stem Cells”, BMES Annual Meeting, San Antonio, TX, October 2014
6. A Dharmarajan, **M Floren**, W Tan. High Temporal Resolution of ERK Activity in Response to Mechano-chemical Stimuli. Society For Biomaterials 2014 Annual Meeting and Exposition, Denver, CO, April 2014
7. **M Floren**, W Bonani, N. Tseng, C. Migliaresi, W Tan “Porous Silk Fibroin Hydrogels with Tunable Stiffness for Vascular Tissue Engineering.” Society For Biomaterials 2014 Annual Meeting and Exposition, Denver, CO, April 2014
8. **M Floren**, N. Tseng, S. Bryant, W Tan. “Synergy of Three-dimensional Soft Matrices with ECM Proteins Augments Stem Cell Differentiation towards Vascular Phenotypes”. Society For Biomaterials 2014 Annual Meeting and Exposition, Denver, CO, April 2014
9. **M Floren**, S. Spilimbergo, A. Motta, C. Migliaresi. “Natural-based Hydrogels with Improved Properties based on Silk Proteins and High Pressure CO<sub>2</sub>” Summer School on Biomaterials & Regenerative Medicine, Riva del Garda, Italy, July 2012
10. **M Floren**, A. Motta, C. Migliaresi. “Gelation Methods for Silk Fibroin” 2nd International Congress on Biohydrogels, Florence, Italy, November 2011
11. **M Floren**, E. Carletti, E. Merzari, C. Migliaresi. “Osteoblast Genotypic Response and Matrix Formation: Effect of Scaffold Morphology and Mechanical Stimuli *In Vitro* – Preliminary Evaluation” Tissue Engineering and Regenerative Medicine International Society- EU Meeting, Galway, Ireland, June 2010

### ***Acknowledgements***

I would like to first acknowledge my advisors, Professors Claudio Migliaresi, Antonella Motta and Wei Tan, for their direction, time, patience and encouragement through five years of my Ph.D. study at both University of Trento, Italy (UNITN) and University of Colorado (CU) Boulder, USA. They not only taught me how to design and execute scientific problems, but also influenced me by their passion to work and persistence to success in research.

I would also like to thank my thesis committee for their time and effort; Virginia Ferguson, Yifu Ding, Stephanie Bryant, and Ralph Nemenoff, who have all provided significant and fruitful technical guidance. Stephanie Bryant collaborated extensively on the materials preparation of for the final progression of this thesis and specifically I must recognize her post-doc Sadhana Sharma for her significant contribution to polymer and peptide synthesis (Chapter 6). In addition to the research ideas she contributed, her support and advice on several levels of this thesis are invaluable. I also wish to recognize Virginia Ferguson for her specific mentoring on the mechanical nature of materials. I also thank all the faculty members and staff and Postdocs at UNITN and CU Boulder who contributed to our excellent graduate education.

I wish to recognize the other members of my research groups (UNITN, CU Boulder) for their outstanding support, shared intellect and above all companionship. It has been a true privilege to work with my friends Devid Maniglio (UNITN), Walter Bonani (UNITN), Winston Elliot (CU Boulder), Anirudh Dharamarjan (CU Boulder). They made research bearable when times were frustrating and provided valuable input on experiments, both design and execution, presentations, and manuscripts. Walter was particularly patient with his preparation of numerous silk hydrogels to later be applied for studies at CU Boulder. I must also recognize Anirudh through his diligence and commitment to countless hours perfecting PCR analysis for a key study within this thesis. I wish to also thank my fellow graduate students who have supported me through critical feedback, technical advice, and experimental protocols: Kathryn Wingate (CU Boulder), Elizabeth Ainsbury (CU Boulder), Fabio Zomer Volpato (UNITN), Elenora Carletti (UNITN).

I would be absent if I did not thank my undergraduate mentors at Colorado State University, Larry Belfiore and Travis Bailey. Travis gave me my first opportunity at real laboratory research and was highly supportive of me to pursue greater research opportunities. Without Larry much of my decision to proceed with research opportunities abroad would not have become a reality, I thank him for his efforts to introduce me to two of my current advisors, Claudio Migliaresi and Antonella Motta, and also for his friendly and intellectual conversations.

I would like to thank my family for all of their support throughout many years of graduate school, both here and abroad, especially my father Dale Floren and brother John Floren for their encouragement, support, and dedication to excellence which has shaped the person that I am today. I also would like to thank my aunts, Marlene and Heather, and uncles, Gus and John, for your unwavering support and adherence to family. I cannot forget my family abroad, Cousin Joe and his wife Catherine, daughter Claire and son Antione; thank you for helping me to realize that beauty exists in many places in this world, without your support and encouragement my time abroad would have not been as special of an endeavor.

*"It had long since come to my attention that people of accomplishment rarely sat back and let things happen to them. They went out and happened to things."*

*- Leonardo Da Vinci*